

THE ROLE OF SEPARATED FLOW IN THE PREDICTION OF THE DYNAMIC
RESPONSE OF OFFSHORE STRUCTURES TO RANDOM WAVES

by

Andrew Bruce Dunwoody
B.A.Sc., University of British Columbia
(1974)

Submitted in Partial Fulfillment
of the Requirements for the Degree of

Doctor of Philosophy

in

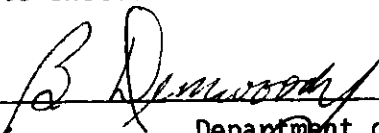
Ocean Engineering

at the

Massachusetts Institute of Technology
May 1980

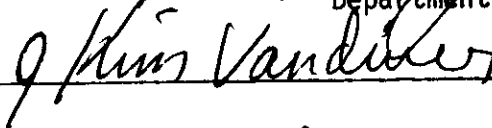
© Massachusetts Institute of Technology 1980

Signature of Author



Department of Ocean Engineering
May 19, 1980

Certified by



J. Kim Vandiver
Thesis Supervisor

Accepted by



Chairman, Department Committee

I. INTRODUCTION

World oil demand is being met increasingly from resources located under the sea. The Gulf of Mexico and the North Sea are the two most important areas in this regard, although offshore oil production exists or is contemplated in many other offshore areas of the world as well. With the rapidly rising cost of crude oil and the uncertainties of supply from some traditional sources, it is becoming economically attractive, if not imperative, to recover the oil from resources located under greater depths of water and more inhospitable seas than was previously thought possible. However, safe and economical designs for these conditions require that it be possible to accurately predict the impact of the environment on the structures being contemplated for use.

The main impact of the environment on the design of most platforms built to date has been limited to the need for the structure to be able to withstand the largest wave likely to be encountered during its lifetime. Recently, though, some platforms have also had to be designed against fatigue failure. An important reason for the significance of fatigue in the design of these platforms has to do with the resonant motion of these platforms in their fundamental flexural modes of vibration. The natural frequencies of these modes in some recent as well as contemplated platforms are sufficiently low as to be in the band of frequencies of the wave spectrum. This fact, coupled with the very light damping in these modes means that these platforms exhibit significant levels of motion even in moderate sea states. Because moderate

seas can be present for much of the life of a platform, low-stress/high-cycle fatigue can be a problem.

At present, proposed platform designs are checked for susceptibility to fatigue using dynamic, finite-element programs, as described by Vugts and Kirra [5]. The response of a proposed design to waves is predicted by subjecting a finite-element model of the structure to representations of a variety of uni-directional, regular waves of different amplitudes, frequencies and directions of propagation. The responses of the platform to these individual waves are then accumulated in some manner in order to predict the overall, weighted-average response to a random sea.

This type of analysis is very expensive and suffers from other problems as well, two of which are listed below.

(1) The analysis treats the motion of a platform as a concatenation of the responses of the platform to a set of discrete, deterministic waves, rather than as the random response of a system to a random input process. Because the method of analysis does not try to accurately model one of the main characteristics of the problem, its randomness, the validity of the method is open to question.

(2) Another problem is that the analysis is specific to one platform. The prediction of motion for one platform does not give much physical insight into the general problem or what influence specific factors have on the motion. As a result, platform design against fatigue may be less efficient than would be possible if a better understanding of the general problem were available.

Against these problems, it must be noted that dynamic, finite-

damage, the emphasis of the research is on predicting platform motion in moderate seas. In moderate seas, non-linearities are less important than they are in severe storms. Therefore, it may be possible to obtain reasonable predictions of platform motion while ignoring most non-linear effects. Also, because resonance plays a significant part in fatigue of offshore platforms, it is important that the model used reflect the dynamic characteristics of a platform.

(2) Whereas it may be possible to neglect many of the non-linearities associated with the wave-structure interaction problem, when predicting platform motion in moderate seas, it is unlikely that the drag force associated with the separation of the flow field behind the members of the structure can be ignored. For want of a better model, it is necessary to use the drag term of Morison's equation for the purpose of predicting this force. Also, in light of the importance of dynamic amplification in response predictions and the possibility of separated-flow, induced damping, it is appropriate to use the relative-velocity formulation of Morison's equation.

(3) The analysis should account for the fundamentally random nature of the sea and of the response of a platform to it. This requirement that the analysis should be a random, or stochastic one restricts the complexity of the model which can be used to describe the system. Fortunately, there are some techniques by which non-linearities can be included in an analysis. In particular, the technique of Gaussian closure, described by Iyengar and Dash [5], has both intuitive and mathematical appeal for this problem. Using this method, it is possible to predict,

approximately, response spectra of a non-linear system.

(4) Most work to date using random vibration techniques to predict structural response has been limited to very idealized structures, such as single, vertical cylinders, and idealized wave environments, it being generally assumed that the sea is unidirectional. Such work is useful for demonstrating trends but the results cannot be directly used in the prediction of the motion of a real platform. To be directly useful, the hydrodynamic and structural models used in this research should be sufficiently general as to be applicable to any arbitrary jacket platform in a directionally distributed sea.

Based on the precepts just listed, the specific goal of this research is to predict the response of an arbitrary, jacket-type, oil production platform to a random sea. The model employed to reach this goal is linear, except for the separated flow drag, which is modelled by the relative velocity formulation of Morison's equation. The model also includes the dynamic behaviour of the structure. The method of analysis is the approximate random vibration technique of Gaussian closure. To reach this goal, three steps are required in the research.

(1) The components of the motion prediction problem must be modelled in a consistent mathematical framework; the two components being the fluid and structural dynamics. After formulating each component independently, they must be combined to form a unified set of equations describing the problem.

(2) Once the problem is well described by a set of equations, these equations must be manipulated, using the Gaussian closure technique,

term in the relative velocity formulation of Morison's equation. Besides setting this drag term in the appropriate mathematical framework, the relationship between the relative velocity formulation and the original, fixed-structure formulation of Morison's equation will be discussed.

For small waves, the behaviour of water beneath a free surface can be described by linear, potential-flow, hydrodynamic theory. This theory, being linear, allows the researcher to describe the solution of any particular problem as a superposition of the solutions for any number of different wave components, each of which propagates independently of all the others. In particular, the forces on a structure immersed in water can be divided into those which would be exerted on the structure due to the incident wave field if the structure were motionless and those which would be exerted on the structure due to its own motion in an otherwise calm sea. The two problems defined by this division are commonly referred to as the diffraction problem and the radiation problem respectively.

The forces associated with the radiation problem do not depend on the incident wave field, but only on the motion of the structure. Therefore, it will be convenient to group these forces with the stiffness, damping and inertial forces of the structural-dynamic model, which also depend only on the motion of the structure. For any given frequency and generalized mode of motion of the structure, the hydrodynamic force on that generalized mode can be regarded as due to added mass and radiation damping terms in the equation of motion of that mode. Similarly, the hydrodynamic force on any other mode due to motion of the first mode can be

associated with added-mass and radiation-damping, cross-coupled terms. A generalized mode is any particular vector displacement function of the structure from its equilibrium configuration. For example, pitch is a generalized mode used to describe the motion of a ship. A unit of pitch displacement corresponds to an angular rotation of the ship about the appropriate axis of one radian. Similarly, the natural modes of vibration of a structure form a set of generalized modes with special properties.

The hydrodynamic forces associated with the radiation problem are not completely analogous to additional inertial and damping forces, because the added mass and radiation damping coefficients in the equations of motion are frequency dependent. As is common in the prediction of platform motion, we will assume that the added-mass and radiation-damping coefficients are constants, their values being based on some mean, response frequency. For the added-mass coefficients, this assumption is justifiable because the effect of the free surface, which induces the frequency dependence, is limited to a thin layer of water adjacent to the surface. Therefore, the frequency-dependent part of the added-mass is only a small portion of the total added mass. The radiation damping has been estimated by Vandiver [13] to account for only 10% of the total damping on typical steel jacket structures, so that ignoring the frequency dependence should have little effect on the final predictions. A more accurate prediction of platform motion spectra could be performed using the Gaussian closure technique and incorporating the frequency dependence of the added-mass and radiation-damping coefficients. Although such an analysis is possible,

Unlike the inertial force term, the separated flow drag term of Morison's equation must be accounted for separately of the potential flow forces. According to Morison's equation, the separated flow drag per unit length is proportional to the square of the component of the fluid velocity perpendicular to the axis of the cylinder. The fluid velocity used in the equation is the velocity which would exist at that point in space due to the incident wave field in the absence of the cylinder. Equation (II-1) expresses the separated-flow drag term of Morison's equation using indicial notation and implied summation.

$$d_i = \frac{1}{2} C_d \rho D v_i |v| \quad (\text{II-1})$$

In equation (II-1), the velocity upon which the drag depends, v , is the component of the incident flow velocity, u , which is perpendicular to the axis of the cylinder. If the orientation of the cylinder is described by a unit vector parallel to the axis of the cylinder, A , then the relationship between v and u can be expressed by equation (II-2).

$$v_i = (\delta_{ij} - A_i A_j) u_j \quad (\text{II-2})$$

The prediction of separated flow drag by equations (II-1) and (II-2) has been confirmed by experiments involving oscillating flows past a stationary cylinder. For an offshore platform, the structural members do move slightly, so that the question arises as to how the drag term should be modified to account for the structural motion and indeed whether the motion of the cylinder has any significant influence on the force. Typically, the relative velocity formulation of Morison's equation has

been used to account for motion of the cylinder. In this formulation, the fluid velocity, u , is replaced by the difference between the fluid velocity and the structural velocity. As noted in the introduction, Burke and Tighe found that inclusion of the relative velocity formulation of Morison's equation led to a significant increase in effective, modal damping in a finite element model of an offshore platform.

If the relative velocity formulation of Morison's equation is reasonable, then it is important that the model of hydrodynamic force use that formulation because damping plays a critical role in the prediction of the motion of a platform for the purpose of fatigue damage estimation. It can be shown that the relative-velocity formulation of Morison's equation would correctly predict the force on a segment of a moving cylinder in a fluid flow, if the original formulation of Morison's equation were an exact predictor of the hydrodynamic force on a fixed cylinder. The argument is based on the application of a coordinate transformation to the Navier-Stokes equation. However, the argument is restricted in that the boundary conditions on the fluid must be kinematic, the boundaries being the cylinder and the far-field of the fluid. For an offshore platform vibrating principally in its fundamental modes, the motion of the platform is almost independent of the instantaneous fluid pressure acting on any portion of it. Therefore, the cylinder can be considered to supply a kinematic boundary condition to the fluid. The far-field of the fluid is all of the volume beyond a few diameters of the cylinder. In this region, the fluid velocity is also nearly independent of the flow in the immediate vicinity of the cylinder. Thus

the far-field flow also constitutes a kinematic boundary condition. The one instance where a dynamic boundary condition is important is for the portions of the platform within a few cylinder diameters of the surface. In this narrow region, the argument based on the Navier-Stokes equation breaks down and the relative-velocity formulation of Morison's equation may not be reasonable.

Separated flow forces have been studied extensively for a fixed cylinder in sinusoidally-oscillating flow. Predictions based on Morison's equation have been found to agree well with measured forces for suitable values of the parameters C_m and C_d . Therefore, the relative velocity formulation should also give good results for the case where flow and cylinder are both oscillating sinusoidally, in-line and at the same frequency with possibly different amplitudes and phases, because the relative velocity is a simple sinusoid. Similarly, the relative velocity formulation should give good results for suitable choices of C_m and C_d when the velocities of the cylinder and the fluid are narrow-band random processes instead of pure sine waves. It is not so clear whether Morison's equation, or the relative velocity formulation of it, will give reasonable results for wide band random processes. An indication that the equations may still give reasonable results for wide band processes is found in the work of Moe and Verley, mentioned previously. They found reasonable agreement between experimental results and predictions based on the relative velocity formulation of Morison's equation for a cylinder oscillating in a steady current. The spectrum of the relative velocity consisted of an impulse at zero frequency and a narrow peak

at the cylinder's natural frequency. In terms of spectra, this experiment was far from the pure sinusoidal oscillations normally studied.

Based on the theoretical relationship between Morison's equation and the relative velocity formulation of it, and on experimental results published in the literature, the relative velocity formulation of Morison's equation was selected for use in the hydrodynamic force model. The inertial term of the equation is already included implicitly in the linear, potential flow force, so that only the separated flow drag term appears explicitly. For the relative velocity formulation, the fluid velocity, u , in equation (II-2) must be replaced by the difference between u and w , where w is the local structural velocity.

$$v_i = (\delta_{ij} - A_i A_j)(u_j - w_j) \quad (\text{II-3})$$

It should be noted that although equations (II-1) and (II-3) are stated for a general three-dimensional fluid flow, most experimental work has been done for separated flow drag on a cylinder in two-dimensional flow conditions. Therefore, caution should be exercised in applying the results of this work, although the equations should still give reasonable results for sufficiently high Keulegan-Carpenter Number.

One final modification of the separated-flow drag term of Morison's equation is necessary because of the mathematical difficulty in dealing with the magnitude of the velocity in equation (II-1). As shown in Appendix A, the term $v|v|$ can be replaced over a range of v by a term of the form $av + bv|v|^2$ by a suitable choice of the constants a and b . This latter term is much more suitable for mathematical manipulations. Thus,

the equation to be used to model the separated flow drag contribution to the hydrodynamic force model is equation (II-4), where v is given by equation (II-3).

$$d_i = \frac{C_d \rho D \sigma_v}{\sqrt{2\pi}} v_i \left\{ 1 + \frac{v_j v_j}{3\sigma_v^2} \right\} \quad (\text{II-4})$$

In equation (II-4), σ_v , the root-mean-square relative velocity component is a function of the incident wave spectrum, the depth below the surface and the structural velocity. The structural velocity is not known, a priori, so that an iterative solution of the motion prediction problem is necessary.

In summary, the hydrodynamic force model has been formulated on the basis of linear, potential flow theory, with an additional contribution to the hydrodynamic force caused by the separation of the flow behind the bluff members of the structure. The potential flow forces can be divided into forces associated with the radiation problem and with the diffraction problem. The forces associated with the radiation problem can be related, with some approximation, to added mass and radiation damping coefficients in the structural equations of motion. The instantaneous force, on any generalized mode of the structure, associated with the diffraction problem has been denoted by $p_\alpha(t)$. This force is a function of the incident wave field, the geometry of the structure and the shape of the mode α , although the functional relationship was not discussed. The hydrodynamic force was modified to

account for separation by inclusion of the relative velocity formulation of Morison's equation. The inertial term of that equation is implicit in the potential flow forces, but the drag term was added separately as a distributed force over the submerged part of the structure.

In the next chapter, this hydrodynamic force model will be combined with a structural dynamic model based on a natural mode description of platform motion. Also, a consistent method by which to define the submerged geometry of an arbitrary jacket platform will be described.

III. STRUCTURAL RESPONSE MODEL

The second component required for the motion prediction model is a structural response model. Before discussing the specific model used, it is necessary to lay down a consistent framework for describing the submerged geometry of an arbitrary platform. This framework is necessary so that integrals over the submerged portion of a platform can be conveniently expressed.

The submerged portion of a jacket platform consists of a number of segments of pipe of various diameters welded together to form an overall framework. Thus, the structure can be described in terms of the diameters of the pipe segments and the positions and orientations of the centerlines of the segments. To facilitate the description of the submerged portion of a platform for the purpose of computing hydrodynamic loads, it is very useful to have a single parameter by which to identify any point along the centerline of any of the pipe segments. The measure employed in this thesis is the accumulated length of submerged pipe, L . To define the measure, L , for any platform requires that each submerged pipe segment be numbered and that one end of each segment be designated as the beginning of that segment. The accumulated length corresponding to any point on the structure is defined as the sum of the lengths of all the segments numbered less than the segment on which the point rests, plus the length from the beginning of that segment to the point. For example, if segments 1 through 5 are each 100 feet long, a point 40 feet from the beginning of segment 5 would

would be assigned an accumulated length of 440 feet. By this definition, there exists a one-to-one relationship between accumulated length, L , and points along the centerlines of the pipe segments which form the submerged structure of the platform. Because the motion-prediction model is linear, except for the separated flow drag, the submerged structure is taken to be all of the structure below the mean waterline, rather than the instantaneous waterline. The only exceptions to the one-to-one relationship are at intersections of two or more pipe segments, where the points of intersection may correspond to more than one value of L . Such exceptions do not constitute a problem in this work. Once the accumulated length is defined for any platform, the submerged geometry of that platform can be defined by the functions, $P(L)$, the position in Cartesian coordinates of the point L , $A(L)$, a unit vector directed along the centerline of the pipe at that point, and $D(L)$, the diameter of the pipe at that point.

The purpose of the structural response model is to predict the motion of the structure resulting from the external forces acting on it. For the purpose of this thesis, it is assumed that the only forces acting on the platform are the hydrodynamic forces outlined in the previous chapter. The response of a structure to applied forces can be expressed in a number of different ways. For a lightly damped structure whose response is a linear function of the applied forces, a convenient method is to decompose the motion of the structure into the motions of the set of natural modes of the structure. In computing the natural mode shapes and the set of modal differential equations to

describe the response of the structure, it is usual to include the forces associated with the hydrodynamic radiation problem with the stiffness, damping and inertial forces associated with the structure, as all of these forces are not functions of the incident wave field but only of the structural motion. Strictly speaking, the modal differential equations so generated are not exact as the added-mass and radiation damping coefficients used are frequency dependent; however, no problem is anticipated as was discussed in the last chapter.

Assuming that the eigenvalue problem has been solved, the form of the modal differential equations are shown in equation (III-1).

$$\delta_{\alpha\beta} \ddot{y}_{\beta} + C_{\alpha\beta} \dot{y}_{\beta} + W_{\alpha\beta} y_{\beta} = g_{\alpha} \quad (\text{III-1})$$

In this equation, $y_{\beta}(t)$ is the modal displacement of mode β and $g_{\alpha}(t)$ is the externally applied force, less the component of the force associated with the radiation problem. $\delta_{\alpha\beta}$ is the Kronecker delta function, indicating that the mode shapes used are ortho-normal. $C_{\alpha\beta}$ and $W_{\alpha\beta}$ are the damping and stiffness matrices respectively. Implicitly included in $C_{\alpha\beta}$ is the radiation-damping term of the hydrodynamic force. $W_{\alpha\beta}$ is a diagonal matrix but is written in this form for consistency. As in the previous chapter, implied summation is used in this equation. A convention employed throughout this thesis is that Greek letter subscripts imply summation over all modes, while the English alphabet is reserved for summation over the three Cartesian coordinates.

The modal, hydrodynamic force, $g_{\alpha}(t)$, is made up of two components: the potential flow force associated with the diffraction problem, $p_{\alpha}(t)$,

and the distributed, non-linear, separated flow drag, $d_i(t)$. If the mode shape vector of the α mode is given by $M_{i\alpha}(L)$, then the α modal, separated flow drag force is given by the integral of the separated flow drag over the accumulated length of the structure, weighted by the mode shape vector. Thus, the α modal differential equation of motion can be rewritten in terms of the potential flow and separated flow modal forces.

$$\delta_{\alpha\beta} \ddot{y}_\beta + C_{\alpha\beta} \dot{y}_\beta + W_{\alpha\beta} y_\beta = p_\alpha + \int_L M_{i\alpha} d_i dL \quad (\text{III-2})$$

In this equation, the distributed, separated-flow drag, d_i , is given by equation (II-4). The structural velocity at any point, L , can be expressed as a weighted sum of the individual modal velocities, so that equation (II-3) for the relative velocity, v , can be rewritten in terms of the incident wave field, fluid velocity and the modal velocities.

$$v_i = (u_j - M_{j\alpha} \dot{y}_\alpha)(\delta_{ij} - A_i A_j) \quad (\text{III-3})$$

Equations (III-2), (II-4), and (III-3) form the mathematical model by which the instantaneous response of an arbitrary platform to incident waves can be predicted. In the next chapter, these three equations will be manipulated with the approximate random vibration technique of Gaussian closure in order to arrive at predictions of the spectra of the platform motion. Because this model can be made to represent an arbitrary jacket platform, the predictions made can also be applied to any platform.

IV. GAUSSIAN CLOSURE TECHNIQUE

Over the last two chapters, a mathematical model has been developed to predict the instantaneous response of an arbitrary, jacket platform to an incident wave field. The purpose of this chapter is to develop a predictor of the second-moment statistics of the motion of this platform, given the model. Because the statistical characteristics of the incident wave field change slowly compared with the response time of a platform, it is appropriate to assume that the wave field is a stationary, random process. If the input is stationary, then the response is also a stationary random process and the second-moment statistics of the response can be expressed in the form of auto- and cross-spectra. A prediction of these response spectra is the desired product of the following analysis.

The model developed is non-linear, and therefore normal spectral analysis techniques cannot be used. Instead, the approximate technique of Gaussian closure has been employed. The approximation in this technique involves the evaluation of higher, statistical moments in terms of second moments. Ordinarily, higher moments of a random process cannot be readily evaluated; however, for a Gaussian process, all higher moments can be expressed as sums and products of first and second moments. For instance, for the joint Gaussian, zero-mean, random variables a , b , c , and d , the fourth moment involving these variables can be decomposed as shown in equation (IV-1).

$$E[abcd] = E[ab]E[cd] + E[ac]E[bd] + E[ad]E[bc] \quad (IV-1)$$

In the following analysis, higher moments will be evaluated using equation (IV-1), even though the joint processes are not strictly Gaussian. The incident wave field is reasonably well modelled as a Gaussian process, but the platform response is not necessarily Gaussian because the response is related to the incident wave field by a non-linear model. We should expect, though, that the platform response would be nearly Gaussian, because a significant portion of the force on the platform is due to the potential flow term in the forcing function, which is a linear function of the incident wave field. Also, the platform response is a spatial and temporal average over the applied force and therefore, by central limit theorem arguments, should be more nearly Gaussian than the applied force. Therefore, it would seem to be a very good approximation for this work to evaluate higher statistical moments using equation (IV-1).

The method by which the response spectra predictor can be developed involves repeated application of the following three steps.

1. Derive a relationship involving second and higher moment statistics in the variables of the model. The relationship can be derived by multiplying all terms of one equation of the model, expressed at time t , by one of the variables, expressed at some other time $t + \tau$, and taking expected values of all the products.

2. Decompose all fourth moments using equation (IV-1) and all sixth moments using a similar equation. Express all the resulting second moments as auto- and cross-correlation functions.

3. Apply the Fourier transform operator to all terms of the

equation in order to replace the auto- and cross-correlation functions with auto- and cross-spectra. Relate the spectra involving derivatives of the modal displacements to the corresponding spectra involving the modal displacements.

Finally, all of the equations relating auto- and cross-spectra can be combined, rearranged and simplified.

Before beginning, note that because there is assumed to be no current acting, all of the random processes have zero mean. This factor greatly simplifies the analysis over that which would be required if a current were present. Also note that, although many of the variables used are functions of position as well as time, this functional dependence will not be explicitly included for convenience.

To start, multiply all terms of equation (III-2) by $y_\epsilon(t + \tau)$, take expected values of all terms and express the statistical moments as cross-correlation functions.

$$E[(\delta_{\alpha\beta}\ddot{y}_\beta(t) + c_{\alpha\beta}\dot{y}_\beta(t) + w_{\alpha\beta}y_\beta(t))y_\epsilon(t+\tau)] =$$

$$E[(p_\alpha(t) + \int_L M_{i\alpha} d_i dL)y_\epsilon(t+\tau)] \quad (IV-2)$$

$$\delta_{\alpha\beta}R\ddot{y}_\beta y_\epsilon(\tau) + c_{\alpha\beta}R\dot{y}_\beta y_\epsilon(\tau) + w_{\alpha\beta}Ry_\beta y_\epsilon(\tau) =$$

$$Rp_\alpha y_\epsilon(\tau) + \int_L M_{i\alpha} Rd_i y_\epsilon(\tau)dL \quad (IV-3)$$

Equation (IV-3) may be simplified by Fourier transforming all terms and relating the cross-spectra involving derivatives of y to cross-spectra

involving y_β .

$$(-\omega^2 \delta_{\alpha\beta} - i\omega C_{\alpha\beta} + W_{\alpha\beta}) S y_\beta y_\epsilon(\omega) = S p_{\alpha} y_\epsilon(\omega) + M_{i\alpha} S d_i y_\epsilon(\omega) dL \quad (IV-4)$$

The second spectrum on the right side of equation(IV-4) can be expanded by multiplying equation(II-4) by $y_\epsilon(t+\tau)$ and taking expected values.

$$E[d_i(t)y_\epsilon(t+\tau)] = \frac{C_d \rho D \sigma_v}{\sqrt{2\pi}} E \left\{ v_i(t) \left[1 + \frac{v_j(t)v_j(t)}{3\sigma_v^2} \right] y_\epsilon(t+\tau) \right\} \quad (IV-5)$$

On the right side of equation(IV-5), there is a fourth, statistical moment involving v and y . Neither of these variables is strictly Gaussian, but using the technique of Gaussian closure, the fourth moment will be evaluated using equation(IV-1).

$$E[d_i(t)y_\epsilon(t+\tau)] = \frac{C_d \rho D \sigma_v}{\sqrt{2\pi}} \left\{ E[v_i(t)y_\epsilon(t+\tau)] + \frac{1}{3\sigma_v^2} \left\{ E[v_i(t)y_\epsilon(t+\tau)]E[v_j(t)v_j(t)] + 2E[v_i(t)v_j(t)]E[v_j(t)y_\epsilon(t+\tau)] \right\} \right\} \quad (IV-6)$$

$$R d_i y_\epsilon(\tau) = \frac{C_d \rho D \sigma_v}{\sqrt{2\pi}} \left\{ R v_i y_\epsilon(\tau) + \frac{1}{3\sigma_v^2} \left\{ R v_i y_\epsilon(\tau) \sigma_v^2 + 2 R v_i v_j(0) R v_j y_\epsilon(\tau) \right\} \right\} \quad (IV-7)$$

$$R d_i y_\epsilon(\tau) = \left\{ \frac{2 C_d \rho D \sigma_v}{3\sqrt{2\pi}} 2\delta_{ij} + \frac{R v_i v_j(0)}{\sigma_v^2} \right\} R v_j y_\epsilon(\tau) \quad (IV-8)$$

Again, equation (IV-8) may be Fourier transformed to put it in terms of cross-spectra.

$$S_{d_i y_\epsilon}(\omega) = \frac{2C_d \rho D \sigma_v}{3\sqrt{2\pi}} \left\{ 2\delta_{ij} + \frac{Rv_i v_j(0)}{\sigma_v^2} \right\} S_{v_j y_\epsilon}(\omega) \quad (IV-9)$$

Continuing along in the same vein, the cross-spectrum between v and y can be expanded by multiplying equation (III-3) by $y_\epsilon(t+\tau)$ and taking expected values.

$$E[v_j(t)y_\epsilon(t+\tau)] = (\delta_{jk} - A_j A_k) E[(u_k(t) - M_{kB} \dot{y}_\beta(t)) y_\epsilon(t+\tau)] \quad (IV-10)$$

$$Rv_j y_\epsilon(\tau) = (\delta_{jk} - A_j A_k) (Ru_k y_\epsilon(\tau) - M_{kB} R \dot{y}_\beta y_\epsilon(\tau)) \quad (IV-11)$$

$$Sv_j y_\epsilon(\omega) = (\delta_{jk} - A_j A_k) (Su_k y_\epsilon(\omega) - i\omega M_{kB} S y_\beta y_\epsilon(\omega)) \quad (IV-12)$$

Equations (IV-4), (IV-9), and (IV-12) can be combined, rearranged and simplified. Definition of two auxiliary constants allows for a more compact expression of the final equation.

$$(-\omega^2 \delta_{\alpha\beta} - i\omega(C_{\alpha\beta} + E_{\alpha\beta}) + W_{\alpha\beta}) S y_\beta y_\epsilon(\omega) = S p_{\alpha\epsilon} y_\epsilon(\omega) + \int_L B_{\alpha k} S u_k y_\epsilon(\omega) dL \quad (IV-13)$$

$$B_{\alpha k} = \frac{2M_{i\alpha} C_d \rho D \sigma_v}{3\sqrt{2\pi}} \left(2\delta_{ij} + \frac{Rv_i v_j(0)}{\sigma_v^2} \right) (\delta_{jk} - A_j A_k) \quad (IV-14)$$

$$E_{\alpha\beta} = \int_L B_{\alpha k} M_{kB} dL \quad (IV-15)$$

The constant $B_{\alpha k}$ contains statistics on the relative velocity, v . As such, $B_{\alpha k}$ cannot be known exactly until after the motion prediction problem has been solved, as the relative velocity is a function of the local, structural velocity as well as the incident fluid velocity. However, it is possible to evaluate $B_{\alpha k}$ assuming that the structural velocity is zero, solve the problem and thus iteratively improve $B_{\alpha k}$. Note in the previous equations that $B_{\alpha k}$, $M_{i\alpha}$, C_d , D , σ_v , $Rv_i v_j(0)$ and A_j are all functions of position, L , although the dependence is not explicitly written in these equations. Note also that the only approximation involved in deriving equation (IV-13) from the mathematical model was that a fourth, statistical moment was decomposed using equation (IV-1) even though the random processes involved were not strictly Gaussian.

Included in equation (IV-14) are references to second moment statistics of the relative velocity, v . Using the same method as has already been employed, a relationship can be derived between the relative velocity spectra and the fluid velocity and modal displacement spectra.

$$\begin{aligned}
 Sv_i v_j(\omega) = & \\
 (\delta_{ik} - A_i A_k)(\delta_{jl} - A_j A_l) \{ & Su_k u_l(\omega) + \omega^2 M_{k\beta} M_{l\epsilon} Sy_\beta y_\epsilon(\omega) + \\
 & + i\omega M_{k\beta} Sy_\beta u_l(\omega) - i\omega M_{l\epsilon} Su_k y_\epsilon(\omega) \} \quad (IV-16)
 \end{aligned}$$

$$\begin{aligned}
 (-\omega^2 \delta_{\alpha\beta} - i\omega(C_{\alpha\beta} + E_{\alpha\beta}) + W_{\alpha\beta}) Sy_\beta u_l(\omega) = & \\
 Sp_\alpha u_l(\omega) + \int_L B_{\alpha k} Su_k u_l(\omega) dL \quad (IV-17)
 \end{aligned}$$

Once the relative velocity spectra have been computed, calculation of the required statistics is simple.

$$Rv_i v_j(\tau) = \mathcal{F}^{-1}(Sv_i v_j(\omega)) \quad (IV-18)$$

$$\sigma_v^2 = Rv_i v_i(0) \quad (IV-19)$$

The next part of the analysis requires the multiplication of equation (III-2), not by a single term expressed at time $t + \tau$, but by itself at time $t + \tau$. Thus, the left side of equation (III-2) is multiplied by the left side of the same equation at a different time, and similarly with the right side of the equation. Different subscripts are used for the time-lagged version of the equation than for the original equation to keep clear over which terms summation is implied.

$$\begin{aligned} & E \left[\left(\delta_{\alpha\beta} \ddot{y}_\beta(t) + C_{\alpha\beta} \dot{y}_\beta(t) + W_{\alpha\beta} y_\beta(t) \right) \left(\delta_{\gamma\epsilon} \ddot{y}_\epsilon(t+\tau) + C_{\gamma\epsilon} \dot{y}_\epsilon(t+\tau) + W_{\gamma\epsilon} y_\epsilon(t+\tau) \right) \right] = \\ & = E \left[\left(p_\alpha(t) + \int_{L_1} M_{i\alpha} d_i(t) dL_1 \right) \left(p_\gamma(t+\tau) + \int_{L_2} M_{j\gamma} d_j(t+\tau) dL_2 \right) \right] \quad (IV-20) \end{aligned}$$

This equation can be expanded and the expectation operator applied to each term individually.

(see next page)

$$\begin{aligned}
 & \delta_{\alpha\beta} \delta_{\gamma\epsilon} E[\ddot{y}_\beta(t) \ddot{y}_\epsilon(t+\tau)] + \delta_{\alpha\beta} C_{\gamma\epsilon} E[\ddot{y}_\beta(t) \dot{y}_\epsilon(t+\tau)] + \delta_{\alpha\beta} W_{\gamma\epsilon} E[\ddot{y}_\beta(t) y_\epsilon(t+\tau)] + \\
 & + C_{\alpha\beta} \delta_{\gamma\epsilon} E[\dot{y}_\beta(t) \ddot{y}_\epsilon(t+\tau)] + C_{\alpha\beta} C_{\gamma\epsilon} E[\dot{y}_\beta(t) \dot{y}_\epsilon(t+\tau)] + C_{\alpha\beta} W_{\gamma\epsilon} E[\dot{y}_\beta(t) y_\epsilon(t+\tau)] + \\
 & + W_{\alpha\beta} \delta_{\gamma\epsilon} E[y_\beta(t) \ddot{y}_\epsilon(t+\tau)] + W_{\alpha\beta} C_{\gamma\epsilon} E[y_\beta(t) \dot{y}_\epsilon(t+\tau)] + W_{\alpha\beta} W_{\gamma\epsilon} E[y_\beta(t) y_\epsilon(t+\tau)] = \\
 & = E[p_\alpha(t) p_\gamma(t+\tau)] + \int_{L_1} M_{i\alpha} E[d_i(t) p_\gamma(t+\tau)] dL_1 + \\
 & + \int_{L_2} M_{j\gamma} E[p_\alpha(t) d_j(t+\tau)] dL_2 + \int_{L_1} M_{i\alpha} M_{j\gamma} E[d_i(t) d_j(t+\tau)] dL_1 dL_2 \quad (IV-21)
 \end{aligned}$$

Equation (IV-21) may be expressed in terms of correlation functions and then Fourier transformed, with spectra involving derivatives of modal displacement related to spectra involving modal displacements.

$$\begin{aligned}
 & \left\{ \begin{aligned}
 & \omega^4 \delta_{\alpha\beta} \delta_{\gamma\epsilon} - i\omega^3 \delta_{\alpha\beta} C_{\gamma\epsilon} - \omega^2 \delta_{\alpha\beta} W_{\gamma\epsilon} + \\
 & + i\omega^3 C_{\alpha\beta} \delta_{\gamma\epsilon} + \omega^2 C_{\alpha\beta} C_{\gamma\epsilon} - i\omega C_{\alpha\beta} W_{\gamma\epsilon} + \\
 & - \omega^2 W_{\alpha\beta} \delta_{\gamma\epsilon} + i\omega W_{\alpha\beta} C_{\gamma\epsilon} + W_{\alpha\beta} W_{\gamma\epsilon}
 \end{aligned} \right\} S y_\beta y_\epsilon(\omega) = \\
 & = S p_\alpha p_\gamma(\omega) + \int_L M_{i\alpha} S d_i p_\gamma(\omega) dL + \int_L M_{j\gamma} S p_\alpha d_j(\omega) dL + \\
 & + \int_{L_1} \int_{L_2} M_{i\alpha} M_{j\gamma} S d_i d_j(\omega) dL_1 dL_2 \quad (IV-22)
 \end{aligned}$$

Equation (IV-22) contains two spectral quantities which mix input and output variables, $S d_i d_j(\omega)$ and $S d_i p_\gamma(\omega)$. In order to express

$Sd_i p_Y(\omega)$ in terms of separate input and output spectra, multiply equation (II-4) by $p_Y(t+\tau)$ and take expected values.

$$E[d_i(t)p_Y(t+\tau)] = \frac{C_d \rho D \sigma_v}{\sqrt{2\pi}} E \left[v_i(t) \left(1 + \frac{v_j(t)v_j(t)}{3\sigma_v^2} \right) p_Y(t+\tau) \right] \quad (IV-23)$$

The right side of equation (IV-23) may be expanded, approximately, by replacing the fourth statistical moment by second moments, using equation (IV-1). As before, the substitution is not exact as one of the processes is not strictly Gaussian.

$$E[d_i(t)p_Y(t+\tau)] = \frac{C_d \rho D \sigma_v}{\sqrt{2\pi}} \left\{ E[v_i(t)p_Y(t+\tau)] + \frac{1}{3\sigma_v^2} \left\{ E[v_i(t)p_Y(t+\tau)]E[v_j(t)v_j(t)] + 2E[v_i(t)v_j(t)]E[v_j(t)p_Y(t+\tau)] \right\} \right\} \quad (IV-24)$$

As before, equation (IV-24) may be simplified and Fourier transformed so as to relate cross-spectral functions.

$$Sd_i p_Y(\omega) = \frac{2C_d \rho D \sigma_v}{3\sqrt{2\pi}} \left(2\delta_{ij} + \frac{Rv_i v_j(0)}{\sigma_v^2} \right) Sv_j p_Y(\omega) \quad (IV-25)$$

The spectral quantity on the right side of equation (IV-25), $Sv_j p_Y(\omega)$, is still a mixture of input and output variables. However, this cross-spectrum can be split by multiplying equation (III-3) by $p_Y(t+\tau)$ and taking expected values.

$$E[v_j(t)p_Y(t+\tau)] = (\delta_{jk} - A_j A_k) E[(u_k(t) - M_{k\beta} \dot{y}_\beta(t))p_Y(t+\tau)] \quad (IV-26)$$

$$Sv_j p_\gamma(\omega) = (\delta_{jk} - A_j A_k)(Su_k p_\gamma(\omega) + i\omega M_{k\beta} Sy_\beta p_\gamma(\omega)) \quad (IV-27)$$

Equations (IV-25) and (IV-27) can be combined and simplified by recalling the constants defined in equations (IV-14) and (IV-15).

$$\int_L M_{i\alpha} Sd_i p_\gamma(\omega) dL = \int_L B_{\alpha k} Su_k p_\gamma(\omega) dL + i\omega E_{\alpha\beta} Sy_\beta p_\gamma(\omega) \quad (IV-28)$$

The term in equation (IV-22) involving $Sp_\alpha d_j(\omega)$ can also be simplified by noting that this cross-spectrum is the complex conjugate of $Sd_i p_\gamma(\omega)$ with different letters used as subscripts. Thus the simplified form of this term in equation (IV-22) can be written down by inspection of equation (IV-28).

$$\int_L M_{j\gamma} Sp_\alpha d_j(\omega) dL = \int_L B_{\gamma\ell} Sp_\alpha u_\ell(\omega) dL - i\omega E_{\gamma\epsilon} Sp_\alpha y_\epsilon(\omega) \quad (IV-29)$$

Equations (IV-28) and (IV-29) will be substituted into equation (IV-22) shortly. However, first it is necessary to deal with the remaining mixed input and output cross-spectrum in equation (IV-22), $Sd_i d_j(\omega)$. For this purpose, multiply the left side of equation (II-4) by a time-lagged version of itself and similarly for the right side, and take expected values.

$$E[d_i(t)d_j(t+\tau)] = \frac{C_d \rho D \sigma_v}{\sqrt{2\pi}} \cdot \frac{C_d \rho D \sigma_v}{\sqrt{2\pi}} E \left[v_i(t) \left(1 + \frac{v_k(t)v_k(t)}{3\sigma_v^2} \right) \cdot v_j(t+\tau) \left(1 + \frac{v_\ell(t+\tau)v_\ell(t+\tau)}{3\sigma_v^2} \right) \right] \quad (IV-30)$$

Equation (IV-30) contains not only two, fourth statistical moments, but also one, sixth moment. As before, equation (IV-1) may be used, approximately, to evaluate the fourth moments and an equivalent relationship may be used to evaluate the sixth moment.

$$E[d_i(t)d_j(t+\tau)] = \frac{C_d \rho D \sigma_v}{2} \frac{C_d \rho D \sigma_v}{2} \cdot$$

$$\left\{ \begin{aligned} & E[v_i(t)v_j(t+\tau)] + \\ & + \frac{1}{3\sigma_v^2} \left\{ \begin{aligned} & E[v_i(t)v_j(t+\tau)]E[v_k(t)v_k(t)] + \\ & + 2E[v_i(t)v_k(t)]E[v_k(t)v_j(t+\tau)] \end{aligned} \right\} \\ & + \frac{1}{3\sigma_v^2} \left\{ \begin{aligned} & E[v_i(t)v_j(t+\tau)]E[v_\ell(t+\tau)v_\ell(t+\tau)] + \\ & + 2E[v_i(t)v_\ell(t+\tau)]E[v_j(t+\tau)v_\ell(t+\tau)] \end{aligned} \right\} \\ & + \frac{1}{9\sigma_v^2 \sigma_v^2} \left\{ \begin{aligned} & E[v_i(t)v_j(t+\tau)]E[v_k(t)v_k(t)]E[v_\ell(t+\tau)v_\ell(t+\tau)] + \\ & + 2E[v_i(t)v_\ell(t+\tau)]E[v_k(t)v_k(t)]E[v_j(t+\tau)v_\ell(t+\tau)] + \\ & + 2E[v_i(t)v_k(t)]E[v_k(t)v_j(t+\tau)]E[v_\ell(t+\tau)v_\ell(t+\tau)] + \\ & + 4E[v_i(t)v_k(t)]E[v_k(t)v_\ell(t+\tau)]E[v_j(t+\tau)v_\ell(t+\tau)] + \\ & + 2E[v_i(t)v_j(t+\tau)]E[v_k(t)v_\ell(t+\tau)]E[v_k(t)v_\ell(t+\tau)] + \\ & + 4E[v_i(t)v_\ell(t+\tau)]E[v_k(t)v_j(t+\tau)]E[v_k(t)v_\ell(t+\tau)] \end{aligned} \right\} \end{aligned} \right\}$$

(IV-31)

The expected values in equation (IV-31) can be replaced by correlation functions and various terms can be grouped together.

$$Rd_i d_j(\tau) = \frac{C_{d\rho D\sigma_v}}{\sqrt{2\pi}} \frac{C_{d\rho D\sigma_v}}{\sqrt{2\pi}} \cdot \left\{ \left(\frac{16}{9} \delta_{ik} \delta_{jl} + \frac{8}{9} \delta_{ik} \frac{Rv_{j\ell} v_{\ell}(0)}{\sigma_v^2} + \frac{8}{9} \delta_{jl} \frac{Rv_{ik} v_k(0)}{\sigma_v^2} + \frac{4}{9} \frac{Rv_{ik} v_k(0)}{\sigma_v^2} \right) \frac{Rv_{j\ell} v_{\ell}(0)}{\sigma_v^2} Rv_{k\ell} v_{\ell}(\tau) \right. \\ \left. + \frac{2Rv_{ij} v_j(\tau) Rv_{k\ell} v_{\ell}(\tau) Rv_{k\ell} v_{\ell}(\tau) + 4Rv_{i\ell} v_{\ell}(\tau) Rv_{kj} v_j(\tau) Rv_{k\ell} v_{\ell}(\tau)}{9\sigma_v^2 \sigma_v^2} \right\} \quad (IV-32)$$

The above equation can be Fourier transformed and further simplified.

$$Sd_i d_j(\omega) = \frac{2C_{d\rho D\sigma_v}}{3\sqrt{2\pi}} \left(2\delta_{ik} + \frac{Rv_{ik} v_k(0)}{\sigma_v^2} \right) \frac{2C_{d\rho D\sigma_v}}{3\sqrt{2\pi}} \left(2\delta_{jl} + \frac{Rv_{j\ell} v_{\ell}(0)}{\sigma} \right) Sv_{k\ell} v_{\ell}(\omega) + S_{Z_{ij}}(\omega) \quad (IV-33)$$

$$S_{Z_{ij}}(\omega) = \frac{C_{d\rho D} C_{d\rho D}}{18\pi\sigma_v\sigma_v} \cdot \mathcal{F} \left\{ 2Rv_{ij} v_j(\tau) Rv_{k\ell} v_{\ell}(\tau) Rv_{k\ell} v_{\ell}(\tau) + 4Rv_{i\ell} v_{\ell}(\tau) Rv_{kj} v_j(\tau) Rv_{k\ell} v_{\ell}(\tau) \right\} \quad (IV-34)$$

The spectral function, $S_{Z_{ij}}(\omega)$, as defined by equation (IV-34), is a mixture of input and output quantities which cannot be further simplified. However, it should be noted that for a typical offshore platform, the relative velocity is dominated by the water velocity, so that a good first guess at $S_{Z_{ij}}(\omega)$ can be made by assuming that the

structural velocity is zero. The estimate of the spectrum can be improved iteratively. Also, the level of the spectrum, $S_{zij}(\omega)$, is only on the order of one-sixth of the level of the other term in equation (IV-33).

The spectral function, $Sv_k v_\ell(\omega)$, can be decomposed by multiplying equation (III-3) by a time-lagged version of itself, as was done previously for $Sd_i d_j(\omega)$.

$$E[v_k(t)v_\ell(t+\tau)] = (\delta_{km} - A_k A_m)(\delta_{\ell n} - A_\ell A_n) \cdot E[(u_m(t) - M_{m\beta} \dot{y}_\beta(t))(u_n(t+\tau) - M_{n\epsilon} \dot{y}_\epsilon(t+\tau))] \quad (IV-35)$$

$$Rv_k v_\ell(\tau) = (\delta_{km} - A_k A_m)(\delta_{\ell n} - A_\ell A_n) \left\{ Ru_m u_n(\tau) - M_{n\epsilon} Ru_m \dot{y}_\epsilon(\tau) + M_{m\beta} R\dot{y}_\beta u_n(\tau) + M_{m\beta} M_{n\epsilon} R\dot{y}_\beta \dot{y}_\epsilon(\tau) \right\} \quad (IV-36)$$

$$Sv_k v_\ell(\omega) = (\delta_{km} - A_k A_m)(\delta_{\ell n} - A_\ell A_n) \left\{ Su_m u_n(\omega) - i\omega M_{n\epsilon} Su_m y_\epsilon(\omega) + i\omega M_{m\beta} Sy_\beta u_n(\omega) + \omega^2 M_{m\beta} M_{n\epsilon} Sy_\beta y_\epsilon(\omega) \right\} \quad (IV-37)$$

Equations (IV-33) and (IV-37) may now be combined, written in a form suitable for substitution in equation (IV-22) and simplified by recalling the constants defined by equations (IV-14) and (IV-15).

$$\int_{L_1} \int_{L_2} M_{i\alpha} M_{j\gamma} Sd_i d_j(\omega) dL_1 dL_2 = \int_{L_1} \int_{L_2} B_{\alpha m} B_{\gamma n} Su_m u_n(\omega) dL_1 dL_2 + i\omega E_{\gamma\epsilon} \int_L B_{\alpha m} Su_m y_\epsilon(\omega) dL + i\omega E_{\alpha\beta} \int_L B_{\gamma n} Sy_\beta u_n(\omega) dL + \omega^2 E_{\alpha\beta} E_{\gamma\epsilon} Sy_\beta y_\epsilon(\omega) + \int_{L_1} \int_{L_2} M_{i\alpha} M_{j\gamma} S_{zij}(\omega) dL_1 dL_2 \quad (IV-38)$$

Equations (IV-28), (IV-29) and (IV-38) may now be used to replace the appropriate terms on the right side of equation (IV-22).

$$\begin{aligned}
 & (-\omega^2 \delta_{\alpha\beta} - i\omega C_{\alpha\beta} + W_{\alpha\beta})(-\omega^2 \delta_{\gamma\epsilon} + i\omega C_{\gamma\epsilon} + W_{\gamma\epsilon}) S_{y_{\beta} y_{\epsilon}}(\omega) = \\
 & = S_{p_{\alpha} p_{\gamma}}(\omega) + \int_L B_{\gamma\ell} S_{p_{\alpha} u_{\ell}}(\omega) dL - i\omega E_{\gamma\epsilon} S_{p_{\alpha} y_{\epsilon}}(\omega) + \\
 & + \int_L B_{\alpha k} S_{u_k p_{\gamma}}(\omega) dL + i\omega E_{\alpha\beta} S_{y_{\beta} p_{\gamma}}(\omega) + \int_{L_1} \int_{L_2} B_{\alpha m} B_{\gamma n} S_{u_m u_n}(\omega) dL_1 dL_2 + \\
 & - i\omega E_{\gamma\epsilon} \int_L B_{\alpha m} S_{u_m y_{\epsilon}}(\omega) dL + i\omega E_{\alpha\beta} \int_L B_{\gamma n} S_{y_{\beta} u_n}(\omega) dL + \\
 & + \omega^2 E_{\alpha\beta} E_{\gamma\epsilon} S_{y_{\beta} y_{\epsilon}}(\omega) + \int_{L_1} \int_{L_2} M_{i\alpha} M_{j\gamma} S_{z_{ij}}(\omega) dL_1 dL_2 \quad (IV-39)
 \end{aligned}$$

Equation (IV-39) may be rearranged and some terms combined.

$$\begin{aligned}
 & (-\omega^2 \delta_{\alpha\beta} - i\omega C_{\alpha\beta} + W_{\alpha\beta})(-\omega^2 \delta_{\gamma\epsilon} + i\omega C_{\gamma\epsilon} + W_{\gamma\epsilon}) S_{y_{\beta} y_{\epsilon}}(\omega) = \\
 & S_{p_{\alpha} p_{\gamma}}(\omega) + \int_L B_{\gamma\ell} S_{p_{\alpha} u_{\ell}}(\omega) dL + \int_L B_{\alpha k} S_{u_k p_{\gamma}}(\omega) dL + \\
 & + \int_{L_1} \int_{L_2} B_{\alpha m} B_{\gamma n} S_{u_m u_n}(\omega) dL_1 dL_2 - i\omega E_{\gamma\epsilon} \left\{ S_{p_{\alpha} y_{\epsilon}}(\omega) + \int_L B_{\alpha m} S_{u_m y_{\epsilon}}(\omega) dL \right\} + \\
 & + i\omega E_{\alpha\beta} \left\{ S_{y_{\beta} p_{\gamma}}(\omega) + \int_L B_{\gamma n} S_{y_{\beta} u_n}(\omega) dL \right\} + \int_{L_1} \int_{L_2} M_{i\alpha} M_{j\gamma} S_{z_{ij}}(\omega) dL_1 dL_2 \\
 & \quad \quad \quad (IV-40)
 \end{aligned}$$

Equation (IV-40) may be further simplified by recalling the relationship expressed in equation (IV-13) and noting that it holds equally for its complex conjugate.

$$\begin{aligned}
 & (-\omega^2 \delta_{\alpha\beta} - i\omega C_{\alpha\beta} + W_{\alpha\beta})(-\omega^2 \delta_{\gamma\epsilon} + i\omega C_{\gamma\epsilon} + W_{\gamma\epsilon}) S_{\beta\gamma\epsilon}(\omega) = \\
 & Sp_{\alpha p_Y}(\omega) + \int_L B_{\gamma\ell} Sp_{\alpha u_\ell}(\omega) dL + \int_L B_{\alpha k} Su_{k p_Y}(\omega) dL + \\
 & + \int_{L_1} \int_{L_2} B_{\alpha m} B_{\gamma n} Su_{m n}(\omega) dL_1 dL_2 - i\omega E_{\gamma\epsilon} (-\omega^2 \delta_{\alpha\beta} - i\omega(C_{\alpha\beta} + E_{\alpha\beta}) + W_{\alpha\beta}) \cdot \\
 & \cdot S_{\beta\gamma\epsilon}(\omega) + i\omega E_{\alpha\beta} (-\omega^2 \delta_{\gamma\epsilon} + i\omega(C_{\gamma\epsilon} + E_{\gamma\epsilon}) + W_{\gamma\epsilon}) S_{\beta\gamma\epsilon}(\omega) + \\
 & + \int_{L_1} \int_{L_2} M_{i\alpha} M_{j\gamma} S_{zij}(\omega) dL_1 dL_2 \tag{IV-41}
 \end{aligned}$$

Finally, after rearranging and grouping terms, equation (IV-41) can be expressed in a rather simple form.

$$\begin{aligned}
 & (-\omega^2 \delta_{\alpha\beta} - i\omega(C_{\alpha\beta} + E_{\alpha\beta}) + W_{\alpha\beta})(-\omega^2 \delta_{\gamma\epsilon} + i\omega(C_{\gamma\epsilon} + E_{\gamma\epsilon}) + W_{\gamma\epsilon}) S_{\beta\gamma\epsilon}(\omega) = \\
 & Sp_{\alpha p_Y}(\omega) + \int_L B_{\gamma\ell} Sp_{\alpha u_\ell}(\omega) dL + \int_L B_{\alpha k} Su_{k p_Y}(\omega) dL + \\
 & + \int_{L_1} \int_{L_2} B_{\alpha m} B_{\gamma n} Su_{m n}(\omega) dL_1 dL_2 + \int_{L_1} \int_{L_2} M_{i\alpha} M_{j\gamma} S_{zij}(\omega) dL_1 dL_2 \tag{IV-42}
 \end{aligned}$$

Using equation (IV-42), we can predict, approximately, the modal response spectra of an offshore platform, given the spectra for the incident flow field. In equation (IV-42), the spectra involving the platform motion have been separated from the spectra involving the incident flow, except for $S_{zij}(\omega)$ which involves both through the relative velocity. Ignoring $S_{zij}(\omega)$ for the moment, equation (IV-42) also describes the relationship between input and response spectra for a much simpler model of the wave-structure interaction than was assumed in the derivation of equation (IV-42).

$$\delta_{\alpha\beta} \ddot{y}_{\beta}(t) + (C_{\alpha\beta} + E_{\alpha\beta}) \dot{y}_{\beta}(t) + W_{\alpha\beta} y_{\beta}(t) = p_{\alpha}(t) + \int_L B_{\alpha k} u_k(t) dL \quad (\text{IV-43})$$

Therefore, as far as the response spectra are concerned, inclusion of a separated flow drag term in the response model has the same effect as the inclusion of a drag force proportional to the local fluid velocity, an effective "hydrodynamic damping", $E_{\alpha\beta}$, and some additional excitation not accounted for by the linear drag term.

The goal of this research has been to predict the response of an arbitrary jacket platform to incident waves, with particular emphasis on the role of separated flow drag. To that end, a model by which to predict platform response was developed, using commonly employed equations to relate fluid kinematics, hydrodynamic forces and structural motions. This model included a non-linear, mixed input and output variables force to account for the separation of the flow from the structural members. The model was then analysed using the approximate technique of Gaussian closure, in order to predict the second-moment statistics of the platform motion.

The final relationship, as expressed in equation (IV-42), showed that the spectra of the platform motion, as predicted using the model developed in chapters II and III, are very similar to the spectra predicted by a much simpler, linear model. If the model used in this analysis is a reasonable reflection of nature over some range of sea states, then examination of the response spectra of a platform should indicate an additional excitation force over that predicted by potential-flow theory and significantly, an additional hydrodynamic damping term which

is sea state dependent. It should be noted that whereas equations (IV-42) and (IV-43) imply an additional hydrodynamic force linearly related to fluid velocity, no linearization of the drag term from Morison's equation has been performed.

As important to the research as the predictions of response spectra themselves, is an understanding of the conditions under which the predictions can be expected to be accurate. Therefore, the next two chapters are devoted to testing the predictions against data generated by numerical simultaneous and small scale experiments in a wave tank.

V. NUMERICAL SIMULATIONS

The derivation over the last three chapters of a predictor for displacement spectra of an offshore platform required that a number of assumptions and idealizations be made. The main assumptions and idealizations were: the manner by which the hydrodynamic force was modified from potential-flow theory to account for separation; the disregard of all other non-linear effects; the replacement of the Morison's equation drag term $v|v|$ by a term of the form $av + bv|v|^2$; and the assumption that the motion of the platform is a Gaussian process. Before considering an experiment to test the validity of all of these assumptions, it is worthwhile to examine the validity of the latter two assumptions separately. A good way to concentrate on these two assumptions is to compare the predicted response spectra of a simple hypothetical system to spectra estimated from sample time histories generated on a computer. The dynamic characteristics of such a hypothetical system can be made to exactly match the model assumed originally.

To perform the numerical simulations, data analysis and comparison with predictions, the following steps are necessary:

1. Describe the system, in this case a simple, spring-mounted, rigid cylinder. Set up the governing differential equations and perform a dimensional analysis to identify the important parameters.
2. Generate sample time histories of the random incident fluid particle velocities and accelerations.
3. Compute time histories of the cylinder's deflections due to

the incident fluid motion.

4. Estimate deflection spectra and half-power bandwidth damping estimates from the cylinder time histories.

5. Use the equations derived in the previous chapter to predict the same quantities and compare.

The hypothetical system to be considered is shown in Figure V-1. The structure consists of a circular cylinder of unit length, diameter D , and mass M . The cylinder's motion is restrained by a spring of stiffness K and a dashpot of resistance R . The one-dimensional, incident fluid velocity is a random process characterized by a root-mean-square velocity, σ_u , and a mean frequency, ω_u . As assumed in Chapter II, the hydrodynamic force acting on the cylinder consists of a potential flow term and a separated-flow drag term. With no free surface, the potential flow force is given by the inertial term in the relative-motion formulation of Morison's equation. Applying conservation of momentum to the structure and the hydrodynamic forces acting on it yields the governing differential equation.

$$M\ddot{y} + R\dot{y} + Ky = \frac{(1 + C_m)\rho\pi D^2}{4} \frac{du}{dt} - \frac{C_m\rho\pi D^2\ddot{y}}{4} + \frac{C_d\rho D}{2} (u-\dot{y})|u-\dot{y}| \quad (V-1)$$

Equation (V-1) can be put in a non-dimensional form by making the following substitutes:

$$m = \frac{C_m\rho\pi D^2}{4} \quad (V-2a)$$

$$\omega_n = \frac{K}{M + m} \quad (V-2b)$$

$$\zeta_s = \frac{R}{2\omega_n(M+m)} \quad (V-2c)$$

$$\gamma = \frac{m}{M+m} \quad (V-2d)$$

$$\tau = \omega_n t \quad (V-2e)$$

$$z = \frac{y}{D} \quad (V-2f)$$

$$w = \frac{u}{D\omega_n} \quad (V-2g)$$

$$\frac{d^2z}{d\tau^2} + 2\zeta_s \frac{dz}{d\tau} + z = \frac{(1+C_m)\gamma}{C_m} \frac{dw}{d\tau} + \frac{2C_d\gamma}{\pi C_m} \left(w - \frac{dz}{d\tau} \right) \left| w - \frac{dz}{d\tau} \right| \quad (V-3)$$

If the non-dimensional parameters ζ_s , C_m and C_d are assigned reasonable values for an offshore platform: 1%, 1.0 and 0.7 respectively, then the motion of this cylinder is governed by the mass ratio, γ , and the characteristics of the incident flow.

The non-dimensional incident flow velocity, w , and acceleration, $\frac{dw}{d\tau}$, are characterized by an rms velocity, $\frac{\sigma_u}{D\omega_n}$, and a mean frequency, $\frac{\omega_u}{\omega_n}$. Any number of different random processes could be constructed which have these two characteristics, so that it is necessary to choose a particular random process for the numerical simulations. The class of random processes which are the responses of single degree of freedom resonators to Gaussian white noise is a good choice for this application because realizations of a joint random process of both the

response function and its derivative can be simply generated on a computer. For this reason, the incident flow velocity was modelled as the response of an SDOF resonator to white noise, the fluid velocity corresponding to the displacement response of the resonator and the fluid acceleration corresponding to the derivative of the displacement response. All fluid velocity/acceleration realizations were generated with a resonator damping of 90% of critical damping as that value of damping yielded smooth, broad, force spectra. No attempt was made to match incident flow spectra to flow spectra associated with Pierson-Moskowitz or any other wave elevation spectra. Further, all realizations were generated with a non-dimensional mean frequency of 1.0, as it was felt that varying the frequency would not add appreciably to the understanding of the validity of the two assumptions being tested. The value, 1.0, was chosen so that both inertial and drag components of force would be appreciable for all tests.

Actual generation of velocity/acceleration time series were performed by successive application of equation (V-4).

$$\begin{Bmatrix} w \\ \frac{dw}{d\tau} \end{Bmatrix}_n = F \begin{Bmatrix} w \\ \frac{dw}{d\tau} \end{Bmatrix}_{n-1} + H \begin{Bmatrix} G_1 \\ G_2 \end{Bmatrix} \quad (V-4)$$

G_1 and G_2 were independent, zero-mean, unit-variance, Gaussian random variables. The matrices F and H were chosen so that the auto- and cross-correlation functions of the time series generated matched those of an SDOF resonator excited by white noise at lags $\tau = 0.0$ and $\tau = \Delta t$,

where Δt was the time increment between successive elements of the time series. Because the joint responses of a SDOF resonator excited by white noise and the time series generated by equation (V-4) both form Markov processes, matching auto- and cross-correlation functions at the two lags mentioned ensures that the correlation functions match at $\tau = m\Delta t$, where m is any integer. Also, both processes are Gaussian because they were generated by linear operations on Gaussian inputs. Therefore, the generated, velocity/acceleration, time series are indistinguishable from the joint response of a SDOF resonator excited by white noise and sampled at time increments of Δt .

Rather than generate a number of joint velocity/acceleration time series for different values of the non-dimensional rms velocity, σ_ω , one time series was generated with unity rms velocity. To estimate the response of the cylinder to an incident flow with some other rms velocity required only that the one time series be scaled appropriately. It should be noted that σ_ω is closely related to the Keulegan-Carpenter number for this problem, based on the rms incident flow velocity and the cylinder natural frequency.

$$N_{K-C} = 2\pi\sigma_\omega \quad (V-5)$$

To estimate the response of the cylinder to the incident flow time series, for any values of the rms velocity, σ_ω , and the mass ratio, γ , the Runge-Kutta method was applied to equation (V-3). The Runge-Kutta method requires that the governing differential equation be evaluated at half-interval points as well as at the ends of the intervals. There-

fore, the time intervals at which the cylinder displacements are calculated must be twice the interval, Δt , used in the incident flow generation.

Once a time series of the cylinder displacement has been computed, estimates of the underlying spectrum can be computed using one of a number of techniques. Since it is expected that the displacement spectrum should be sharply peaked at the cylinder's natural frequency, a good spectral estimation technique to use is the maximum entropy method. Besides being better at resolving peaks than either the Blackman-Tukey or averaged periodograms methods, Campbell [3] has developed a statistically efficient, damping estimator using the maximum entropy method. The damping estimator, which is based on the estimation of the half-power bandwidth from ambient motion records, not only provides an estimate of the damping, but also an approximate variance of the estimate.

Of course, the purpose of performing the numerical simulations and estimating the cylinder displacement spectra was to compare the estimates against the spectra predicted by the technique developed in the previous chapter. The significant equations from that chapter are equations (IV-14) to (IV-19), (IV-34) and (IV-42). The following prediction is based on the application of these equations to equation (V-3), the non-dimensional form of the governing differential equation for the motion of the cylinder.

$$|-\omega^2 - 2i\omega(\zeta_s + \zeta_h) + 1|^2 S_z(\omega) = \left(\frac{1 + C_m}{C_m} \gamma\right)^2 \omega^2 S_w(\omega) + B^2 S_w(\omega) + \frac{16}{3\pi^3 \sigma_v^2} \left(\frac{C_d}{C_m} \gamma\right)^2 \mathcal{F}\{R_v^3(\tau)\} \quad (V-6a)$$

$$B = 2 \left(\frac{2}{\pi}\right)^{3/2} \frac{C_d}{C_m} \gamma \sigma_v \quad (V-6b)$$

$$\zeta_h = \frac{B}{2} \quad (V-6c)$$

$$S_v(\omega) = S_w(\omega) + \omega^2 S_z(\omega) + 2\omega \text{Re}\{S_{zw}(\omega)\} \quad (V-6d)$$

$$(-\omega^2 - 2i\omega(\zeta_s + \zeta_h) + 1) S_{zw}(\omega) = \left\{ -i\omega \frac{(1 + C_m)}{C_m} \gamma + B \right\} S_w(\omega) \quad (V-6e)$$

$$R_v(\tau) = \mathcal{F}^{-1}\{S_v(\omega)\} \quad (V-6f)$$

$$\sigma_v = R_v(0) \quad (V-6g)$$

Numerical simulations were performed for three values of the mass ratio, γ , and five values of the rms fluid velocity, σ_w . In each test, the cylinder deflection was computed over approximately 2000 oscillations of the cylinder, with eight values of the displacement computed for each cycle. The results of the simulation tests are summarized over the next seven figures. Figures V-2, V-3, and V-4 are for the test with $\gamma = 0.079$ and $\sigma_w = 1.0$. Figure V-2 is a normalized histogram of the cylinder's deflections, with a Gaussian distribution of the same mean and variance overlaid. There appears to be no significant departure of the displacement histogram from a Gaussian distribution. Although this argument does not guarantee that the fluid and cylinder velocities form a joint, Gaussian process, it does indicate that the Gaussian closure assumption is reasonable. Figure V-3 shows estimated and predicted deflection spectra. The agreement between the

two spectra is excellent, with the discrepancy at low frequency probably due to the characteristics of the spectral estimator rather than a fault of the predictor. Figure V-4 shows the predicted relative contributions to the force spectrum on the right side of equation V-6a. The inertial force dominates the total force spectrum in this test, with the non-linear contribution, defined by equation (IV-34), being barely significant.

Figures V-5, V-6, and V-7 are for the most severe case tested, $\gamma = 0.079$ and $\sigma_w = 2.5$. Again, the normalized histogram appears to be Gaussian and the predicted and estimated spectra are in good agreement. However, in this test the predicted force spectrum is dominated by the separated-flow drag, although the non-linear component of the drag spectrum is still small.

Figure V-8 shows the comparison between predicted and estimated effective damping for all fifteen tests. The lines are the predicted effective damping ratio for the three different values of γ , as a function of rms velocity. The crosses represent the damping ratios estimated from the numerical simulation time histories, with 95% confidence intervals superimposed. Again, all predicted and estimated results agree within the statistical uncertainty of the estimator.

The range of Keulegan-Carpenter numbers and damping ratios covered by these tests was chosen to encompass the values of interest when predicting motions of offshore platforms for the purpose of fatigue damage calculations. Over this range, it would appear that the Gaussian closure assumption and the replacement of the term $v|v|$ by a term of the form

$av + bv|v|^2$ are valid approximations when predicting displacement spectra. Therefore, these tests are a good indication that the predictor developed is useful. The other main assumptions made during the course of developing the motion predictor concerned the form of hydrodynamic force model chosen. The purpose of the next chapter is to describe the results of a test designed to examine that area.

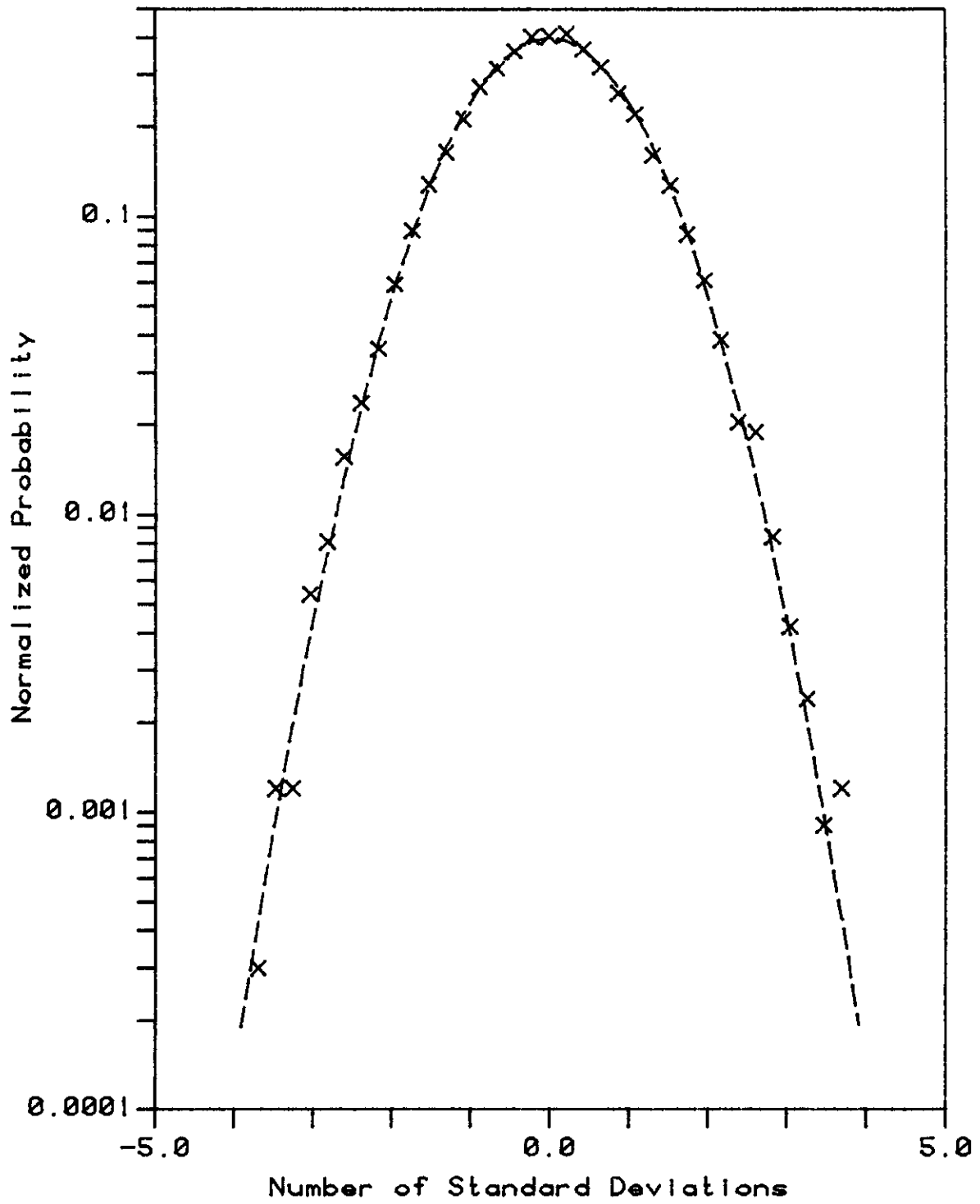


Fig V-2: Normalized Displacement Histogram ($\gamma=0.079, \sigma_W=1.0$)

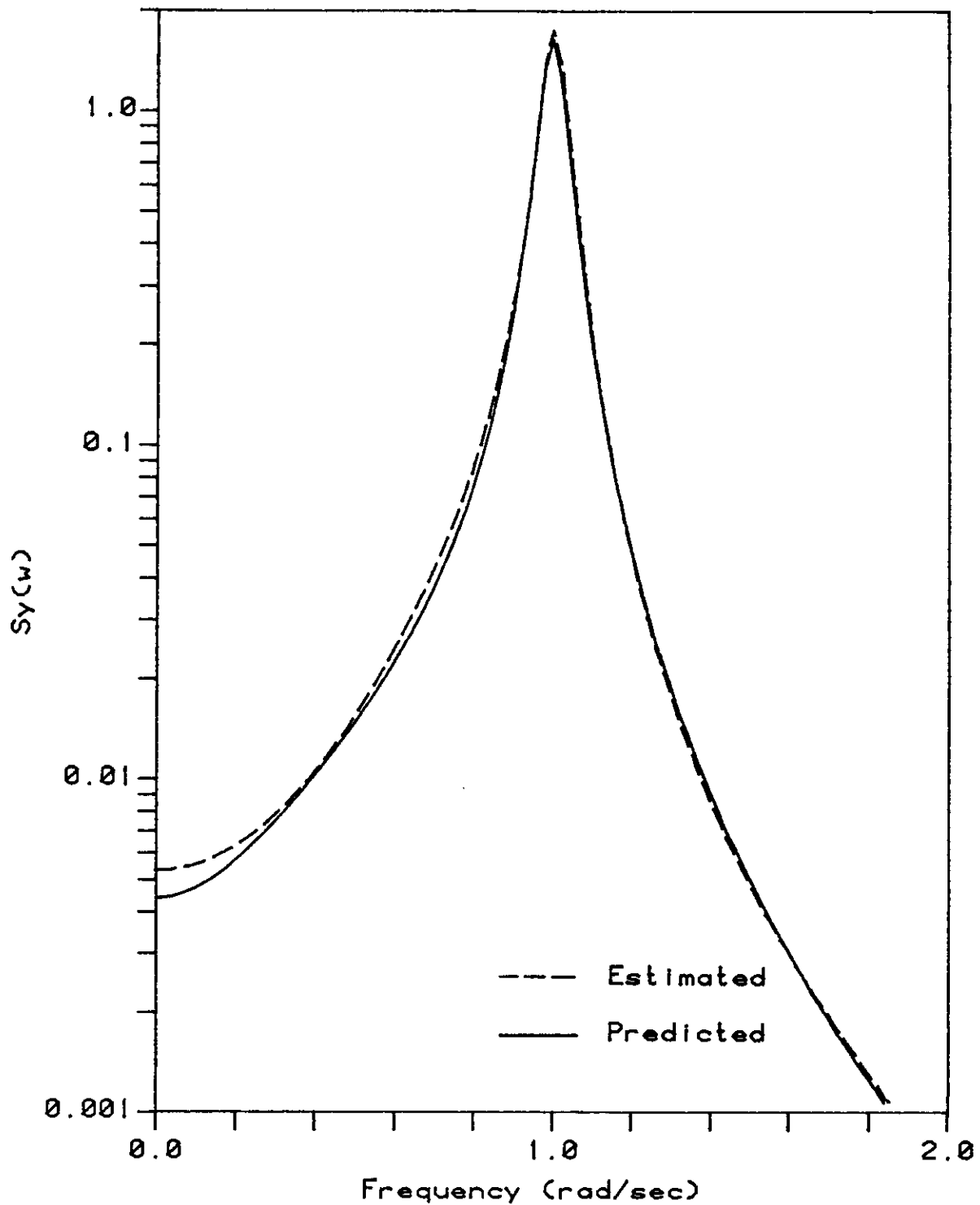


Fig V-3: Cylinder Deflection Spec.
($\gamma=0.079, \sigma_w=1.0$)

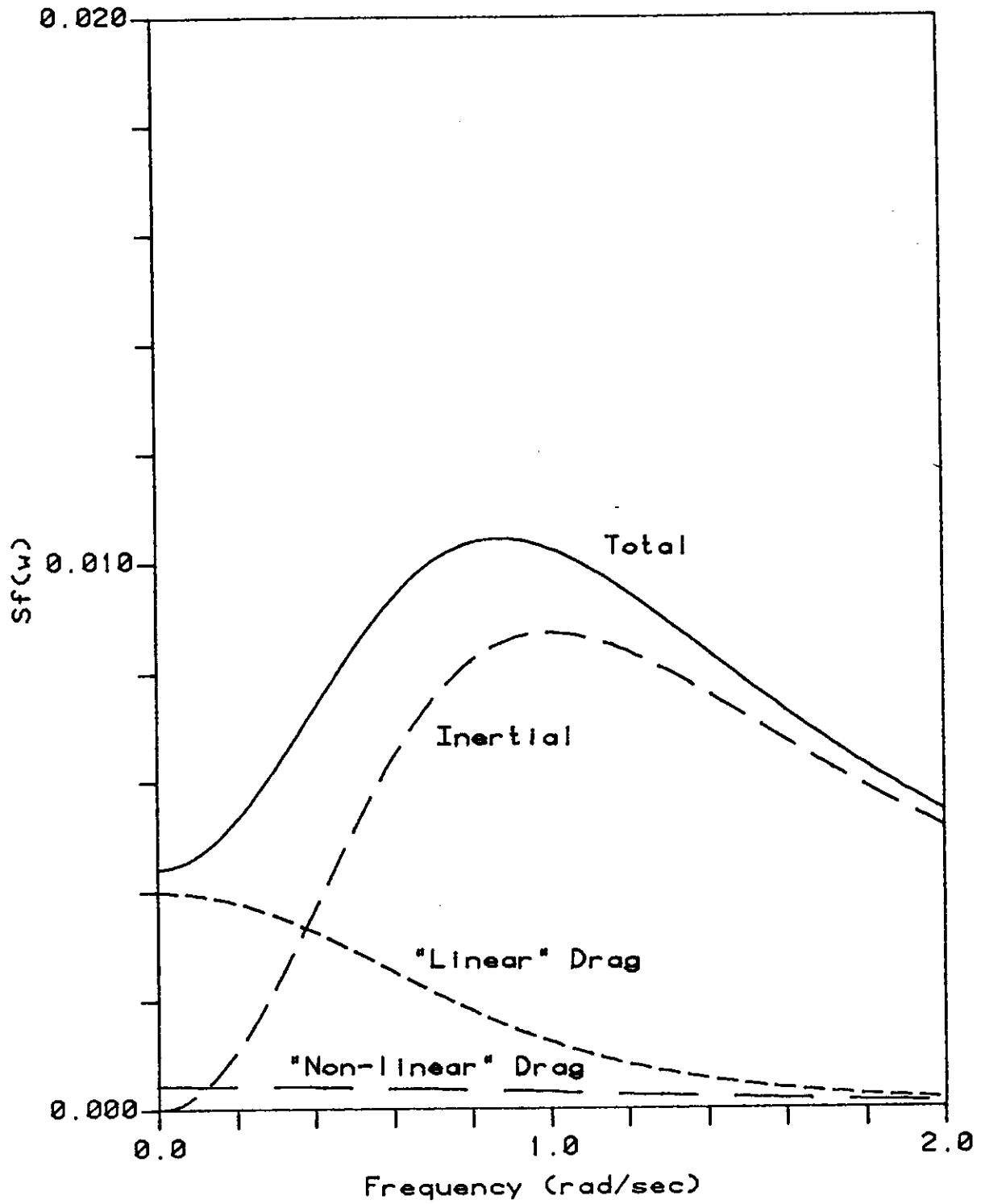


Fig V-4: Components of Hydro. Force
($\gamma=0.079, \sigma_W=1.0$)

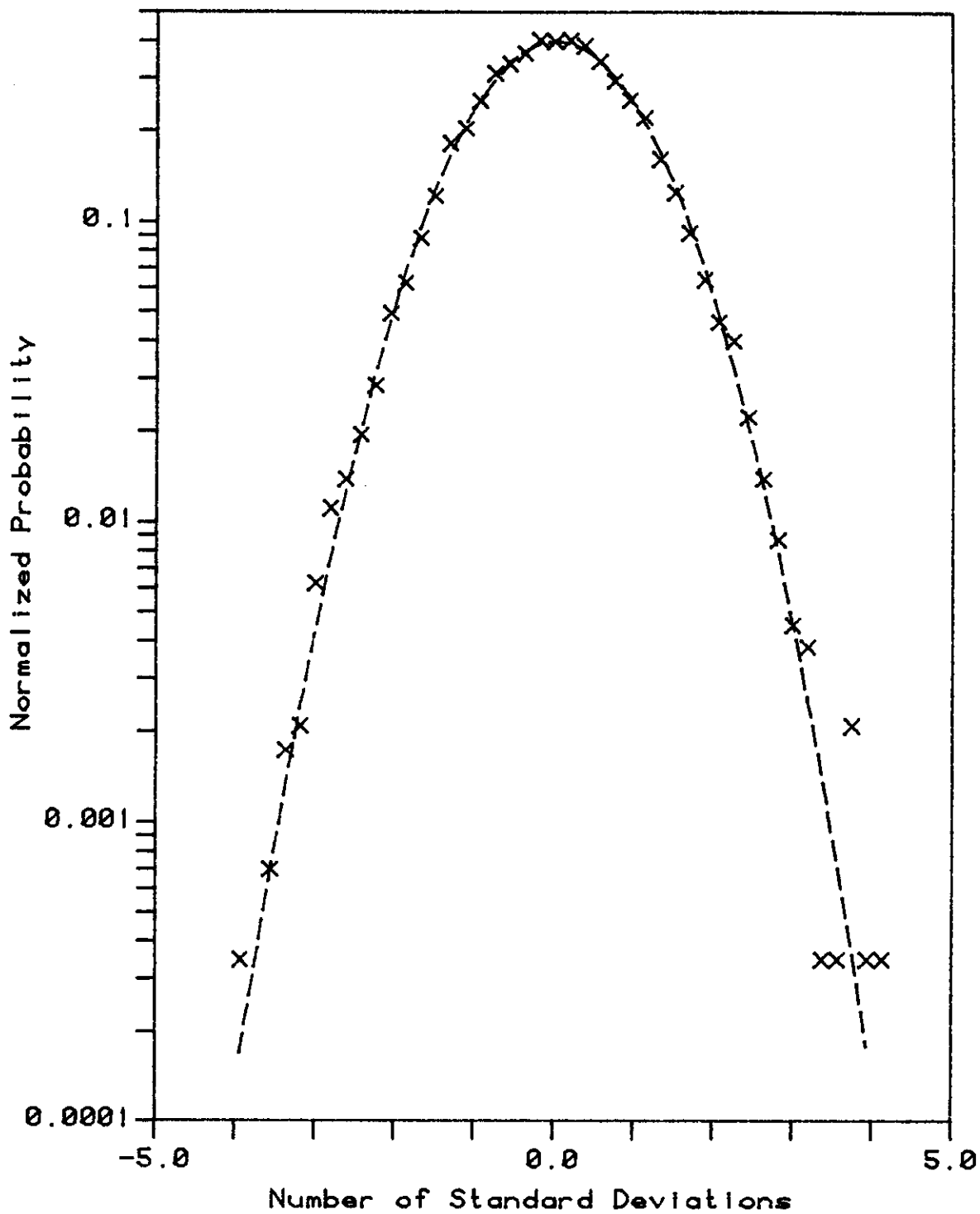


Fig V-5: Normalized Displacement Histogram ($\gamma=0.079, \sigma_w=2.5$)

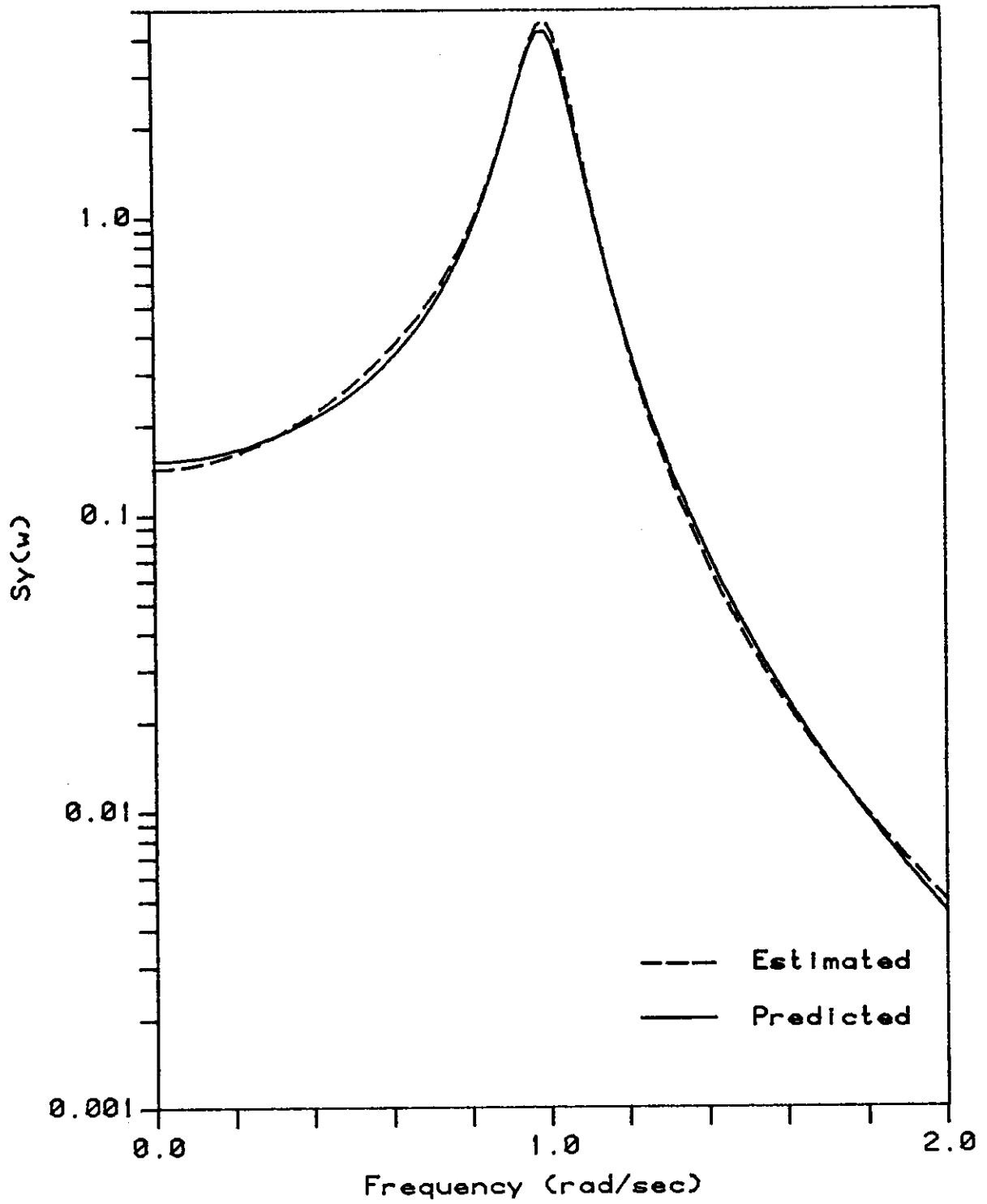


Fig V-6: Cylinder Deflection Spec.
($\gamma=0.079, \sigma_w=2.5$)

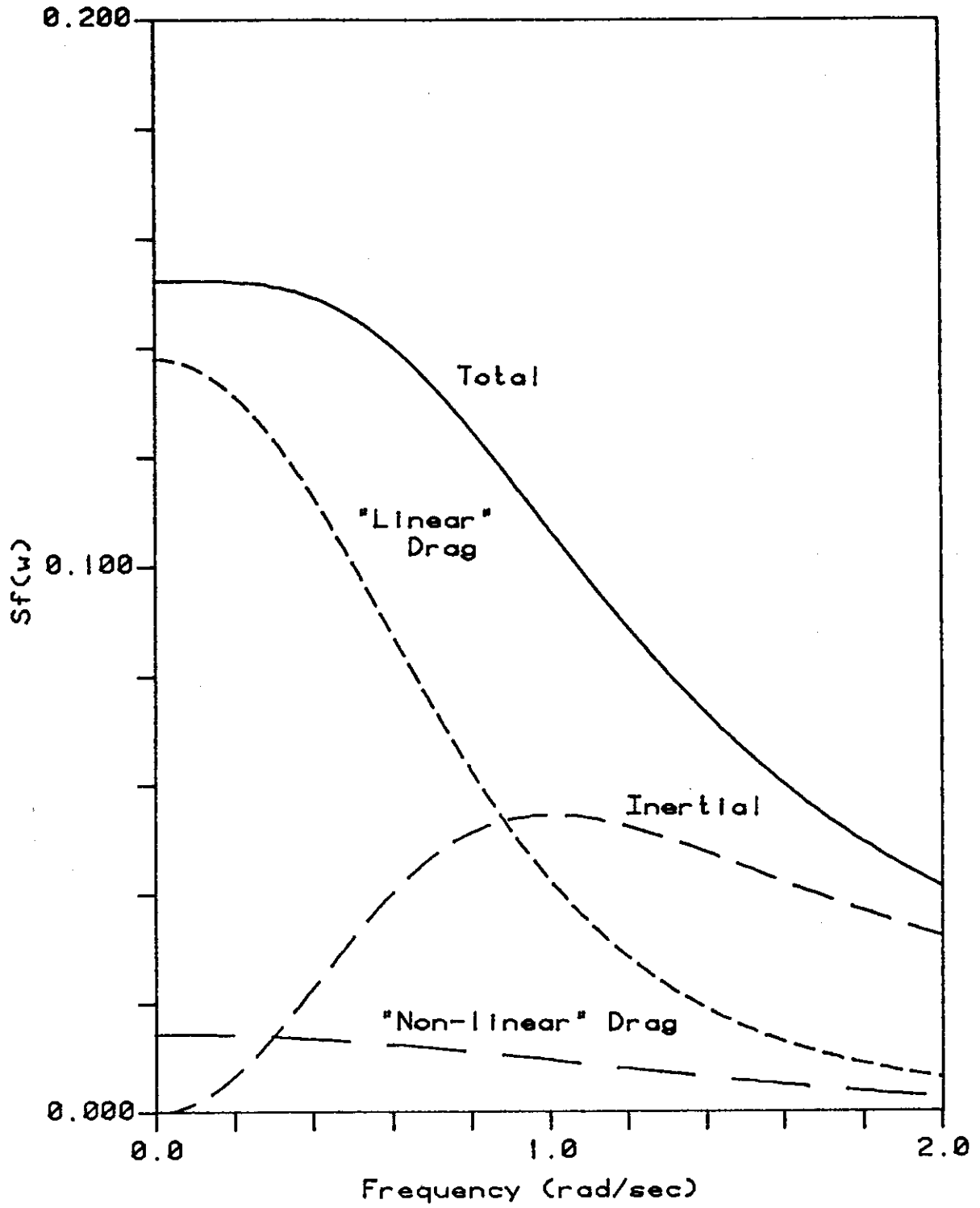


Fig V-7: Components of Hydro. Force
($\gamma=0.079, \sigma_w=2.5$).

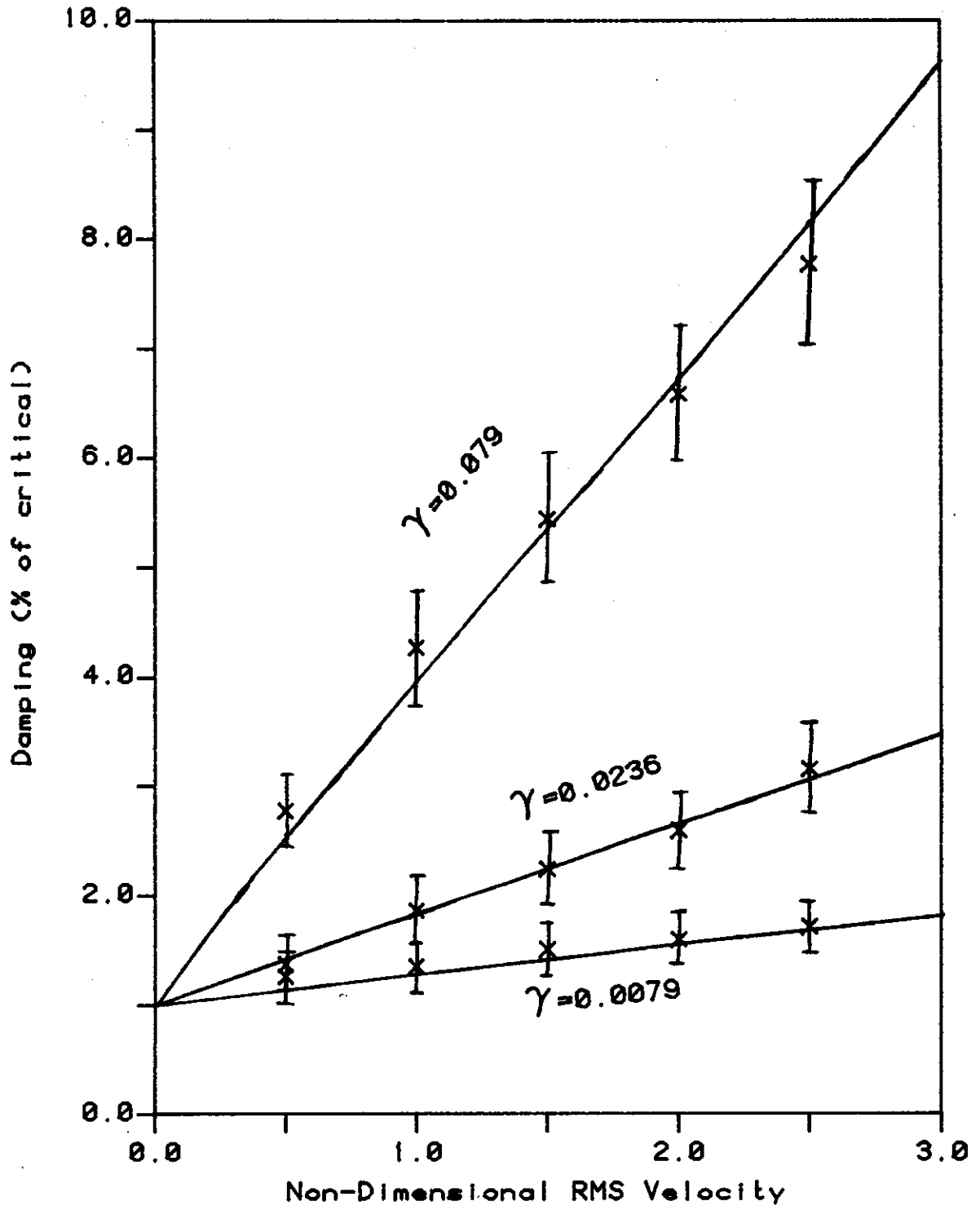


Fig V- 8: Effective Damping for Numerical Simulations

VI. A SMALL SCALE TEST

In chapters II and III, a model was developed to describe the instantaneous response of an offshore platform to the incident wave field. Using that model and the Gaussian closure technique, a relationship was derived for predicting the motion spectra of a platform given the incident flow field spectra. In the last chapter, predictions of deflection spectra were compared with spectra estimated from sample time histories for a simple, hypothetical system simulated on a computer. The agreement between predicted and estimated spectra demonstrated the suitability of the Gaussian closure technique and the replacement of the " $v|v|$ " term in Morison's equation by a term of the form " $av + bv^3$ ".

To test the overall ability to predict deflection spectra of a structure excited by random waves, a small scale test of a simple structure mounted in a wave tank was devised. Since the numerical simulations verified the applicability of the Gaussian closure technique, this experiment was mainly a test of the model for the instantaneous response, particularly the validity of employing the relative velocity form of the drag term of Morison's equation. For the experiment, a vertical, 0.025 m in diameter, surface-piercing cylinder with a wetted length of 0.52 m was suspended in a wave tank. The cylinder was free to oscillate in the direction of wave propagation, with a natural frequency within the band of the wave spectrum. The object of the test was to estimate displacement spectra from records of the motion of the cylinder in unidirectional random waves and compare those spectra to predicted spectra. For fatigue damage estimation, the most important aspect of the theory developed is

the prediction of an effective hydrodynamic damping which is sea-state dependent. Therefore, particular emphasis was placed on the comparison of estimated and predicted damping.

The experimental apparatus is shown in Figure VI-1. The apparatus was designed specifically to minimize structural damping, so that any hydrodynamic damping could be accurately measured. The shaft, which supported the surface-piercing cylinder, rode on air bearings. The leaf springs, made from pairs of hacksaw blades bolted together at the ends, not only acted as the system springs, but also provided torsional restraint to prevent rotation of the support shaft without introducing any rubbing contact. The displacement sensor, not shown in Figure VI-1, was a linear, variable, differential transformer (LVDT). The sensor was mounted so that the core, which moved with the cylinder, did not contact the coils, which were fixed to the support structure. As a result of these features, the structural damping was only from viscosity in the air bearings and hysteresis in the hacksaw blades.

Figure VI-2 is a logarithmic plot of the freely decaying oscillations of the cylinder in air. Approximately 150 cycles of motion are included in the graph, with the damping estimated at 0.10% of critical damping at an amplitude of motion of 5 mm. The natural frequency of oscillation in air was 9.525 rad/sec. The distinctive pattern observed in the plot resulted from the sampling frequency being almost exactly eight times the natural frequency of the cylinder. As a result, every eighth sample is taken at nearly the same phase in the cycle.

In addition to the oscillating cylinder, a second cylinder and a

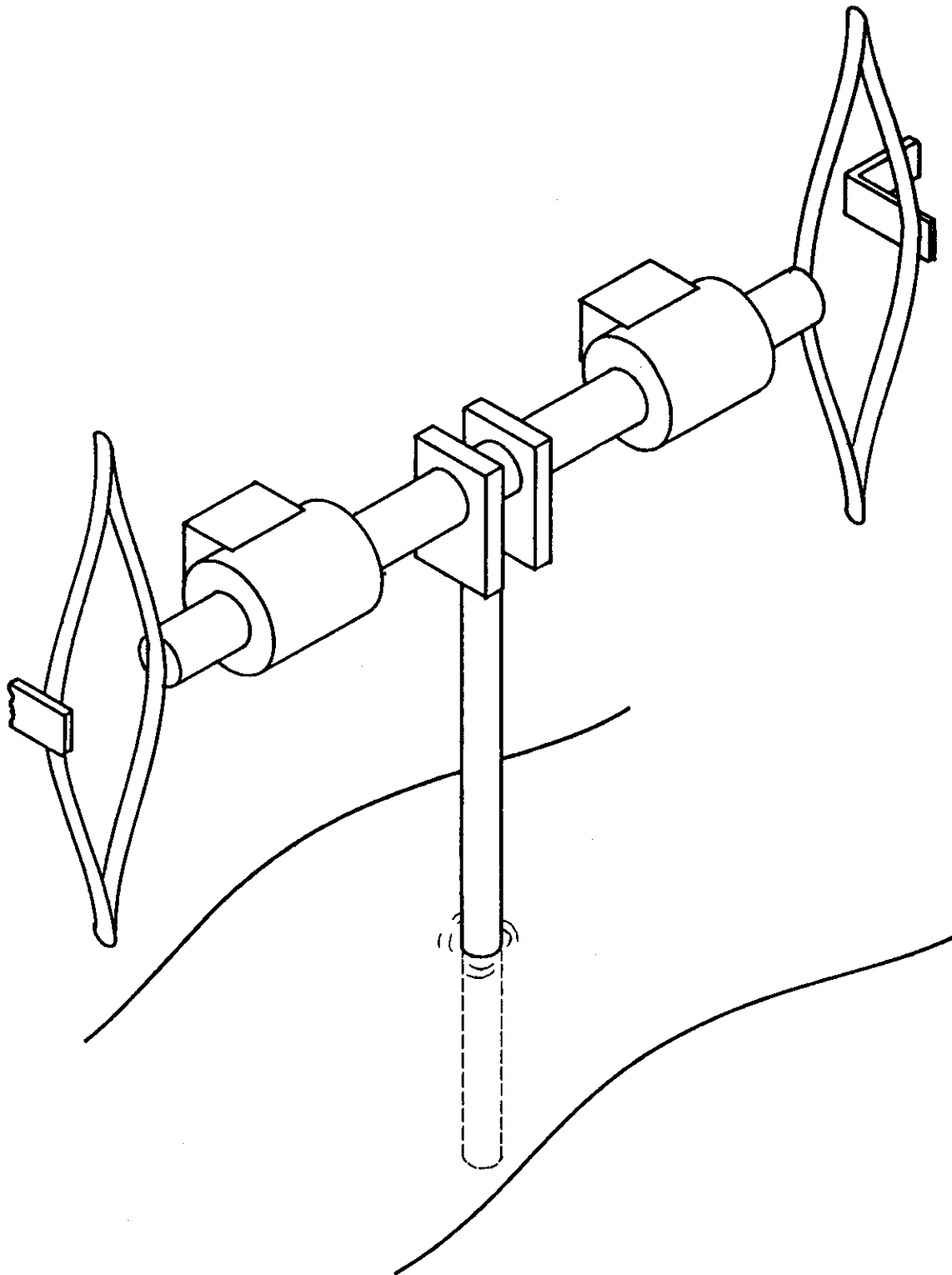


Fig VI- 1: Experimental Apparatus
for Oscillating Cylind.

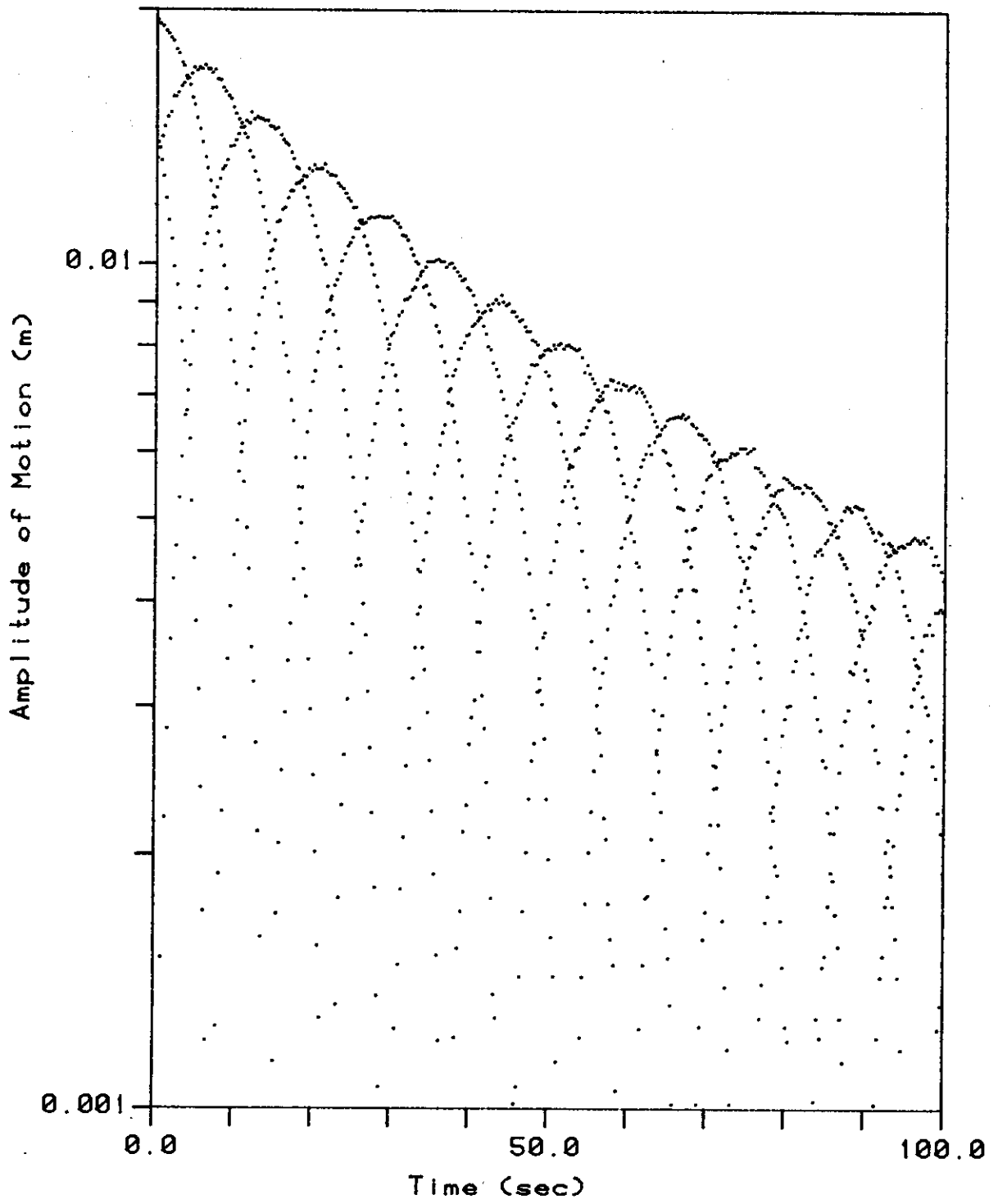


Fig VI-2: Damped Oscillations of Cylinder in Air

wave probe were also mounted in the wave tank. The three pieces of equipment were mounted in a line parallel to the wave crests, so that they all experienced the same water at the same time. The second cylinder had the same diameter and submerged length as the oscillating cylinder, but was held above the waver by a force transducer rather than being free to move. The second cylinder was included in the experiment as a test of the validity of Morison's equation.

Each run of the experiment involved generating random waves corresponding to a given sea state and recording the outputs of the three transducers on a four-channel, FM tape recorder. Based on a length ratio of 100:1 and Froude scaling, the waves generated corresponded approximately to Pierson-Moskowitz sea states for wind speeds of 20, 30, 40, and 50 knots. For each run, 25 minutes of data were recorded, or over 2,000 oscillations of the cylinder. In addition, free vibrations of the cylinder in air and in calm water were also recorded.

Data analysis began with digitization of the recorded data. Analog to digital conversion, as well as all subsequent analysis, was performed using a GenRad, four-channel, spectral analysis system built around a PDP-11/34 minicomputer. Once digitized, all data was stored on a disk for later processing.

The objective of the processing was to compare the observed force on the fixed cylinder and deflection of the oscillating cylinder to the predicted behaviour for the same incident wave spectra. As a preliminary step to that processing, histograms were computed for each channel of each run. The histograms indicated whether any clipping of the signals

had occurred during the A/D conversion as well as indicating any departures from a Gaussian probability distribution for each process. In preparation for comparing estimated with predicted response spectra, autocorrelation functions were estimated out to 20 seconds lag for all processes. In addition, cross-correlation functions between wave elevation and force on the fixed cylinder were estimated out to the same lag.

Before comparing the observed behaviour in the experiment with the predicted behaviour, it is necessary to discuss the choice of values for C_m and C_d used in the prediction of the hydrodynamic forces. Unfortunately, little work has been done on hydrodynamic force measurements in random seas, so it is necessary to infer appropriate values for C_m and C_d from experiments performed with uniform, harmonically oscillating flows. As is commonly assumed, the variation in flow conditions along the length of the cylinder was treated by a strip theory approach. To relate values of C_m and C_d from harmonic flows to values for random flows, a rational method was proposed. The method, described in Appendix B, required computing weighted averages of C_m and C_d , for harmonic flows, over the range of cycle amplitudes likely to be encountered in a particular random process. The end result is that functional relationships were developed between C_m and C_d and the non-dimensional parameters N^*_{K-C} and R^* .

$$N^*_{K-C} = \frac{2\pi\sigma_u}{\omega D} \quad (VI-1)$$

$$R^* = \frac{\sigma_u D}{\nu} \quad (VI-2)$$

In these equations, σ_u is the RMS fluid velocity and $\bar{\omega}$ is the mean frequency of the random process.

As mentioned previously, the fixed cylinder was included in the experiment as a test of the applicability of Morison's equation. To determine whether the values of C_m and C_d from harmonic flow tests could predict the forces on a fixed cylinder in waves, estimated and predicted spectra were compared. The Gaussian closure technique was applied to the problem to determine the predicted relationship between wave elevation spectra and wave-elevation to force cross-spectra. Using the hydrodynamic force model described in Chapter II, with the potential flow component of the force given by the inertial term of Morison's equation, and assuming that the incident wave kinematics are adequately described by linear, potential flow theory, the following relationship was derived.

$$S_{nf}(\omega) = H_{nf}(\omega) S_{nn}(\omega) \quad (\text{VI-3})$$

$$\text{Re}\{H_{nf}(\omega)\} = \int_{-h}^0 \frac{C_d \rho D \sigma_u}{\sqrt{2\pi}} \omega \exp\left[\frac{-\omega^2 y}{g}\right] dy \quad (\text{VI-4a})$$

$$\text{Im}\{H_{nf}(\omega)\} = \int_{-h}^0 \frac{(1 + C_m) \rho \pi D^2}{4} \omega^2 \exp\left[\frac{-\omega^2 y}{g}\right] dy \quad (\text{VI-4b})$$

$$\sigma_u^2(y) = \int_0^\infty \omega^2 \exp\left[\frac{-2\omega^2 y}{g}\right] S_{nn}(\omega) d\omega \quad (\text{VI-5a})$$

$$\bar{\omega}^2(y) = \sigma_u^2(y) / \int_0^\infty \exp\left[\frac{-2\omega^2 y}{g}\right] S_{nn}(\omega) d\omega \quad (\text{VI-5b})$$

Even though the relationship between fluid particle kinematics and hydrodynamic force was taken to be non-linear, a transfer function could be identified, relating the wave spectrum, $S_{\eta\eta}(\omega)$, to the cross-spectrum, $S_{\eta f}(\omega)$. Using the wave elevation autocorrelation function and the wave elevation to force cross-correlation function estimated from the data, the same transfer function could be estimated for each run of the experiment. Comparison of the predicted and estimated transfer functions was particularly useful because the influences of the coefficients C_d and C_m could be separately examined in the real and imaginary components of the transfer function. However, "correct" values of C_m and C_d could not be derived from an examination of the transfer functions because both C_m and C_d were strong functions of position along the cylinder due to their dependence on N_{K-C}^* and R^* . Rather, the transfer functions yielded weighted averages of the coefficients over the length of the cylinder.

For each run, graphs were plotted of the ratio between the two components of the transfer function estimated from the data and the transfer function predicted using the Gaussian closure technique. To aid in the interpretation of this graph, the wave-elevation spectrum, the wave-force spectrum and the square of the coherence between the wave elevation and the wave force were also plotted. The spectra and cross-spectra were estimated from the auto- and cross-correlation functions by the Blackman-Tukey method. A Bartlett window was used with a maximum lag length of 20 seconds.

To complete the processing of the data, the estimated and predicted

deflection spectra for the oscillating cylinder were compared. The maximum entropy method (MEM) was used to estimate deflection spectra from the observed motion, as it had the spectra from the numerical simulations. The number of poles to be used in estimating each spectrum were selected according to the criterion outlined by Campbell [3].

The predicted motion spectra were computed using equations (IV-14) through (IV-19), (IV-34) and (IV-42). Evaluation of the equations was relatively simple as the structure responded in only one mode and the submerged geometry was simple. The structural-dynamic parameters of natural frequency, orthonormal mode shape and modal damping were required as input to the predictions. The modal damping, estimated at 0.13% of critical, included the hydrodynamic radiation damping as well as the system damping measured in air. The natural frequency and amplitude of the mode shape varied between runs because the hydrodynamic added mass depended on the severity of the sea state through N^*_{K-C} . For each run, the natural frequency was estimated from the data and, based on the natural frequency measured in air and the weights of the components, the virtual mass of the system was estimated. The orthonormal mode shape could then be computed, given the virtual mass. As an example, the natural frequencies in air and in calm water were 9.526 rad/sec and 9.348 rad/sec respectively. Since the mass of the structure in air was 5.21 kg, the virtual mass in calm water was 5.41 kg. Therefore, the amplitude of the orthonormal mode shape, M_{11} , was $0.430 \text{ kg}^{-1/2}$ in calm water. The amplitude of the mode shape is in keeping with the orthonormal require-

ment that the modal mass, equal to the virtual mass multiplied by the square of the mode shape, must be unity.

Values of C_m and C_d required in the prediction were selected as described previously, except that the relative velocity was used in the calculation of N_{K-C}^* , rather than the fluid velocity alone. The coefficients were then adjusted, based on the ratios of estimated to predicted transfer functions of the wave elevation to the hydrodynamic force on the fixed cylinder. Also required as input to the predictions were the spectra for the incident fluid kinematics. These were computed from the estimated, wave elevation spectra and linear, potential flow theory.

Prediction of the motion spectra of the cylinder had to be performed iteratively, although only two iterations were required for each prediction. To simplify the computation, the double integral of $S_{zij}(\omega)$ in equation (IV-42) was evaluated approximately. The integral is difficult to evaluate but the influence of the integral is minor compared with the other terms in the equation.

Figures VI-3 through VI-42 are plots showing for each run the results of the processing described. Ten plots for each run are presented. Of each group of ten, the first three are normalized histograms of the wave elevation, wave force and cylinder deflection with a Gaussian distribution overlaid on each. The next three plots are the wave-elevation spectrum, the wave-force spectrum and the square of the coherence between the two. The next two plots show respectively the ratios between the estimated and predicted components of the transfer function corresponding to the inertial

and drag forces. The ninth plot shows the damping estimated as a function of the number of poles in the MEM model. The last plot of each group shows, superimposed, the estimated deflection spectrum and the predicted deflection spectrum. The estimated spectrum is plotted as a dashed line while the predicted spectrum is plotted as a solid line.

Concerning the plotted results, a number of comments can be made.

1. The wave-force histograms are much more non-Gaussian than the wave-elevation histograms. Therefore, the relationship between the fluid kinematics and the hydrodynamic force must be non-linear.

2. Although the wave-force histograms are non-Gaussian, all of the cylinder-deflection histograms appear to be Gaussian. This observation indicates that the Gaussian closure technique should yield reasonable predictions of the deflection spectra for this problem.

3. All coherence functions between wave elevation and wave force are close to unity at least over the range of frequencies around the peaks of the wave-elevation and wave-force spectra. The high coherence implies that the wave-elevation and wave-force spectra can be related to each other through a transfer function. There is an apparent paradox between the conclusion based on the histograms, that the relationship between wave elevation and wave force must be non-linear and the conclusion based on the coherence, that the wave-elevation and wave-force spectra can be related through a transfer function. Normally transfer functions are associated with linear systems. However, one of the consequences of applying the Gaussian closure technique is that a transfer function can be identified between the spectra of two random processes which are non-linearly

related.

4. The ratios of the estimated to the observed, real and imaginary components of the transfer functions were generally flat over a significant frequency band, indicating that Morison's equation is providing a reasonable prediction of hydrodynamic force for a cylinder excited by random waves. However, the ratios are not exactly equal to one. Some of the plots do show departures from a constant ratio. In particular, both the inertial and drag component ratios show significant departures for the 50 kt. sea state. However, it is not possible to draw any conclusions about the cause of the departure without further experiments.

5. Typical behaviour of the damping estimates as a function of the number of poles in the MEM model show large swings at low numbers of poles but converging to a reliable estimate as the number of poles increases, in accordance with the guidelines established by Campbell.

6. Generally good agreement was found between the estimated and predicted deflection spectra although the predictions tended to underpredict the response.

Table VI-1 contains a listing of the significant numbers associated with each run of the experiment. Of particular interest are the estimated and predicted RMS deflection of the cylinder and the estimated and predicted damping. As noted previously, the predictions of response were less than the observed responses. At least partially explaining the underprediction of response, the predicted damping tended to be higher than the damping estimated from the observed behaviour. A number of explanations of the overprediction are possible. One possibility is that the

relative velocity formulation of Morison's equation does not accurately predict the hydrodynamic force very close to the free surface. Certainly the argument presented in Chapter II as justification of the relative velocity formulations breaks down near the free surface. Another possibility is that Morison's equation does not accurately predict the frequency components of the force on the fringes of the frequency band of significant velocity. Although there are differences between the estimated and predicted damping and response, the qualitative agreement is good. The prediction of a sea-state dependent hydrodynamic damping is dramatically demonstrated in the experimental results, as shown in Figure VI-43.

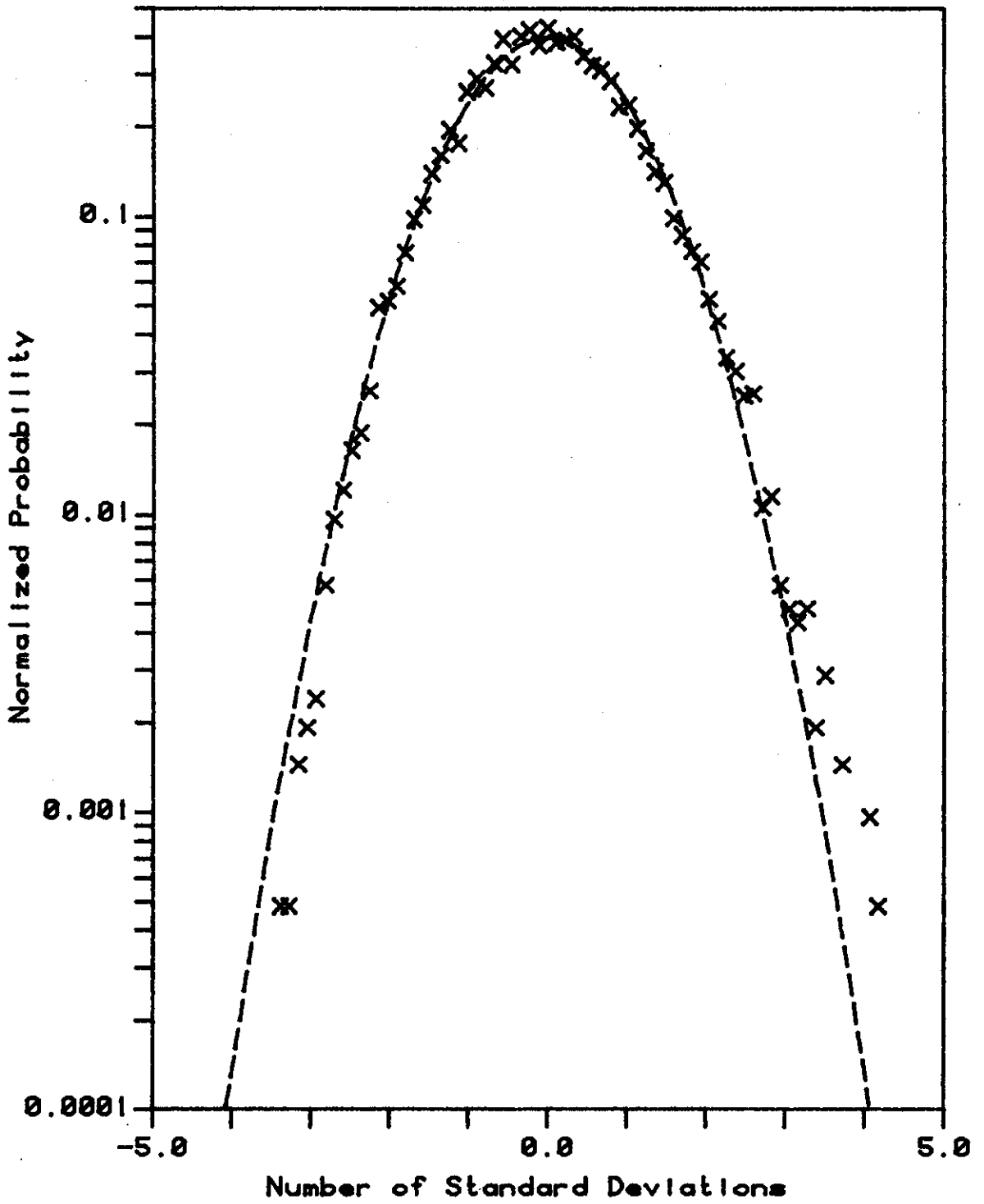


Fig VI- 3: Wave Elevation Histogram
for 20 kt. Sea State

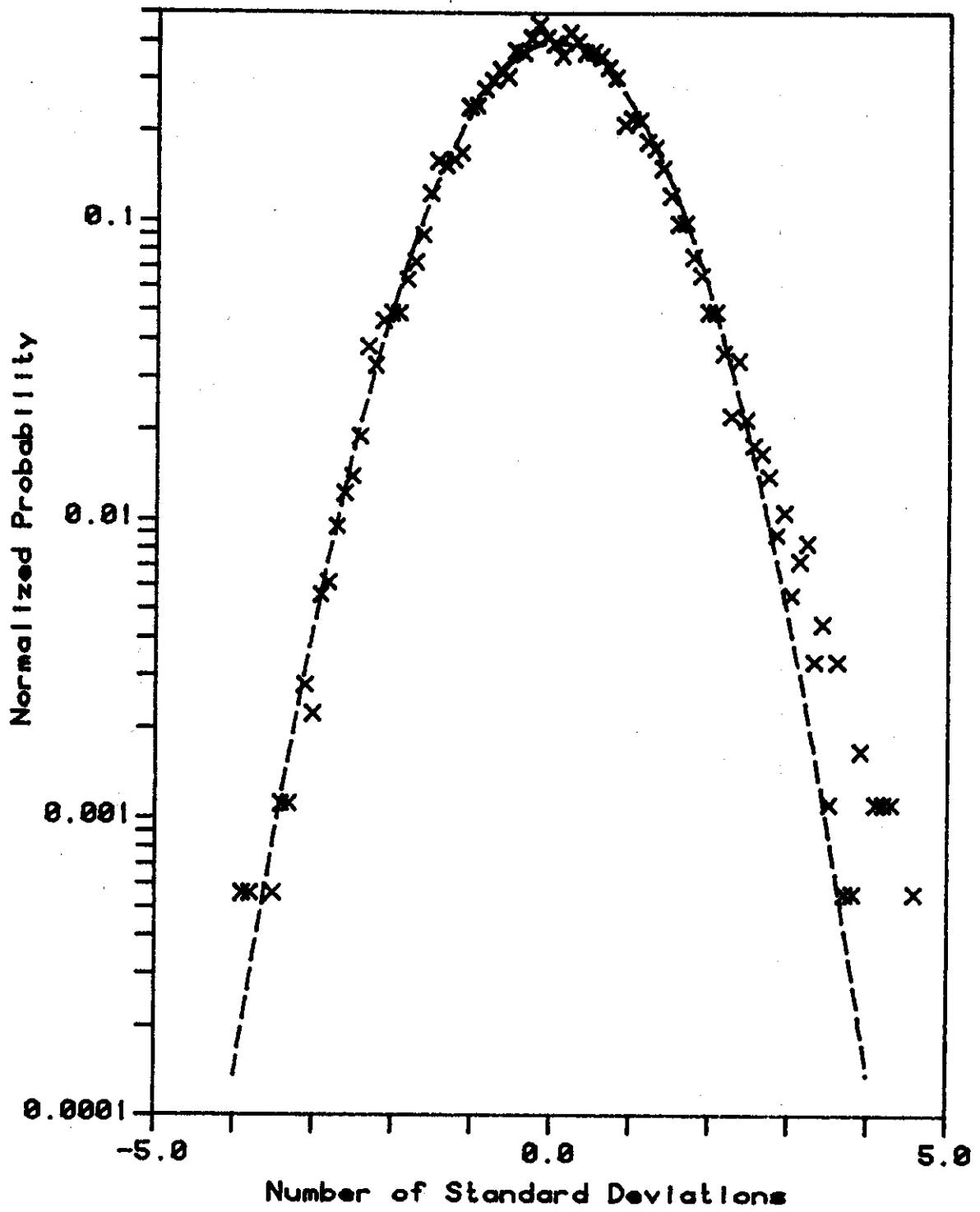


Fig VI- 4: Wave Force Histogram for 20 kt. Sea State

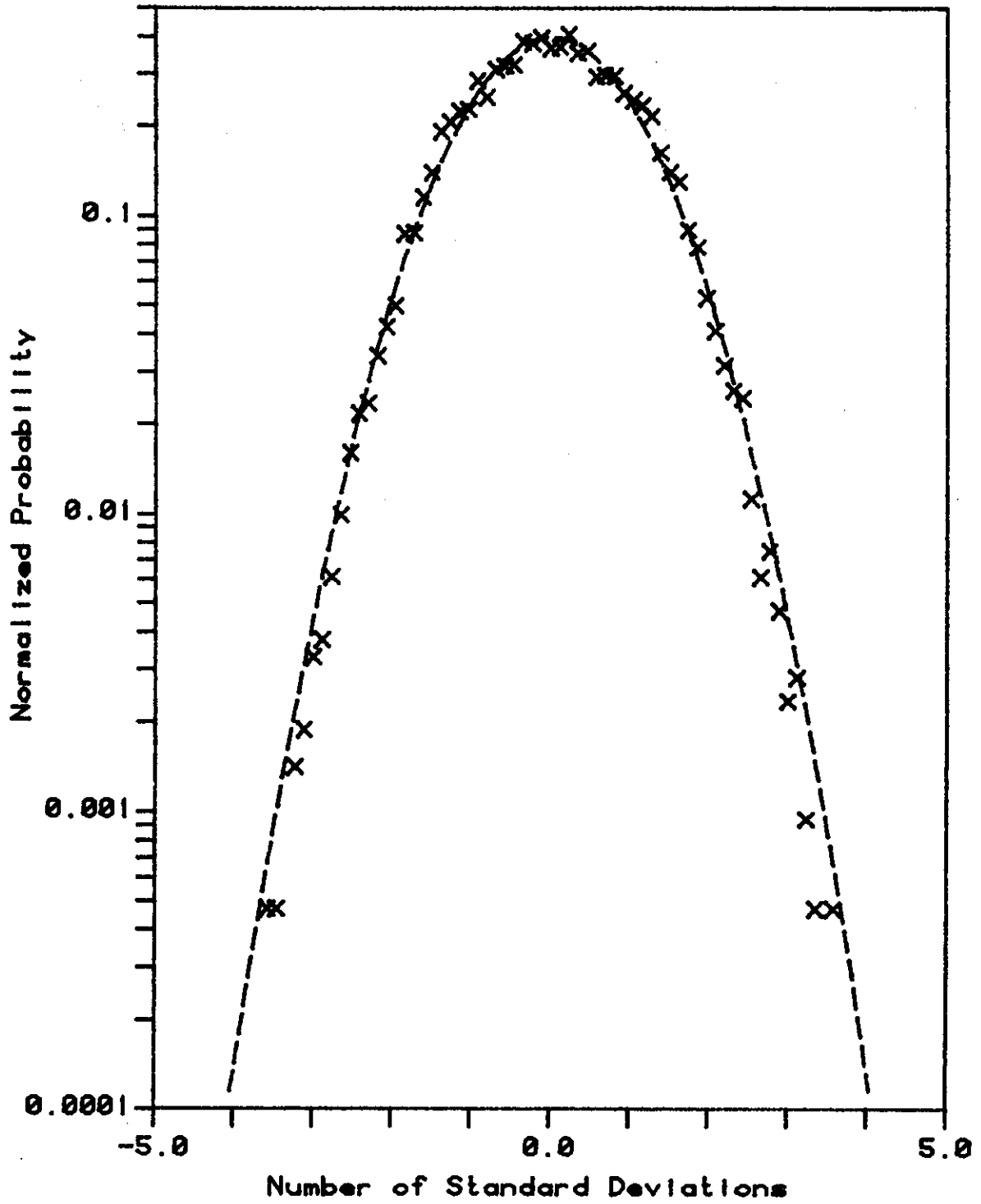


Fig VI- 5: Cylinder Deflection Hist.
for 20 kt. Sea State

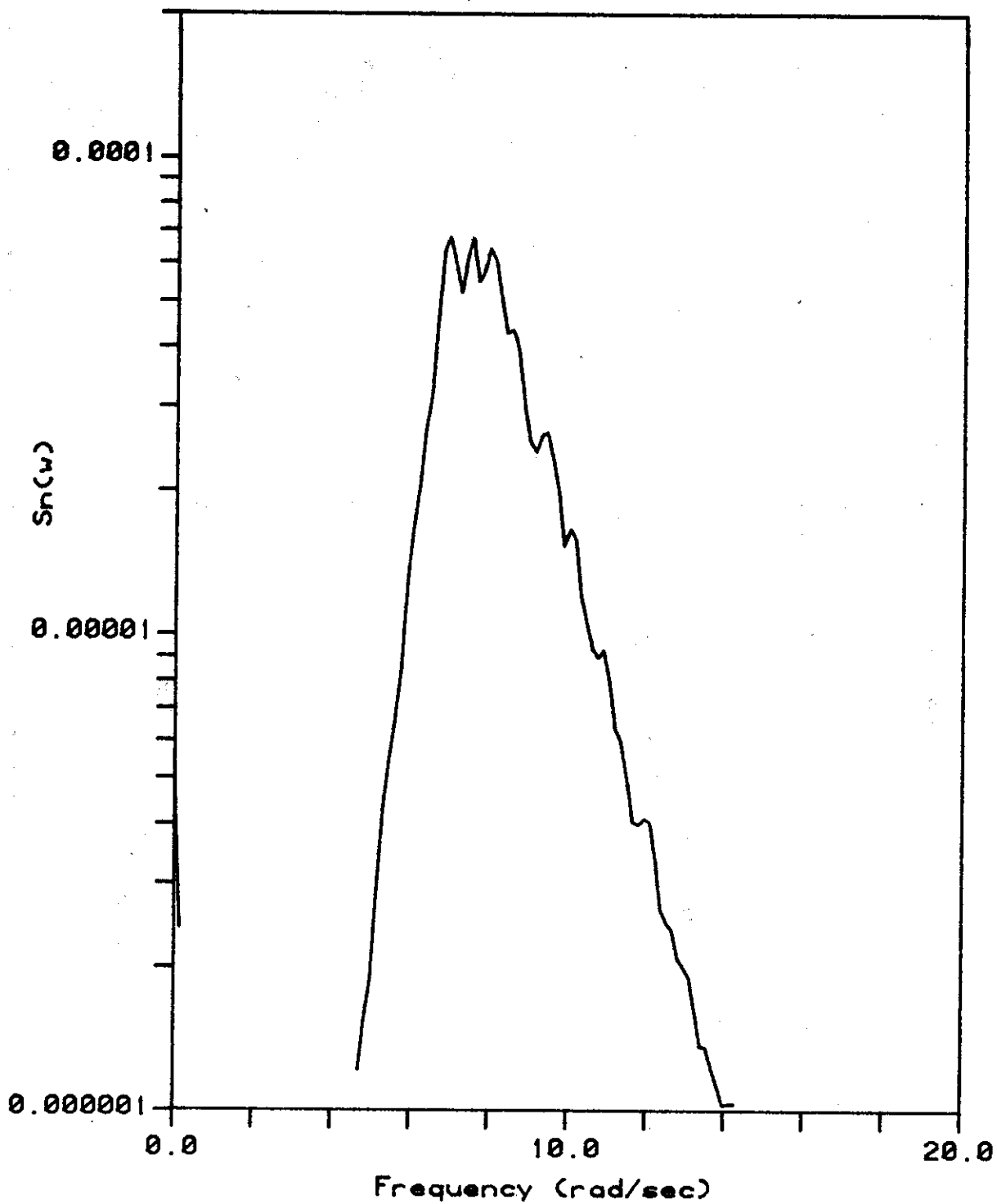


Fig VI- 6: Wave Elevation Spectrum
for 20 kt. Sea State

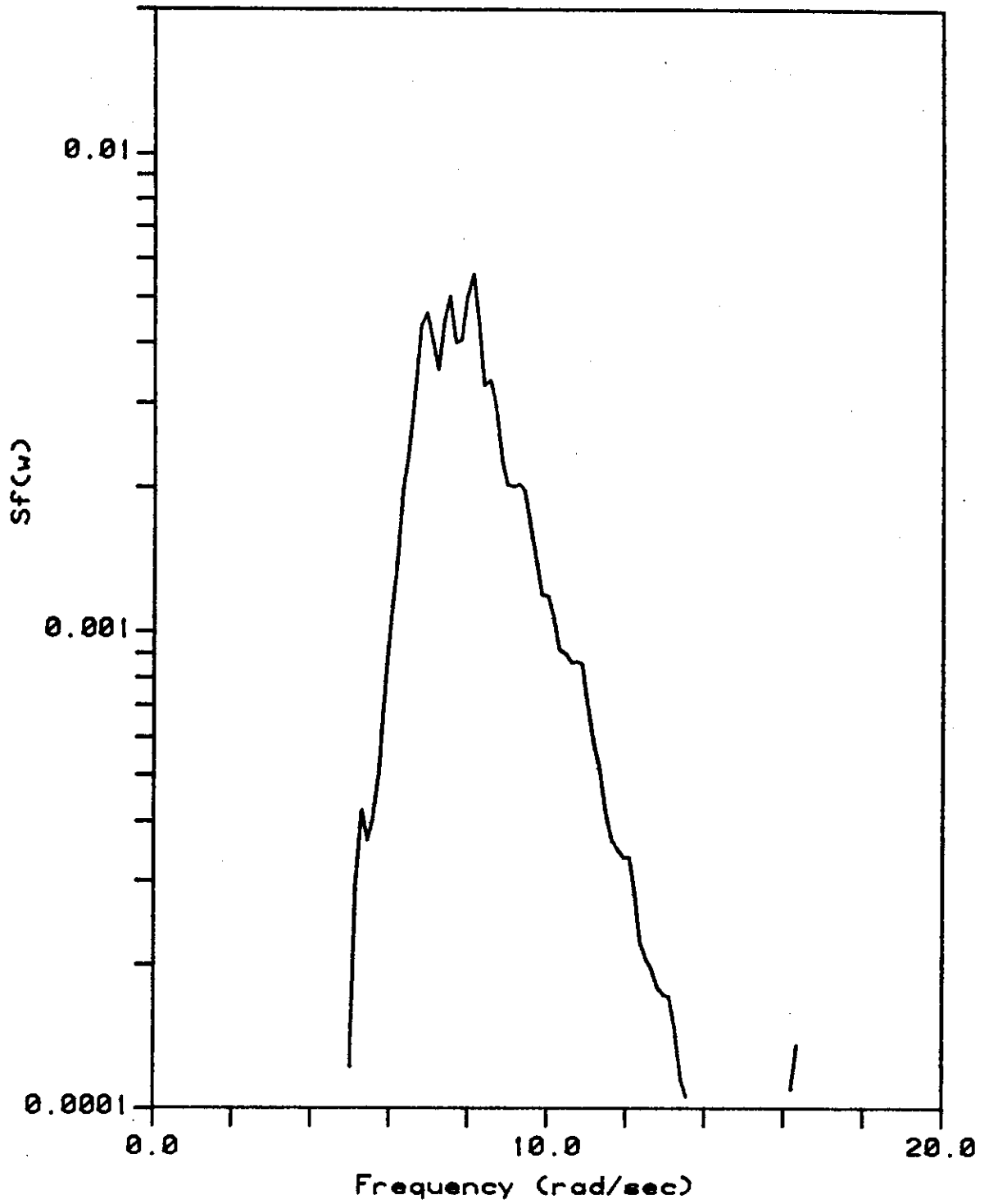


Fig VI- 7: Wave Force Spectrum
for 20 kt. Sea State

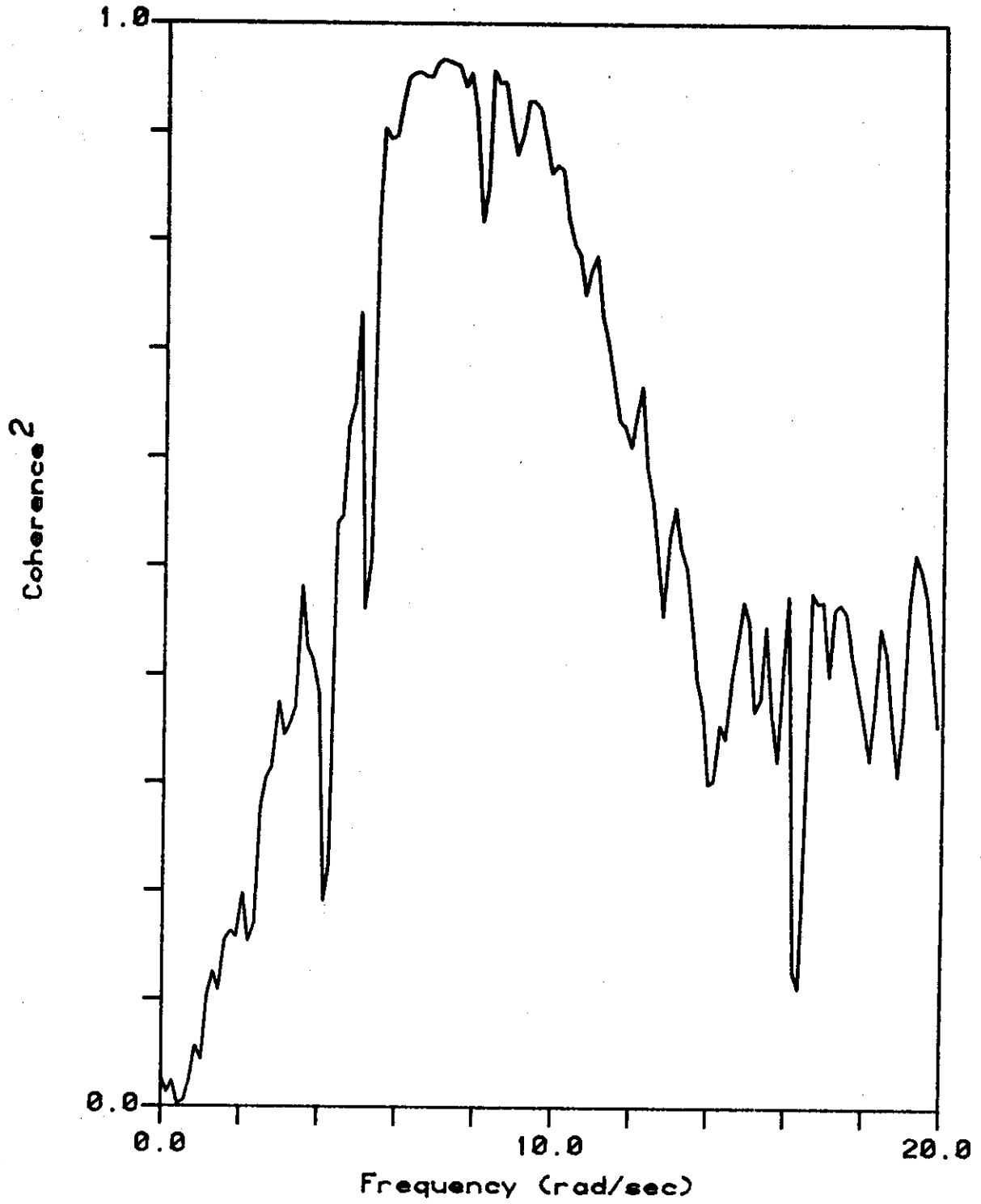


Fig VI- 8: Wave Elevation/Force Coh.
for 20 kt. Sea State

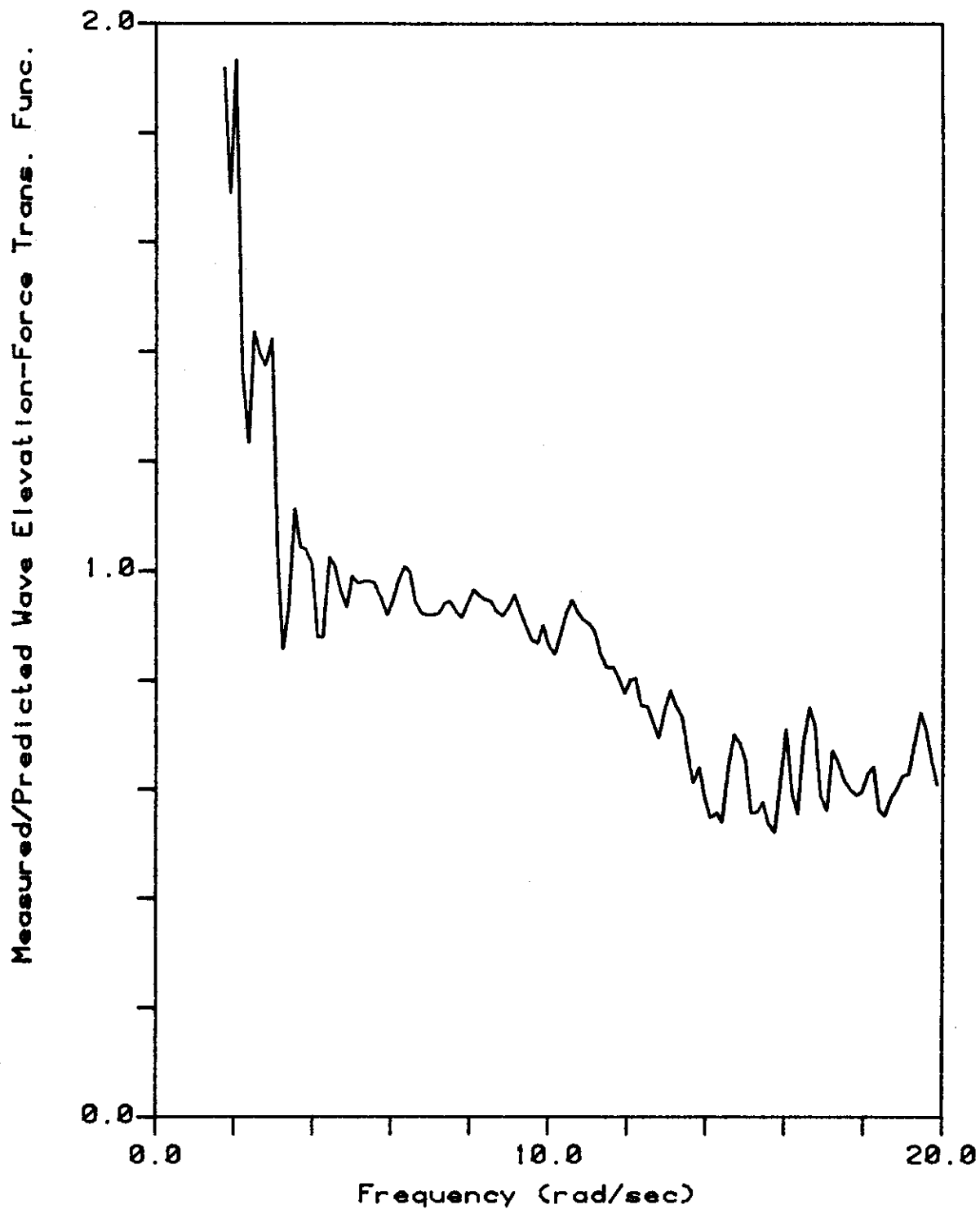


Fig VI- 9: Inertial Force on Cylind.
for 20 kt. Sea State

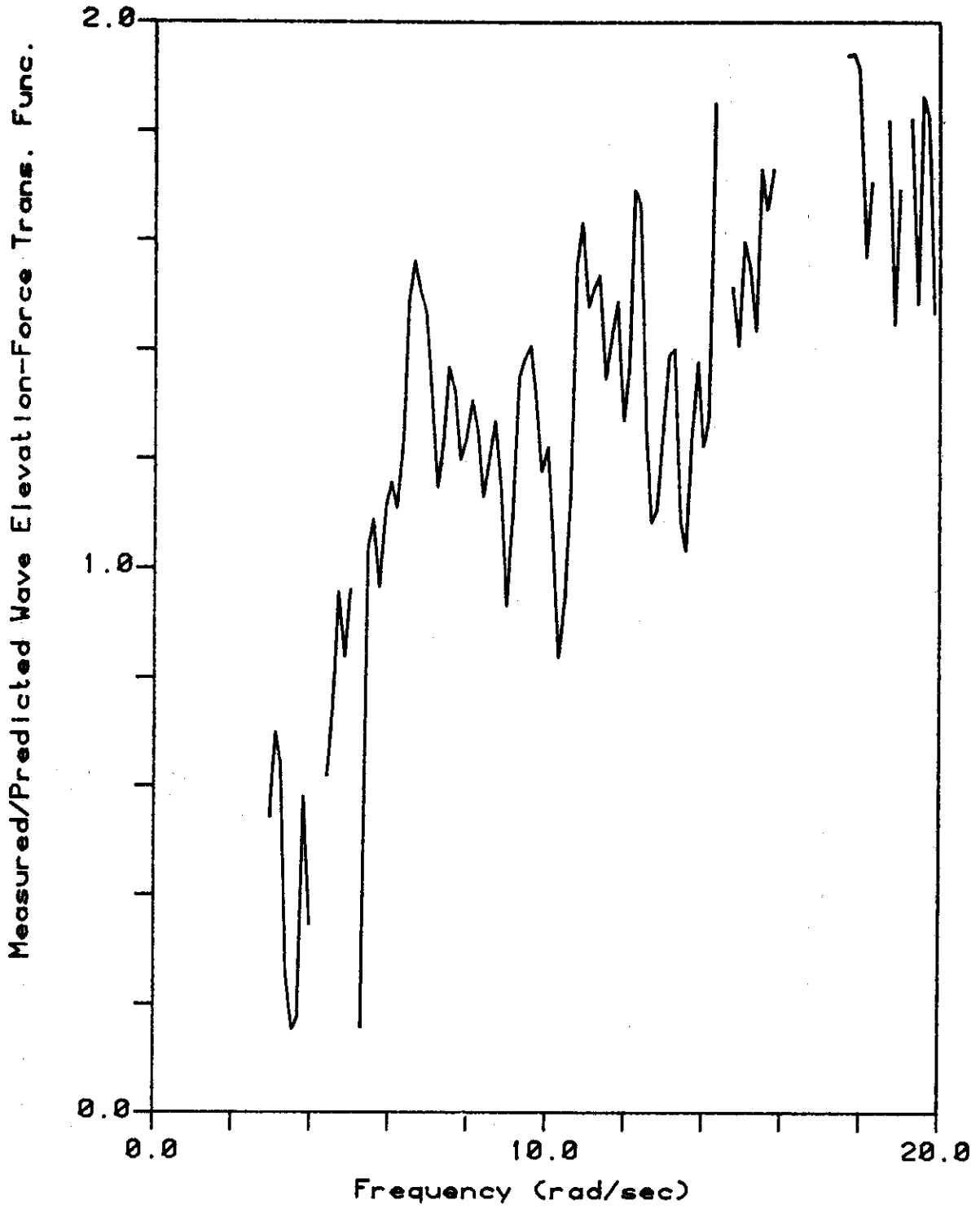


Fig VI-10: Drag Force on Cylinder for 20 kt. Sea State

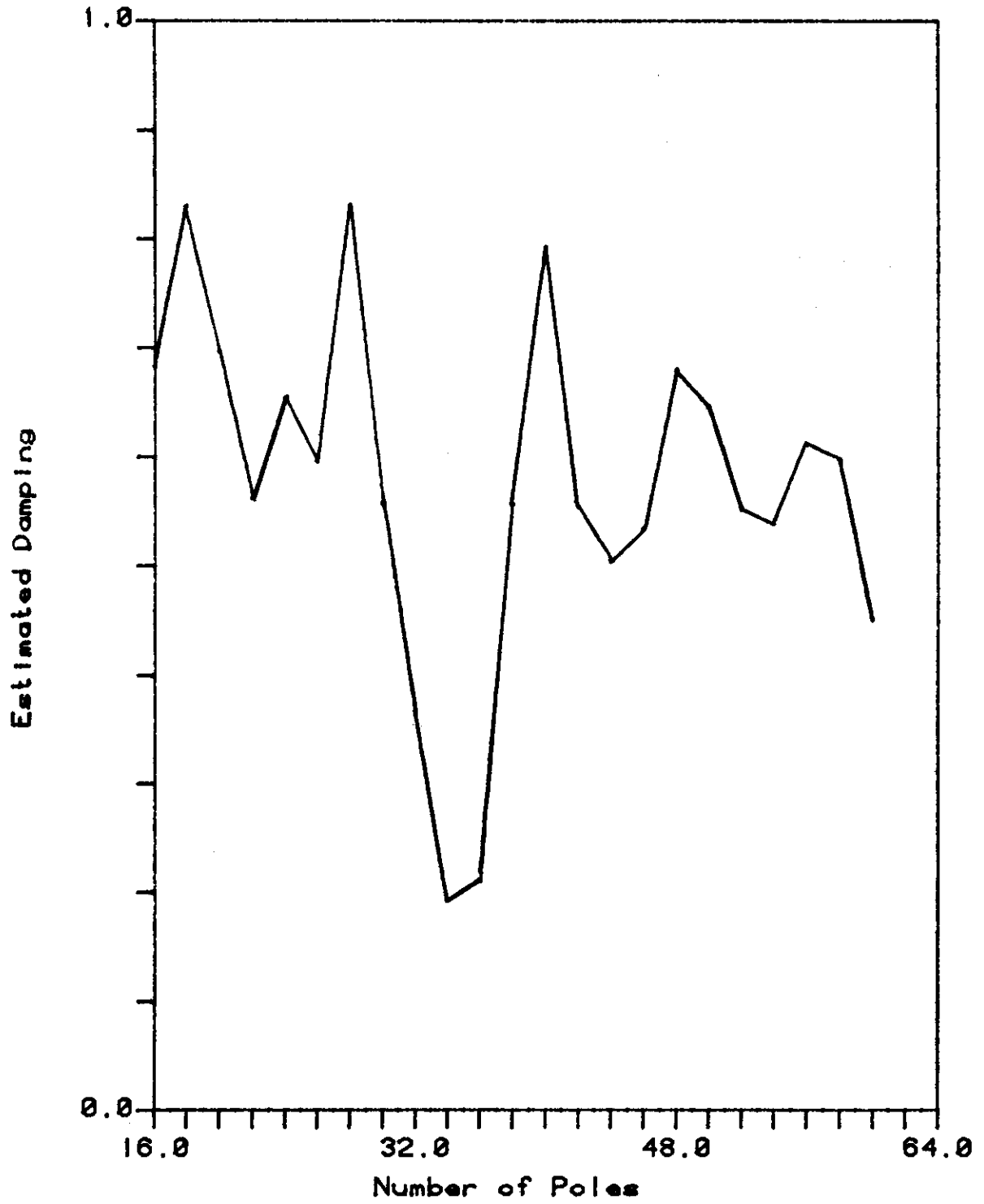


Fig VI-11: MEM Damping Estimates for 20 kt. Sea State

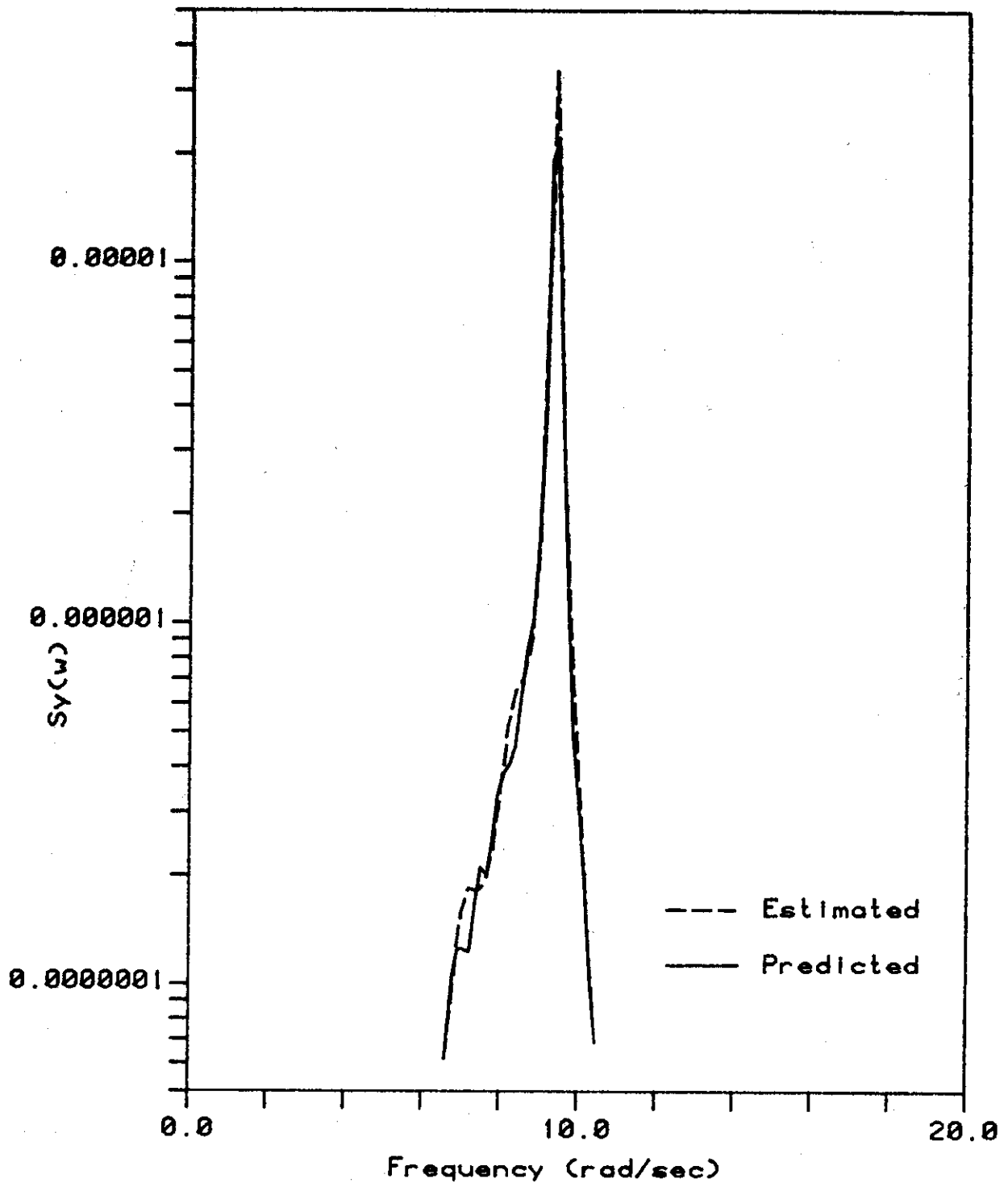


Fig VI-12: Cylinder Deflection Spec.
for 20 kt. Sea State

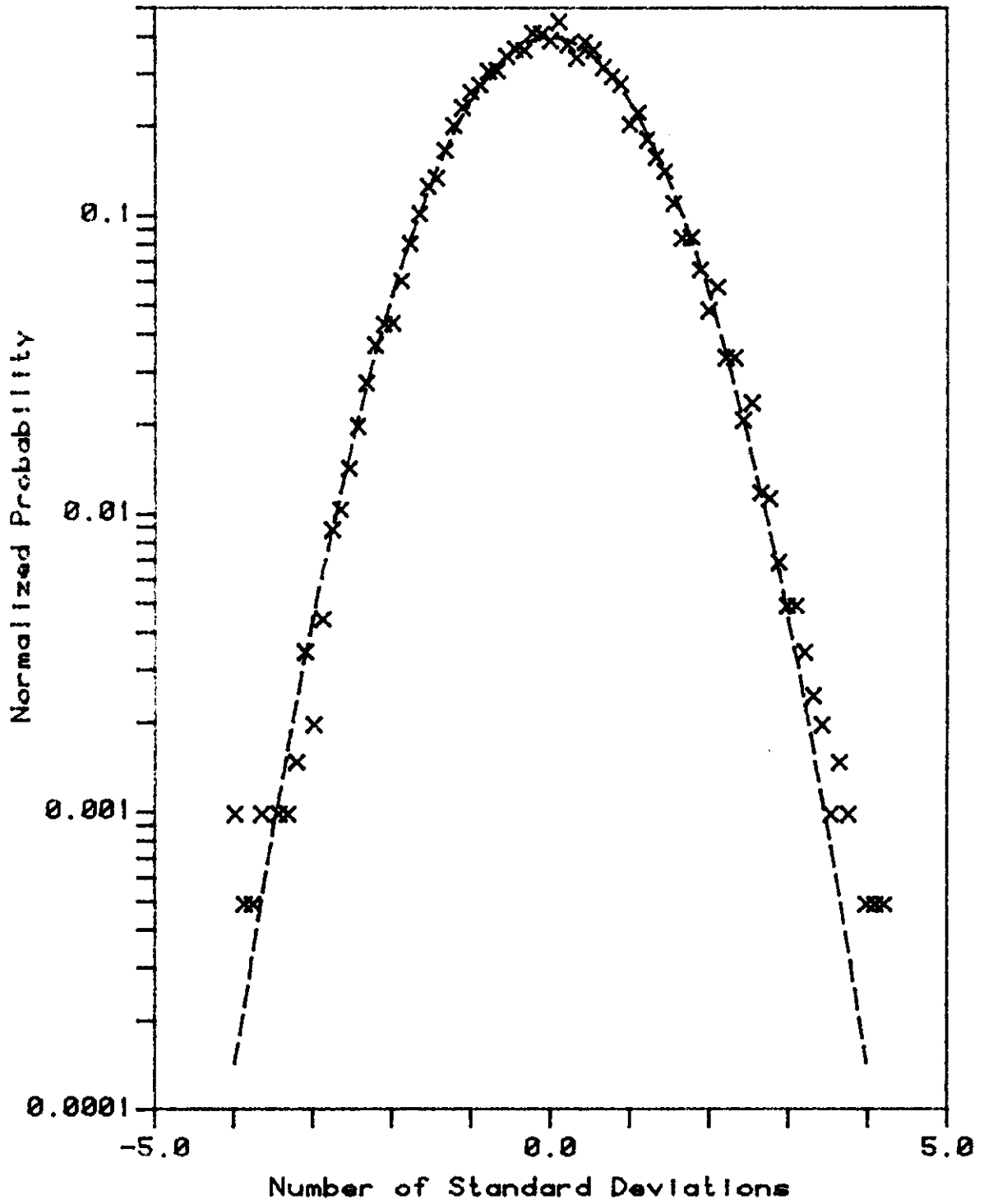


Fig VI-13: Wave Elevation Histogram for 30 kt. Sea State

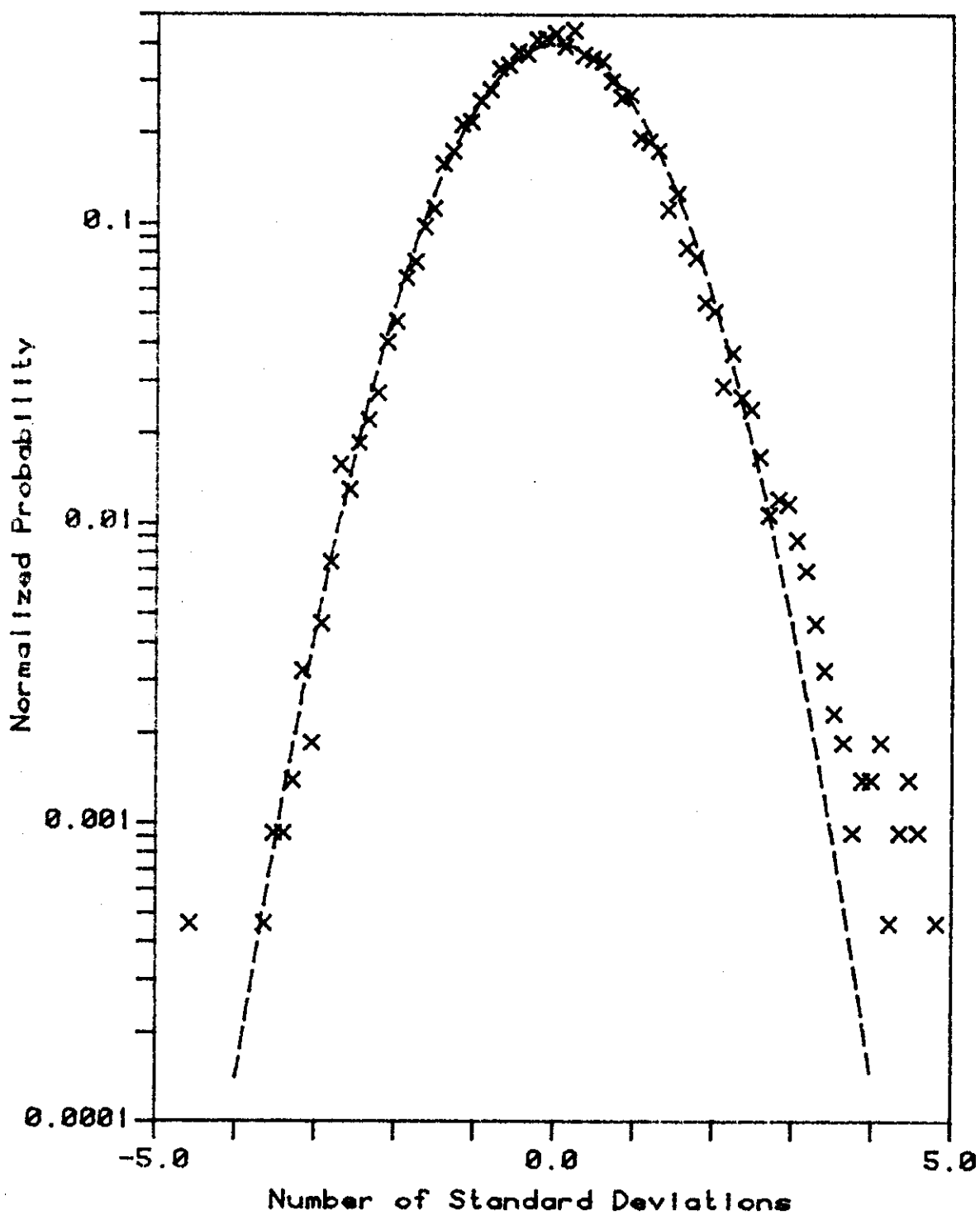


Fig VI-14: Wave Force Histogram for 30 kt. Sea State

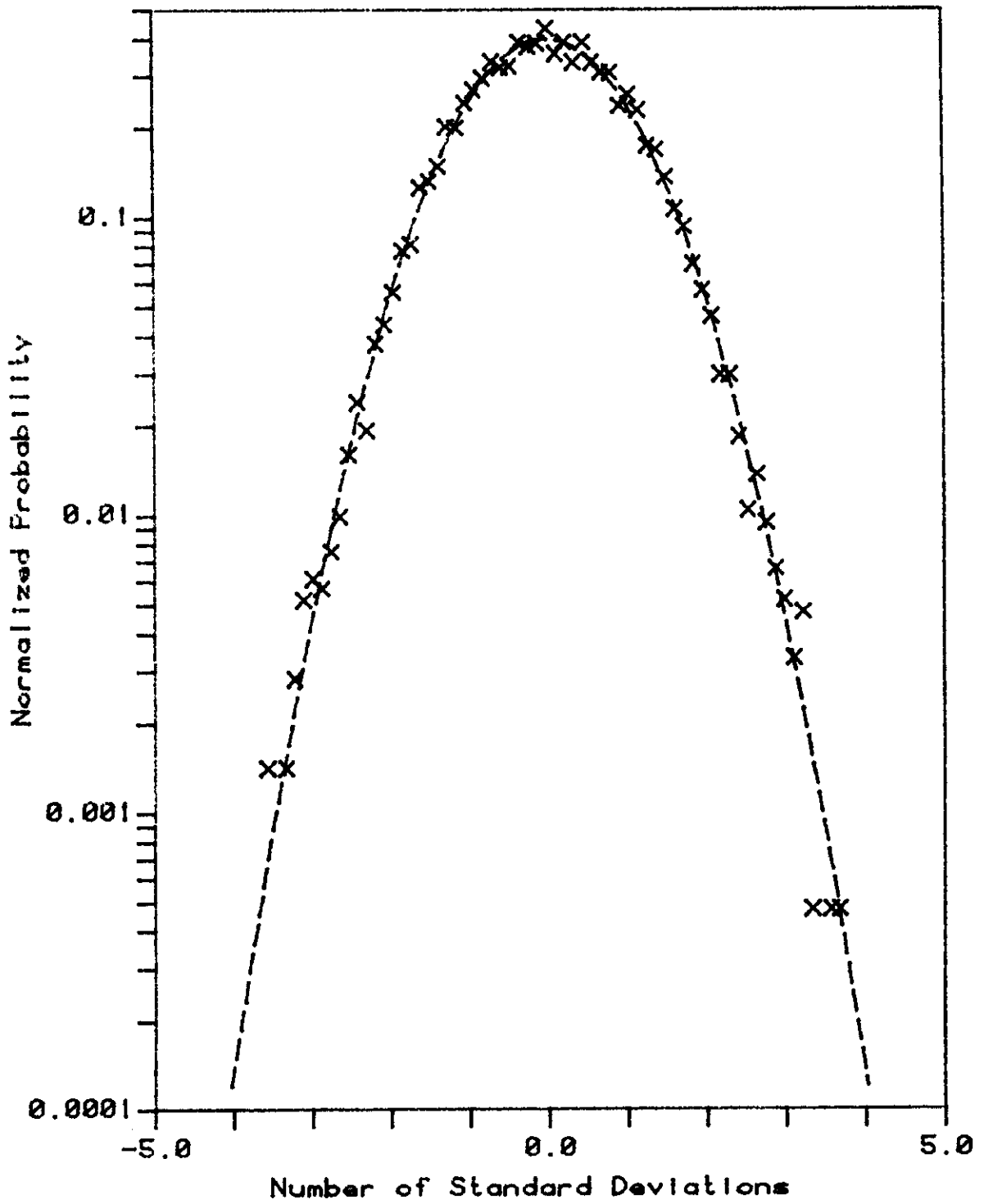


Fig VI-15: Cylinder Deflection Hist.
for 30 kt. Sea State

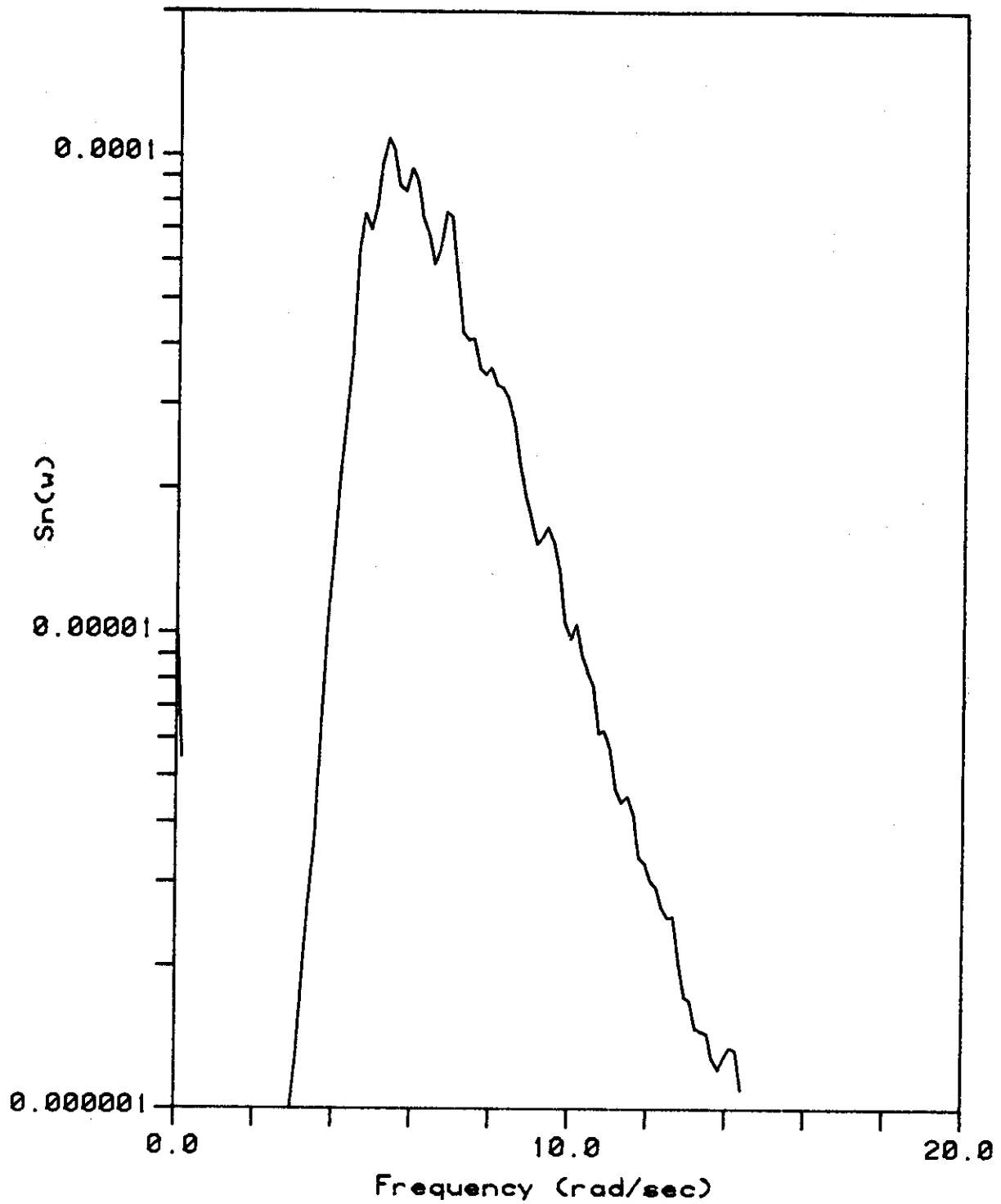


Fig VI-16: Wave Elevation Spectrum for 30 kt. Sea State

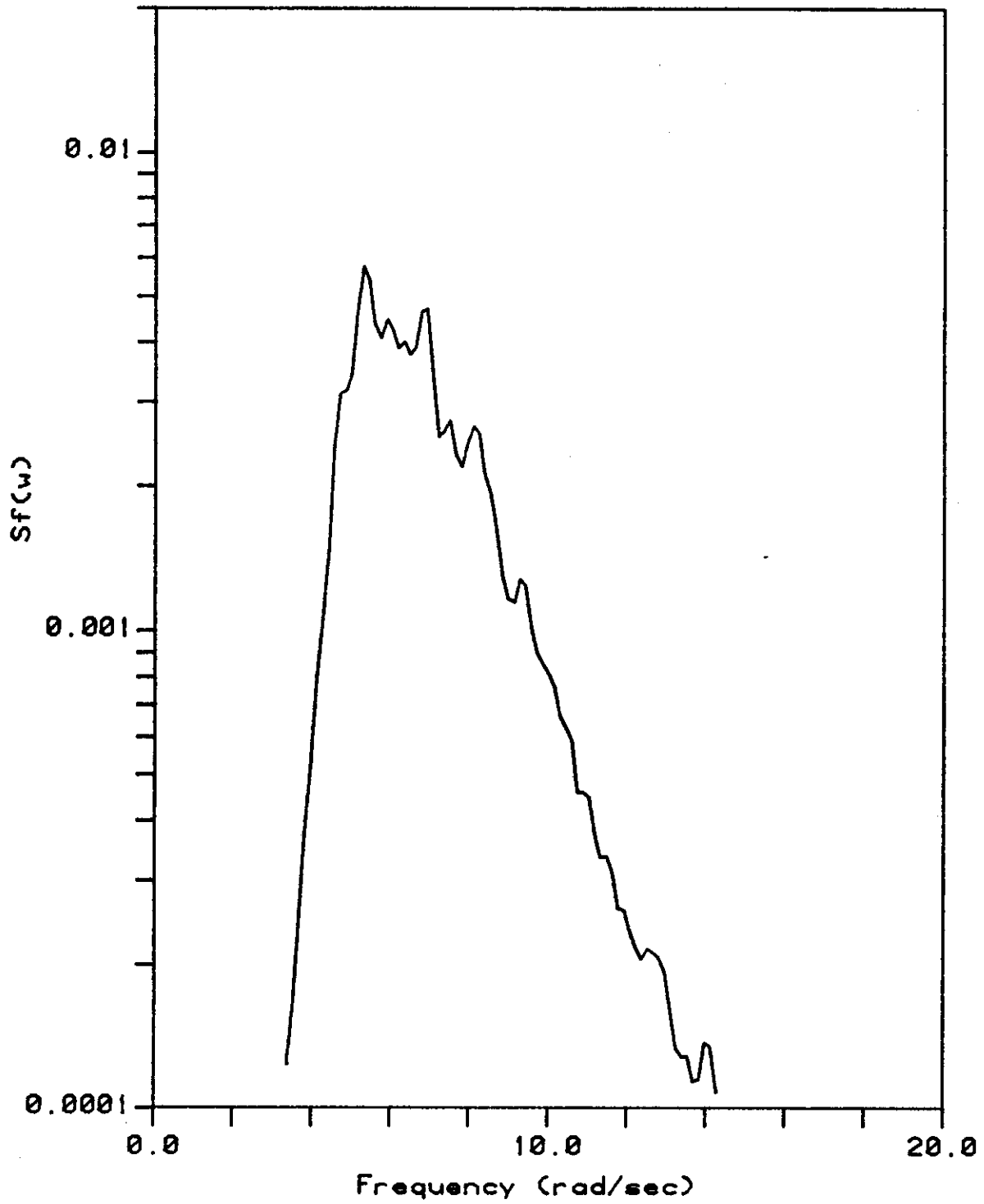


Fig VI-17: Wave Force Spectrum
for 30 kt. Sea State

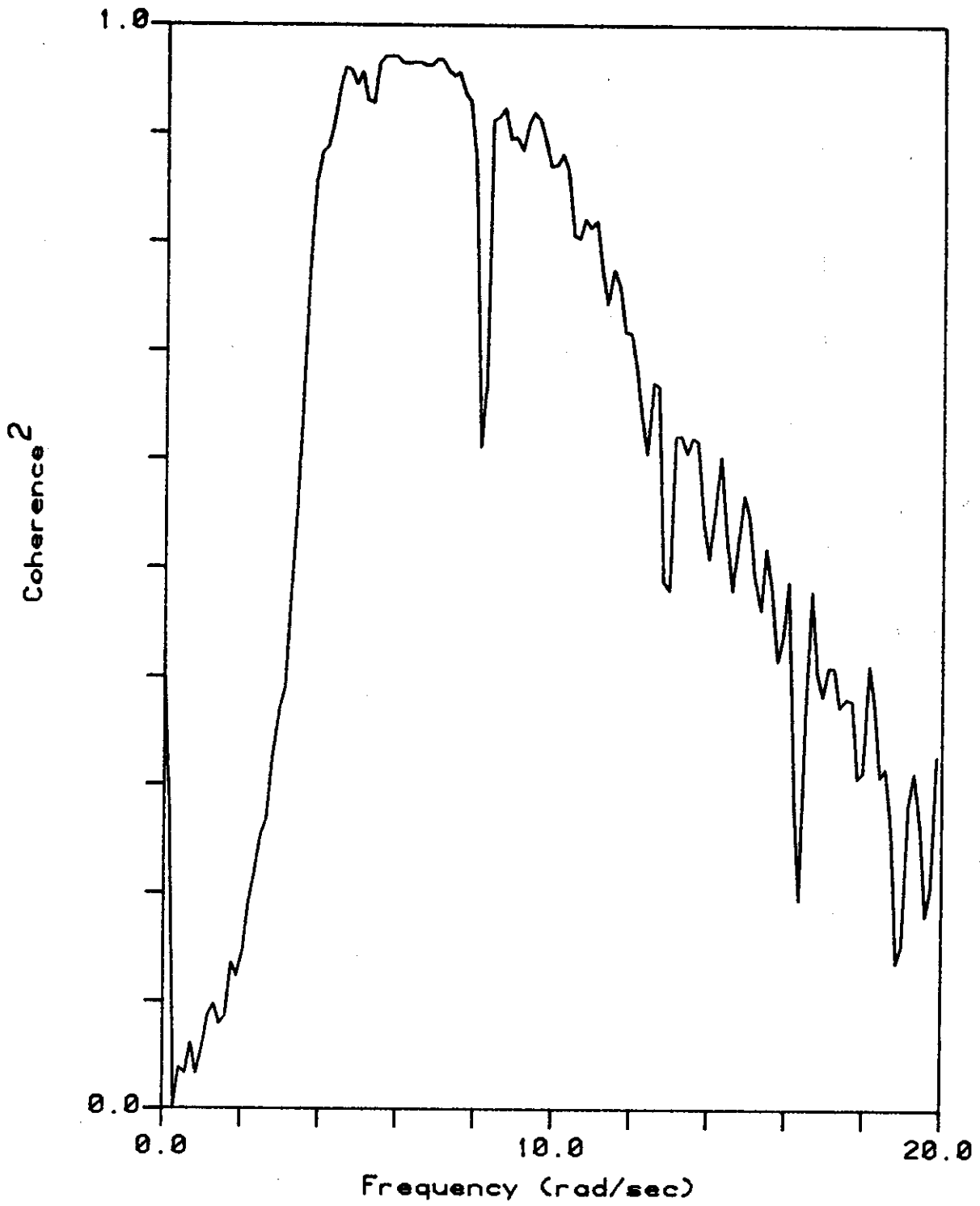


Fig VI-18: Wave Elevation/Force Coh.
for 30 kt. Sea State

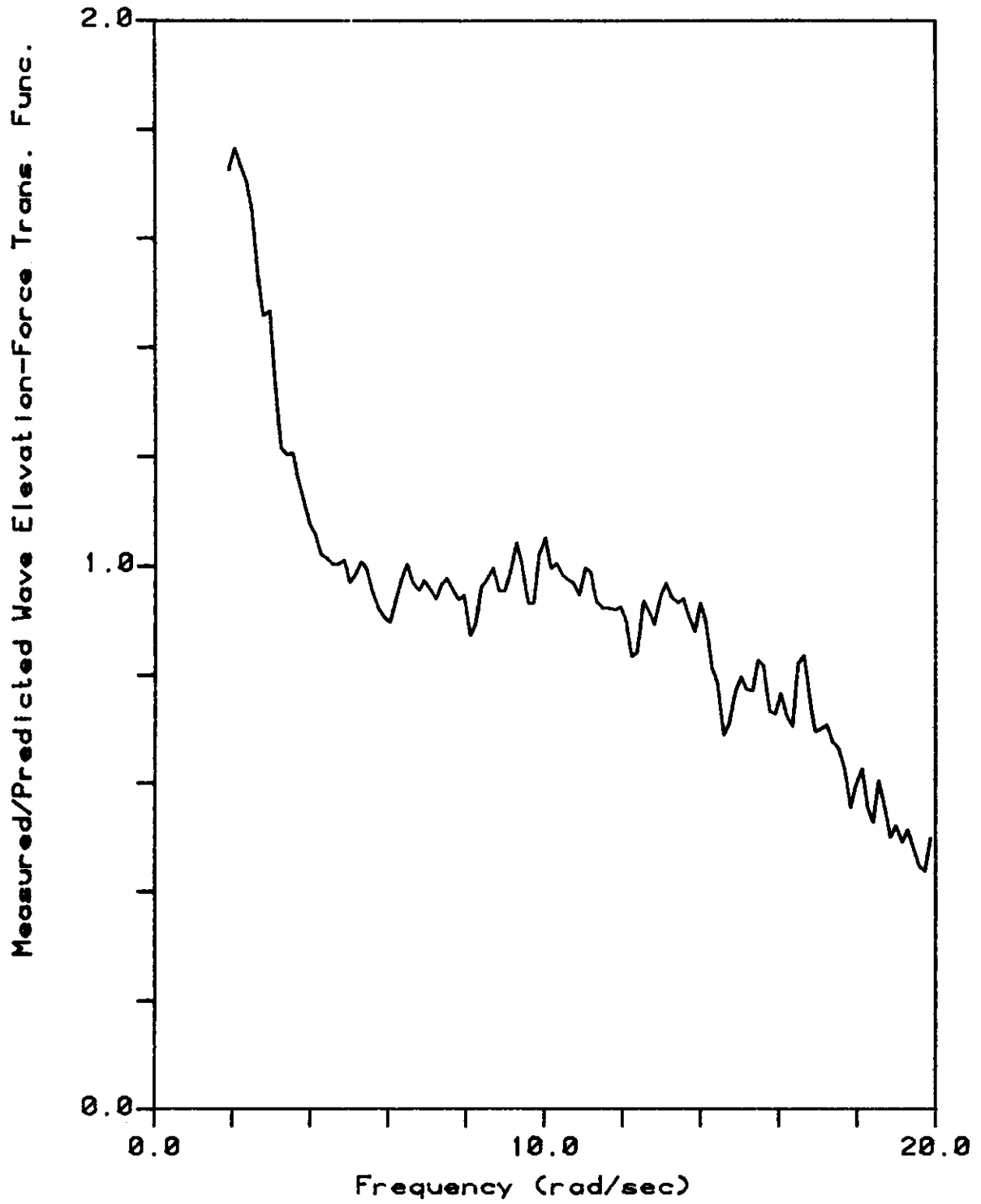


Fig VI-19: Inertial Force on Cylind.
for 30 kt. Sea State

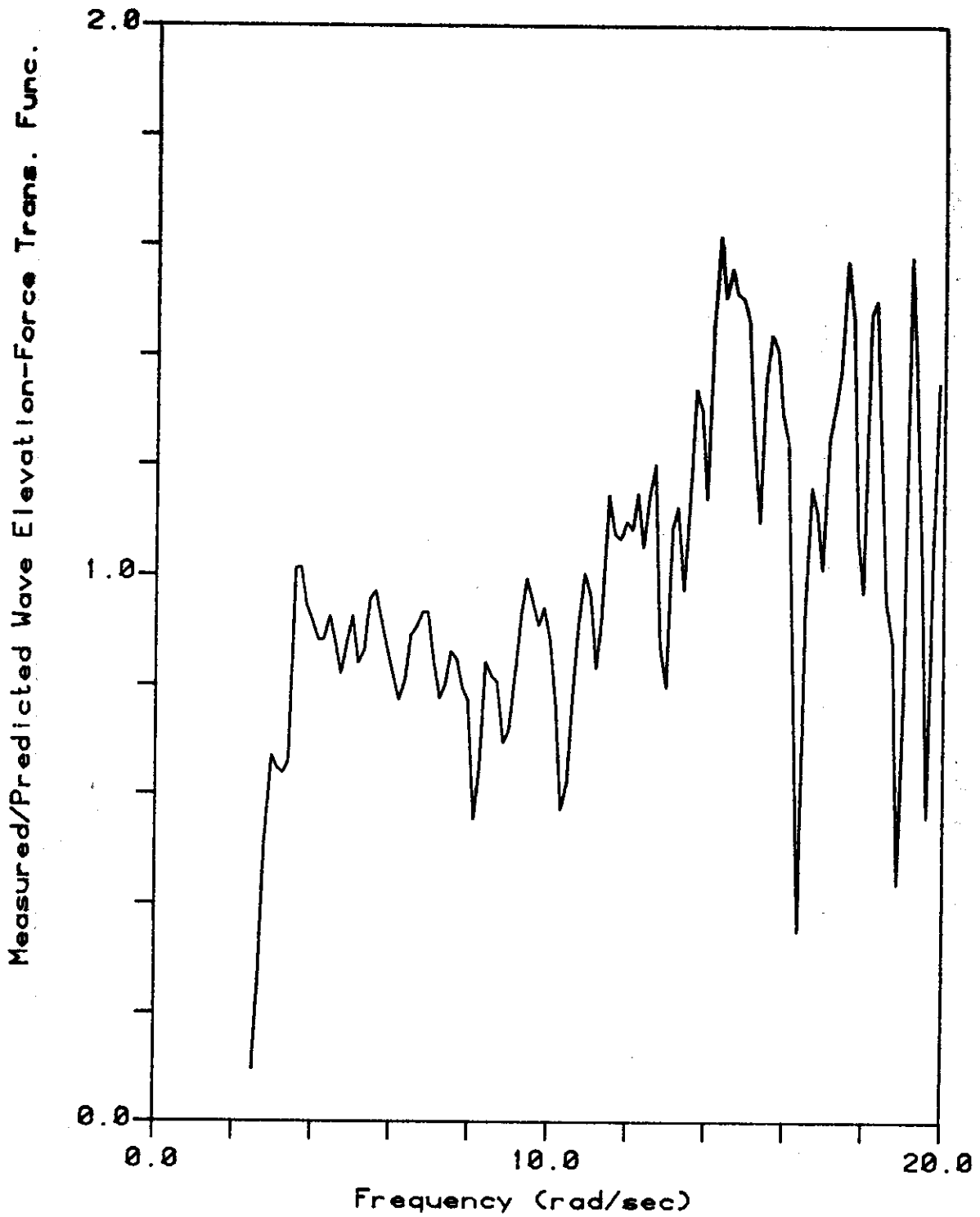


Fig VI-20: Drag Force on Cylinder for 30 kt. Sea State

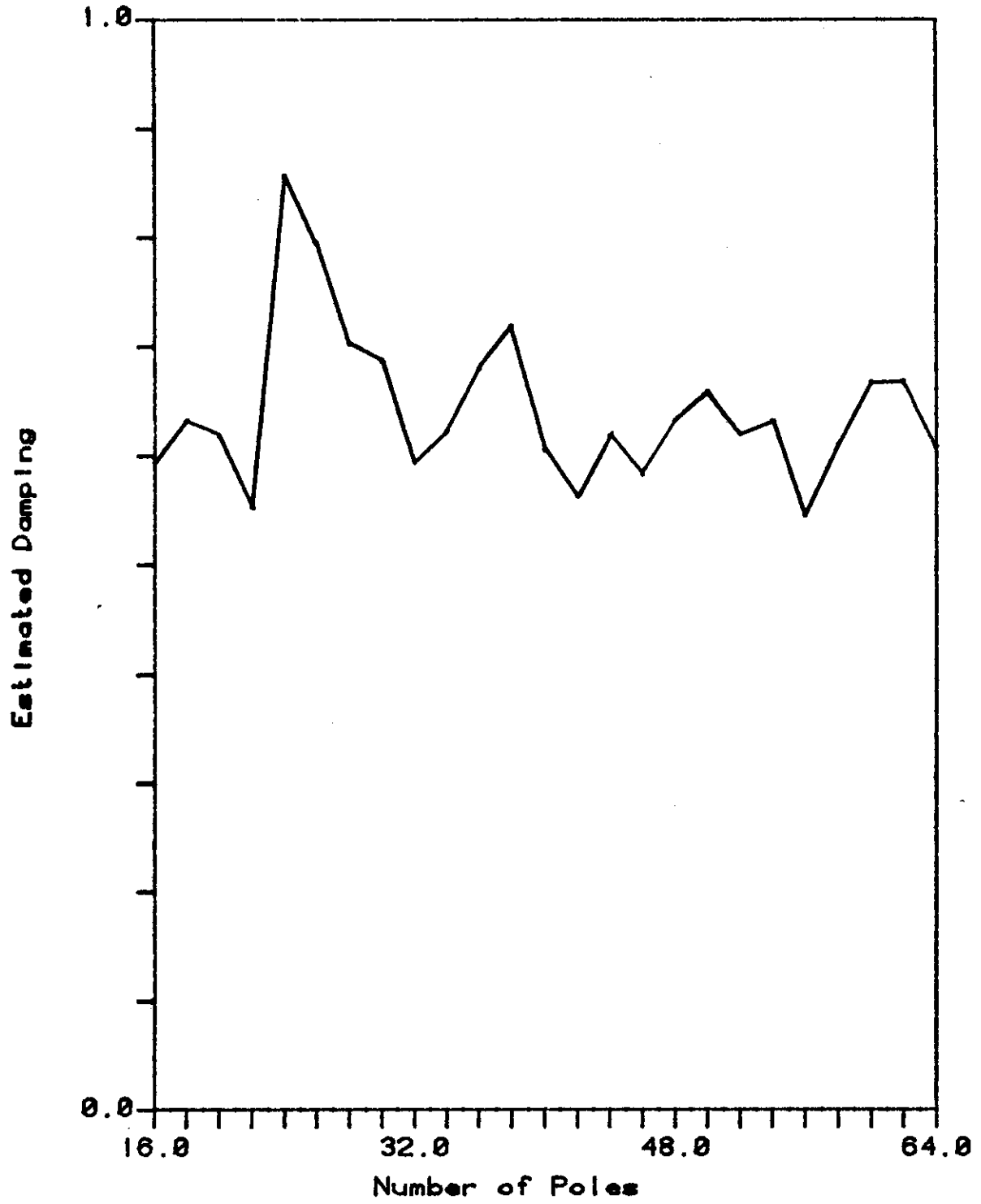


Fig VI-21: MEM Damping Estimates for 30 kt. Sea State

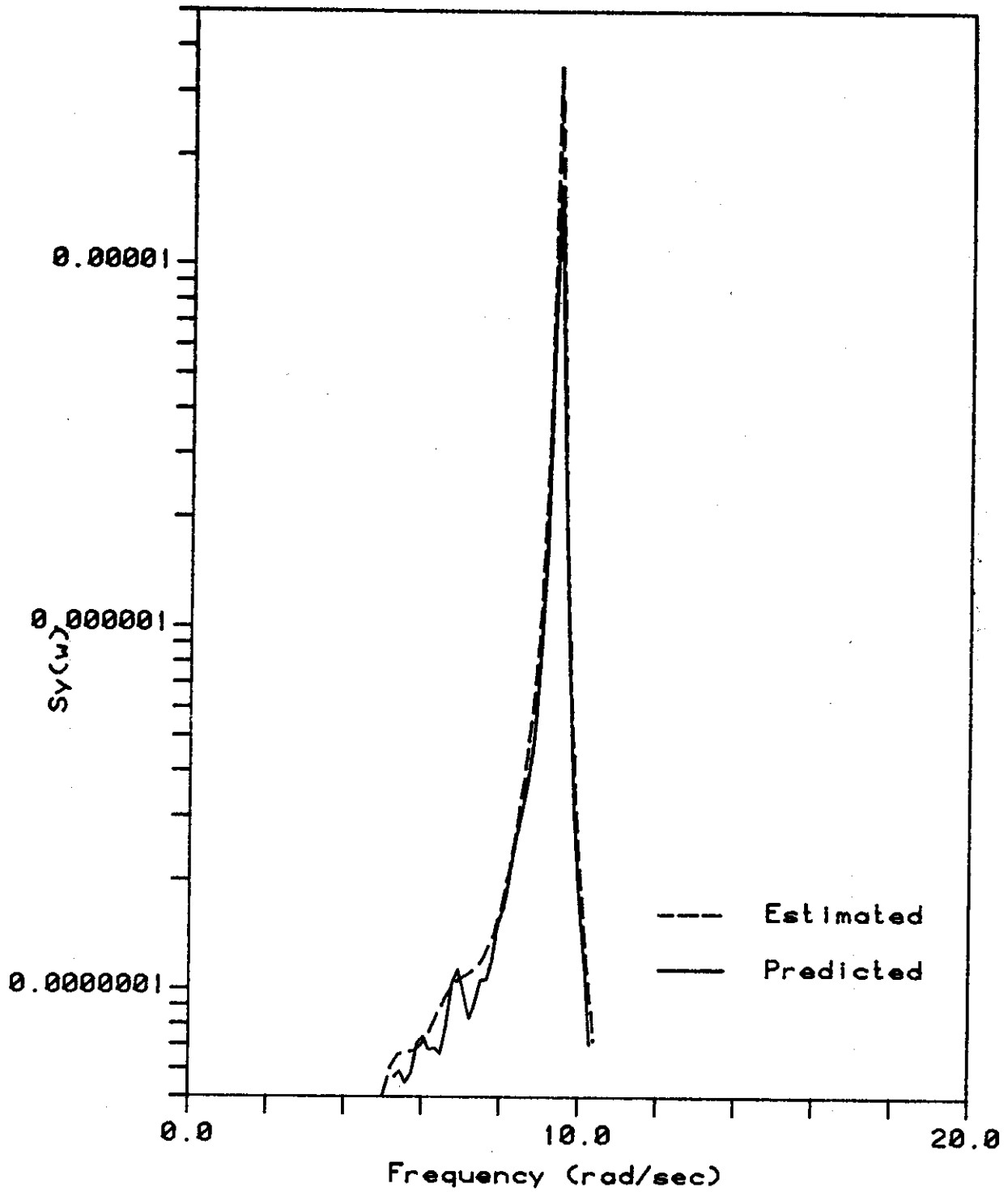


Fig VI-22: Cylinder Deflection Spec.
for 30 kt. Sea State

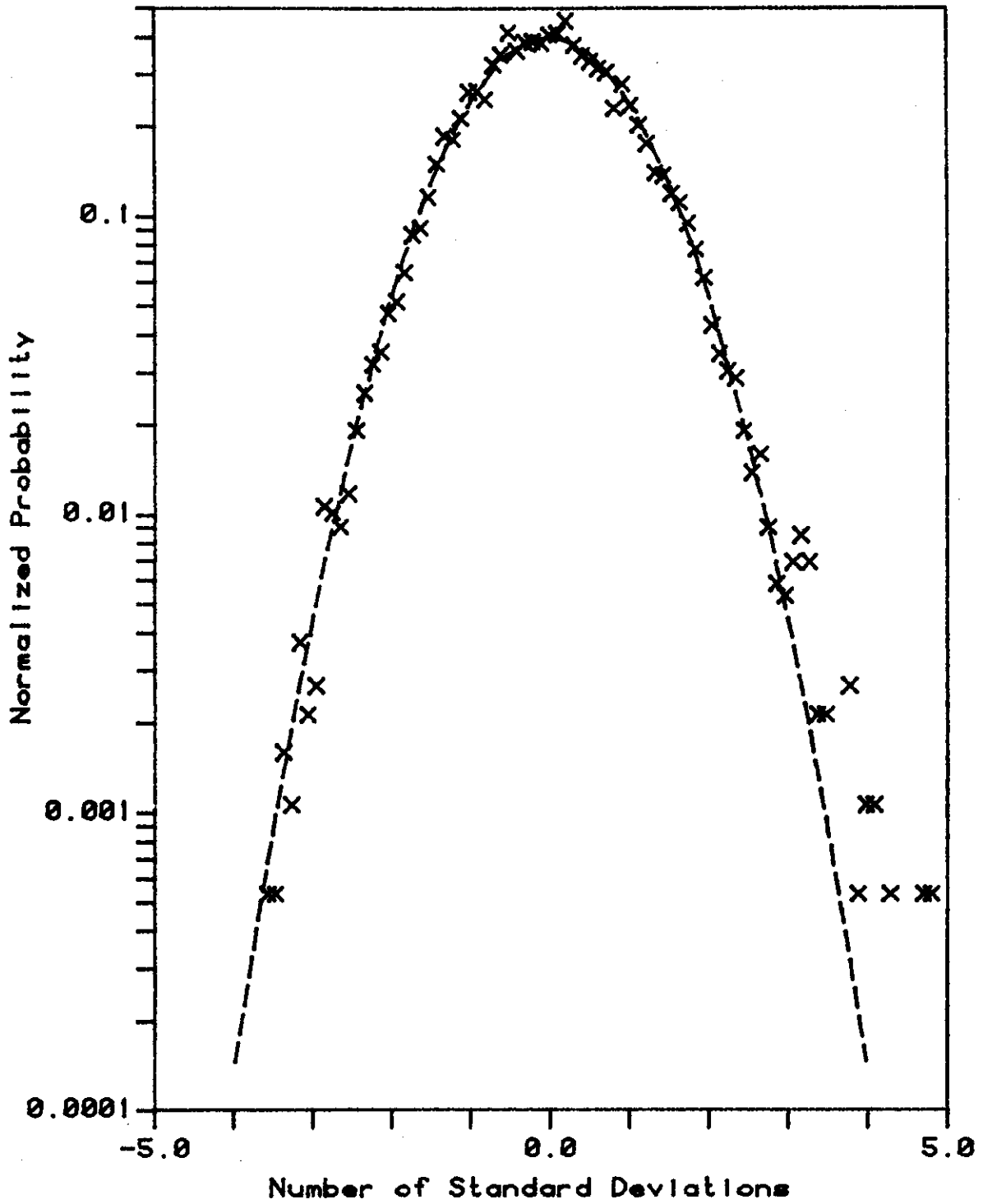


Fig VI-23: Wave Elevation Histogram for 40 kt. Sea State

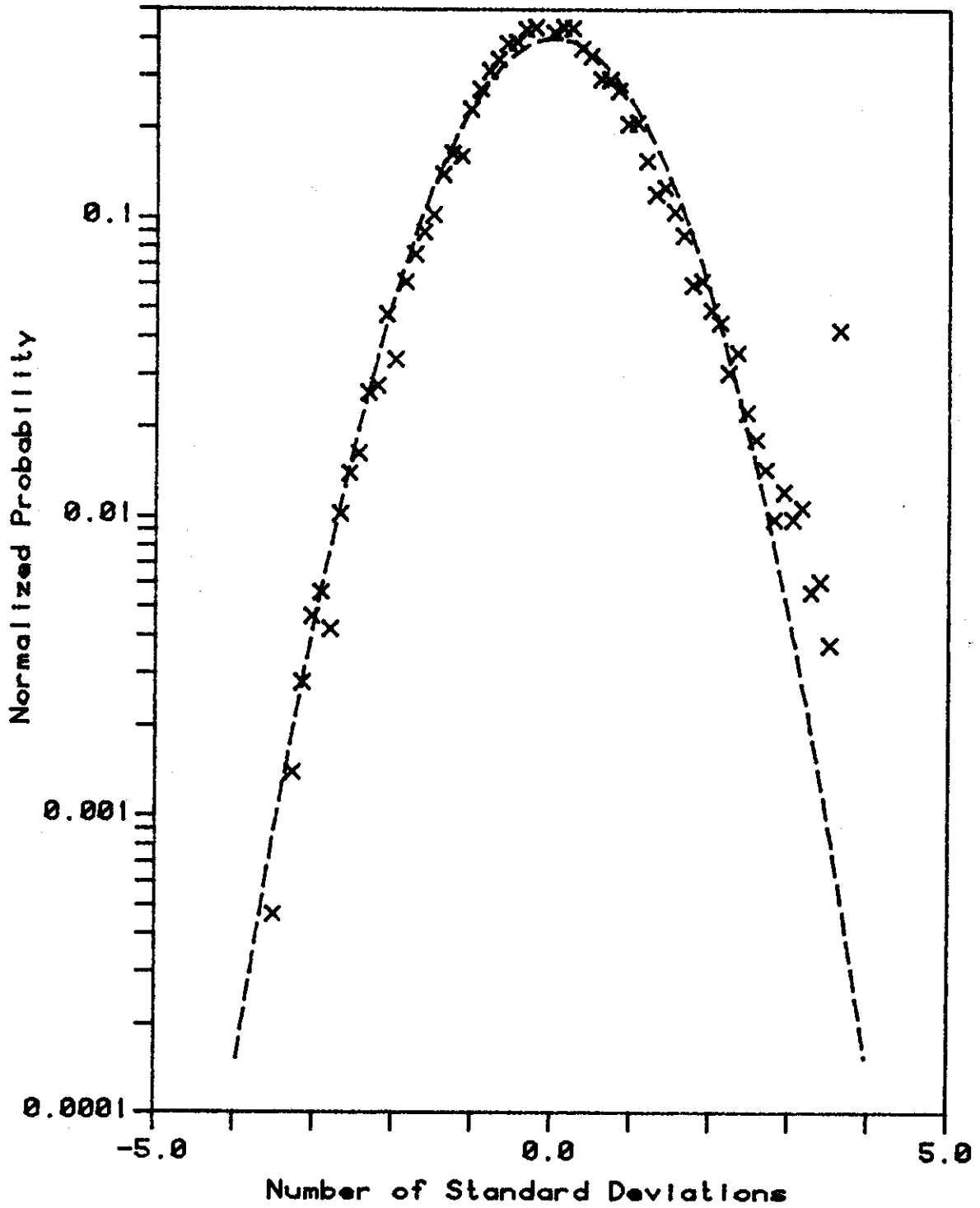


Fig VI-24: Wave Force Histogram for 40 kt. Sea State

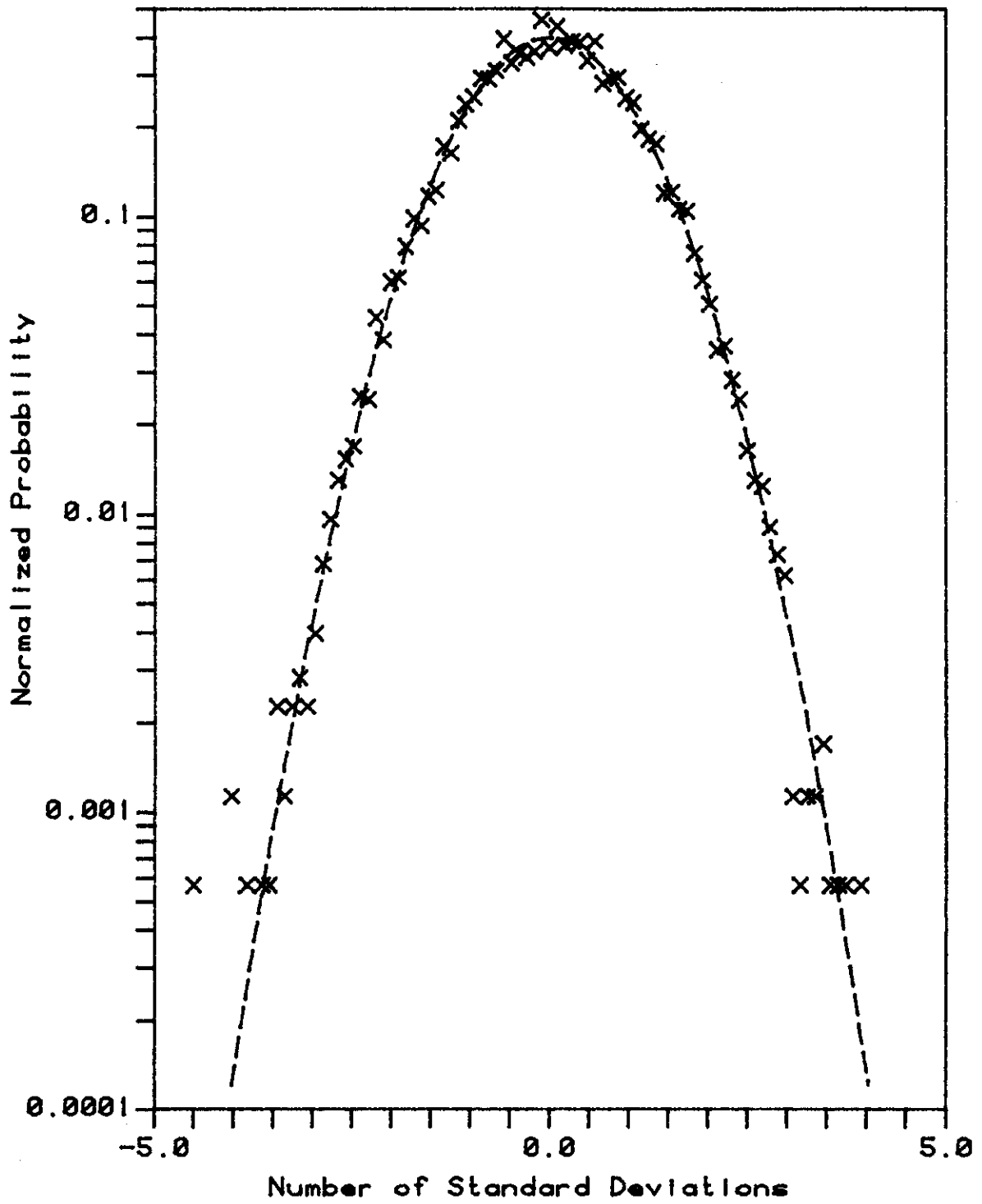


Fig VI-25: Cylinder Deflection Hist.
for 40 kt. Sea State

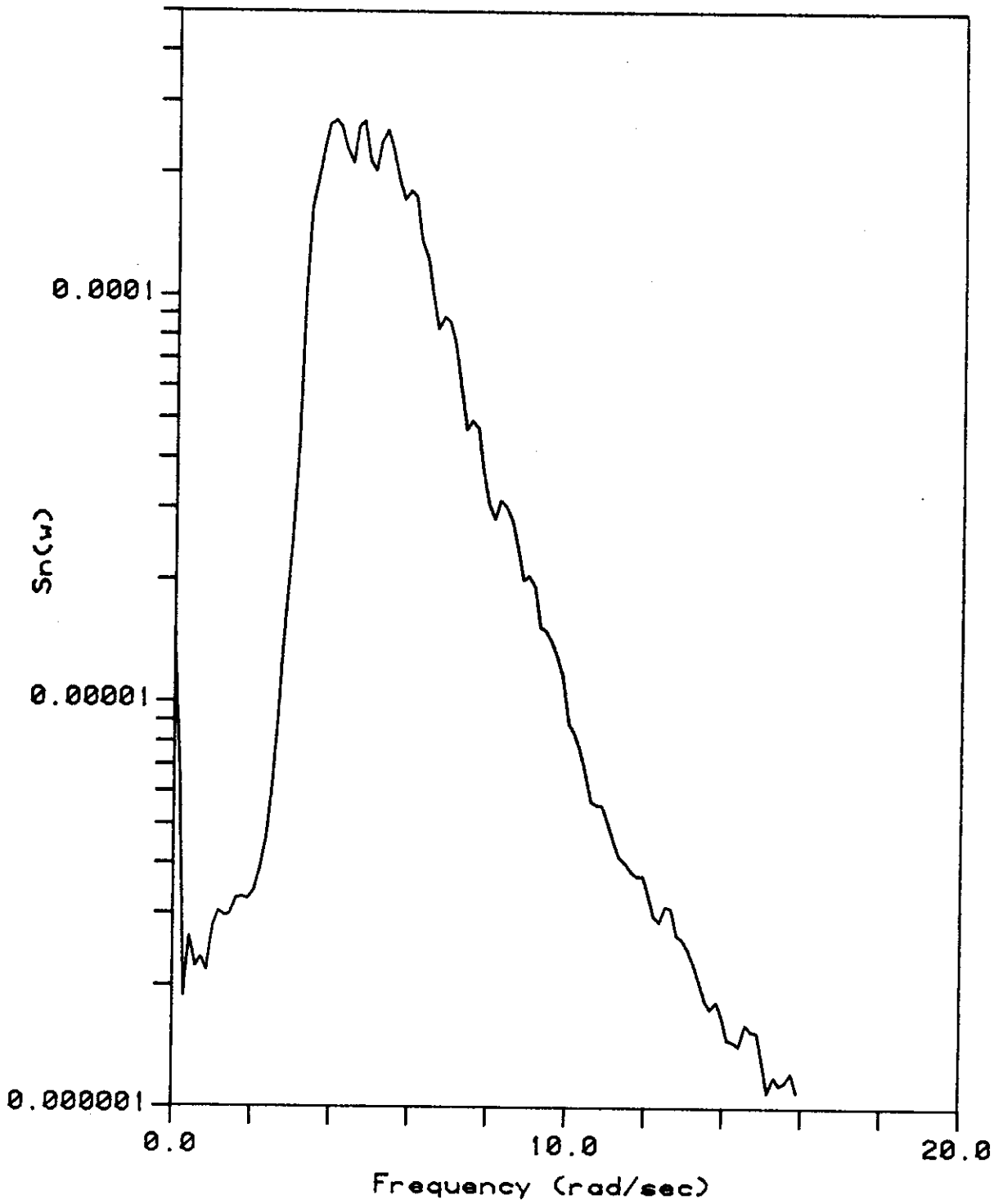


Fig VI-26: Wave Elevation Spectrum for 40 kt. Sea State

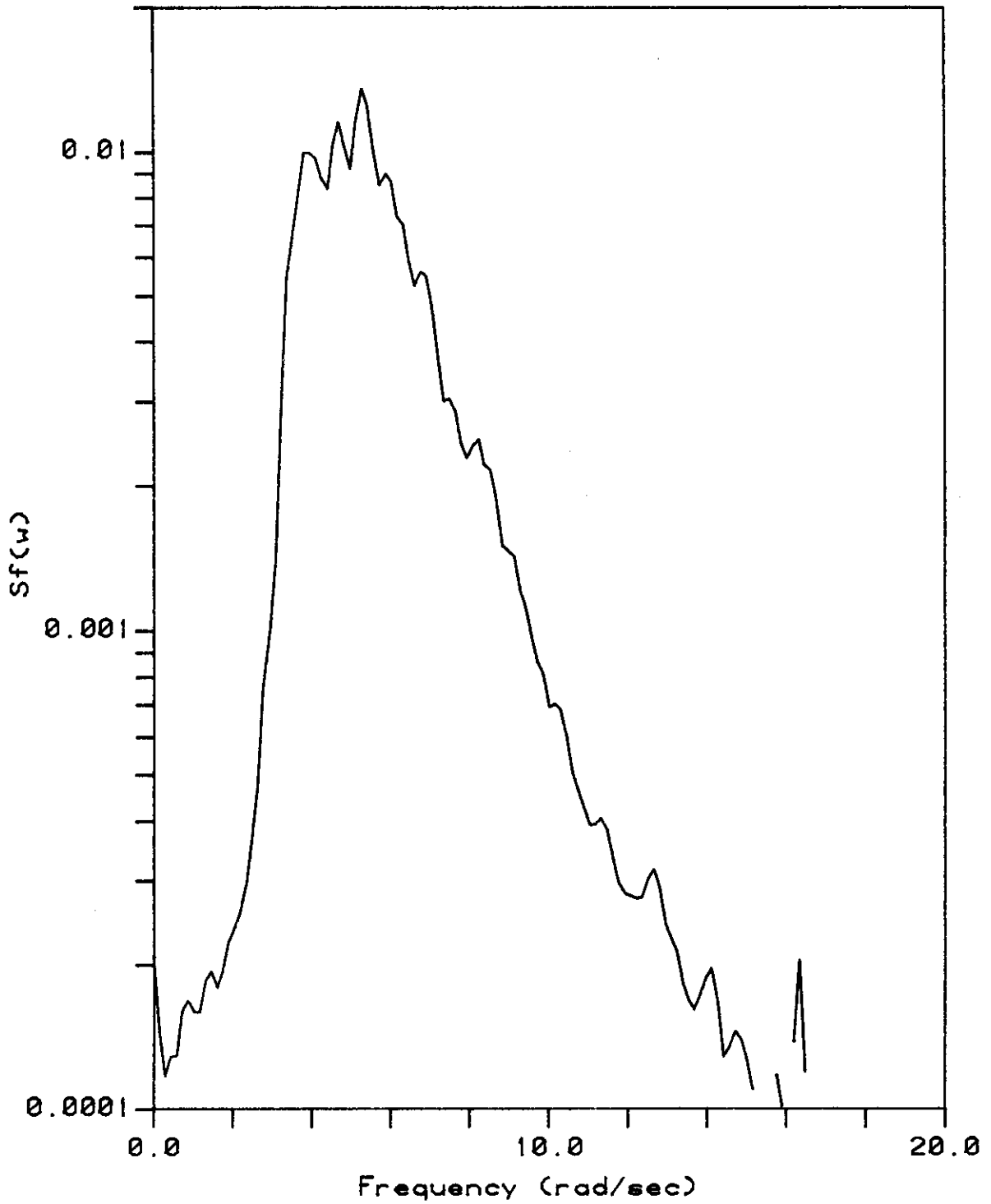


Fig VI-27: Wave Force Spectrum
for 40 kt. Sea State

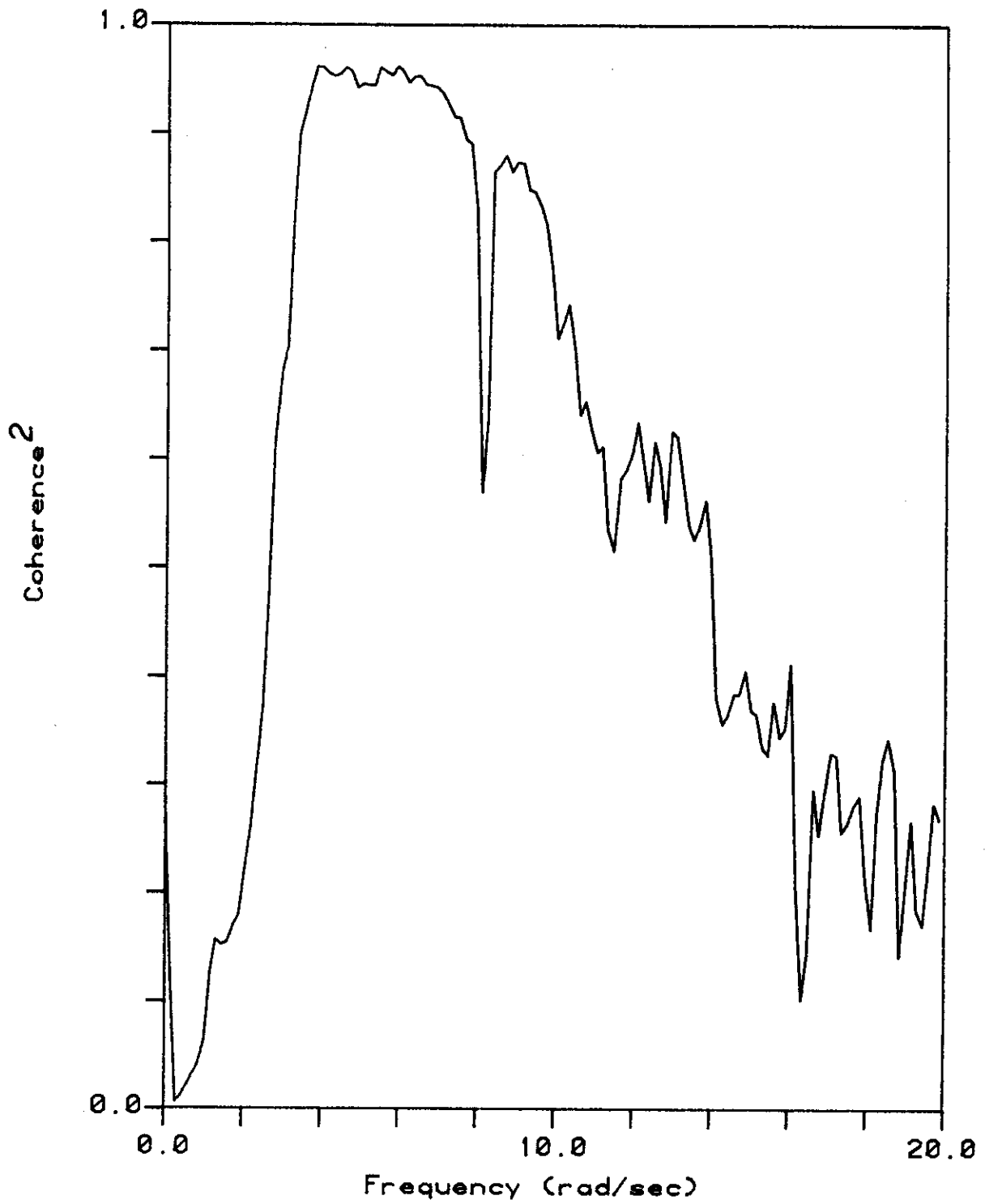


Fig VI-28: Wave Elevation/Force Coh. for 40 kt. Sea State

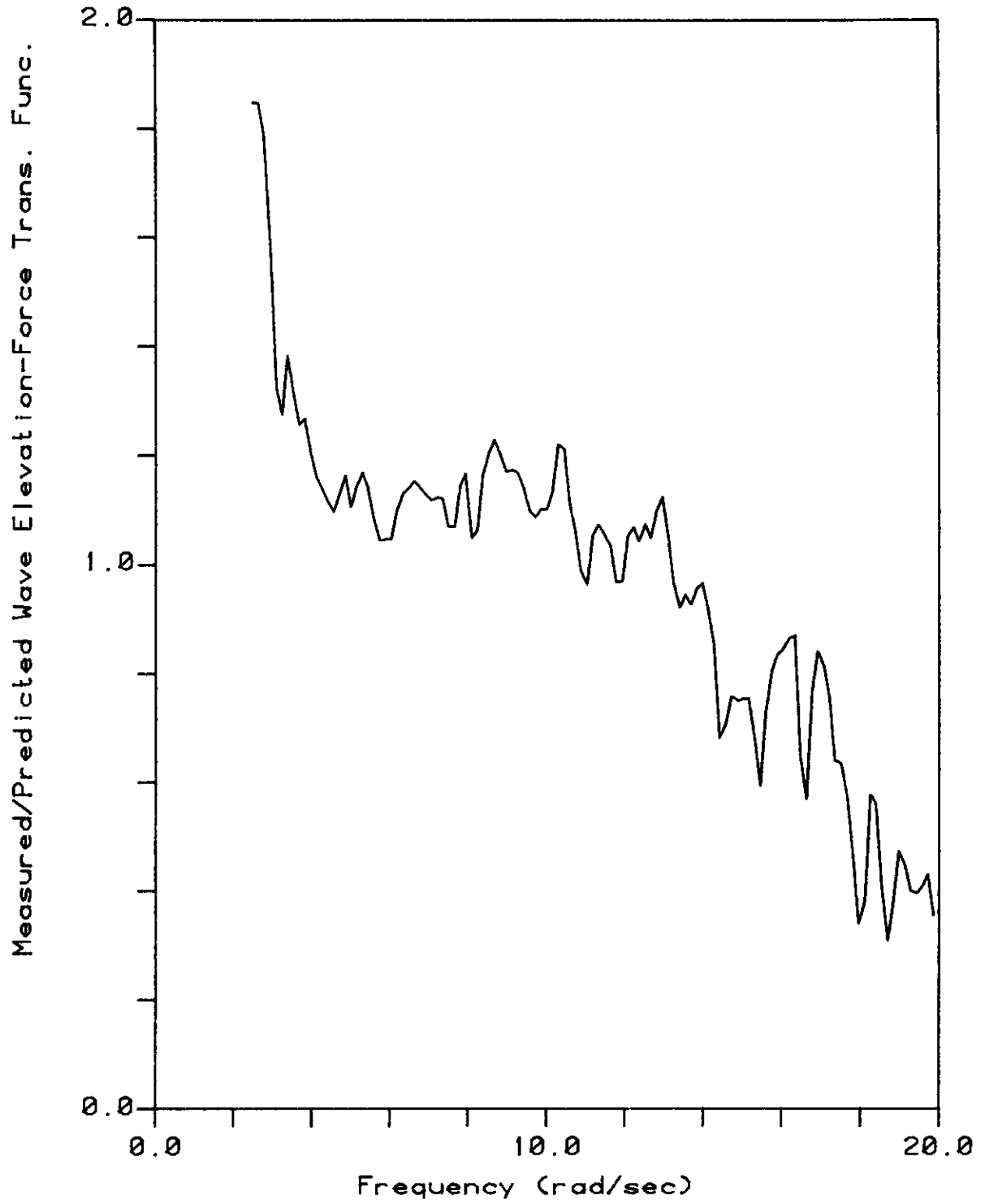


Fig VI-29: Inertial Force on Cylind.
for 40 kt. Sea State

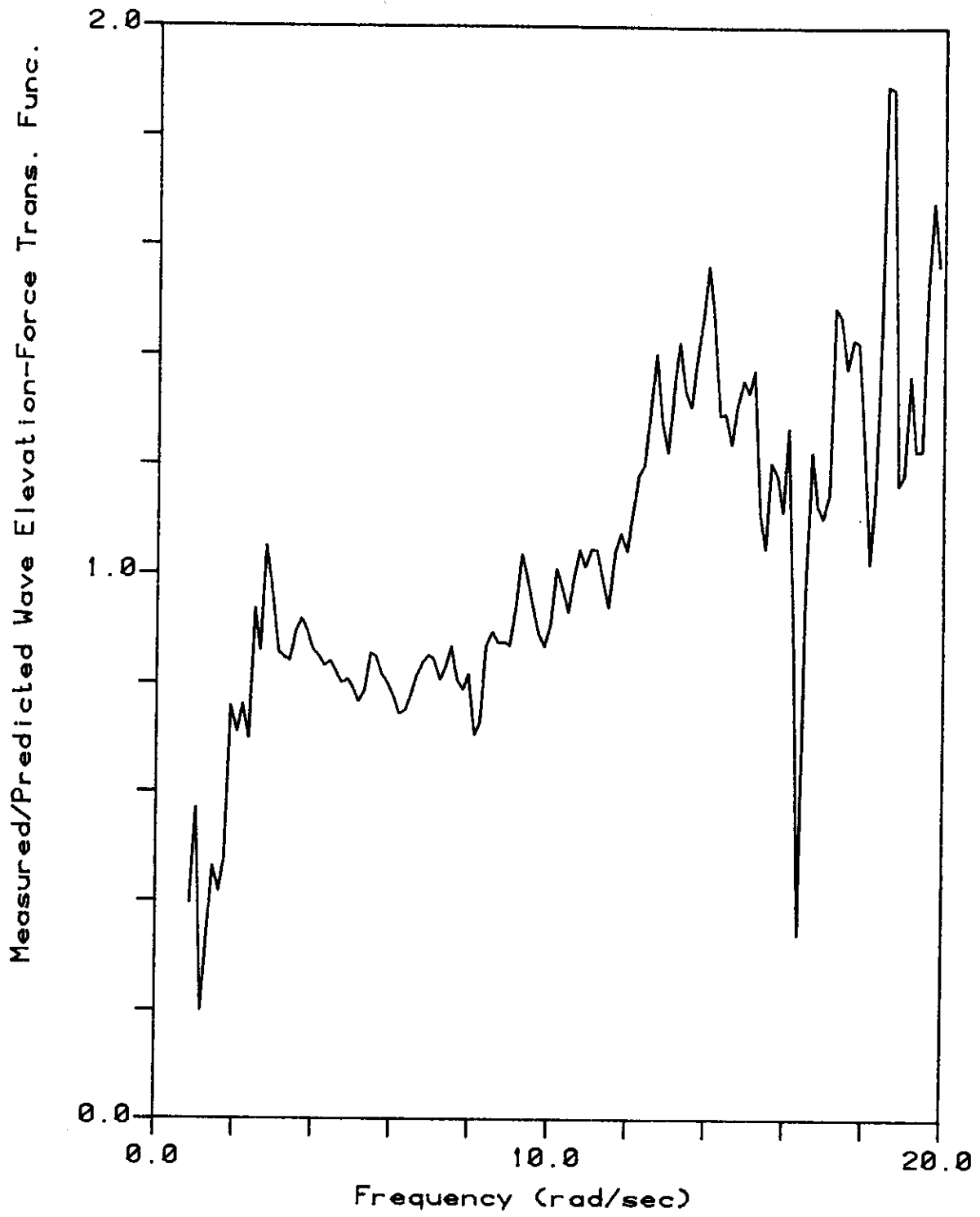


Fig VI-30: Drag Force on Cylinder for 40 kt. Sea State

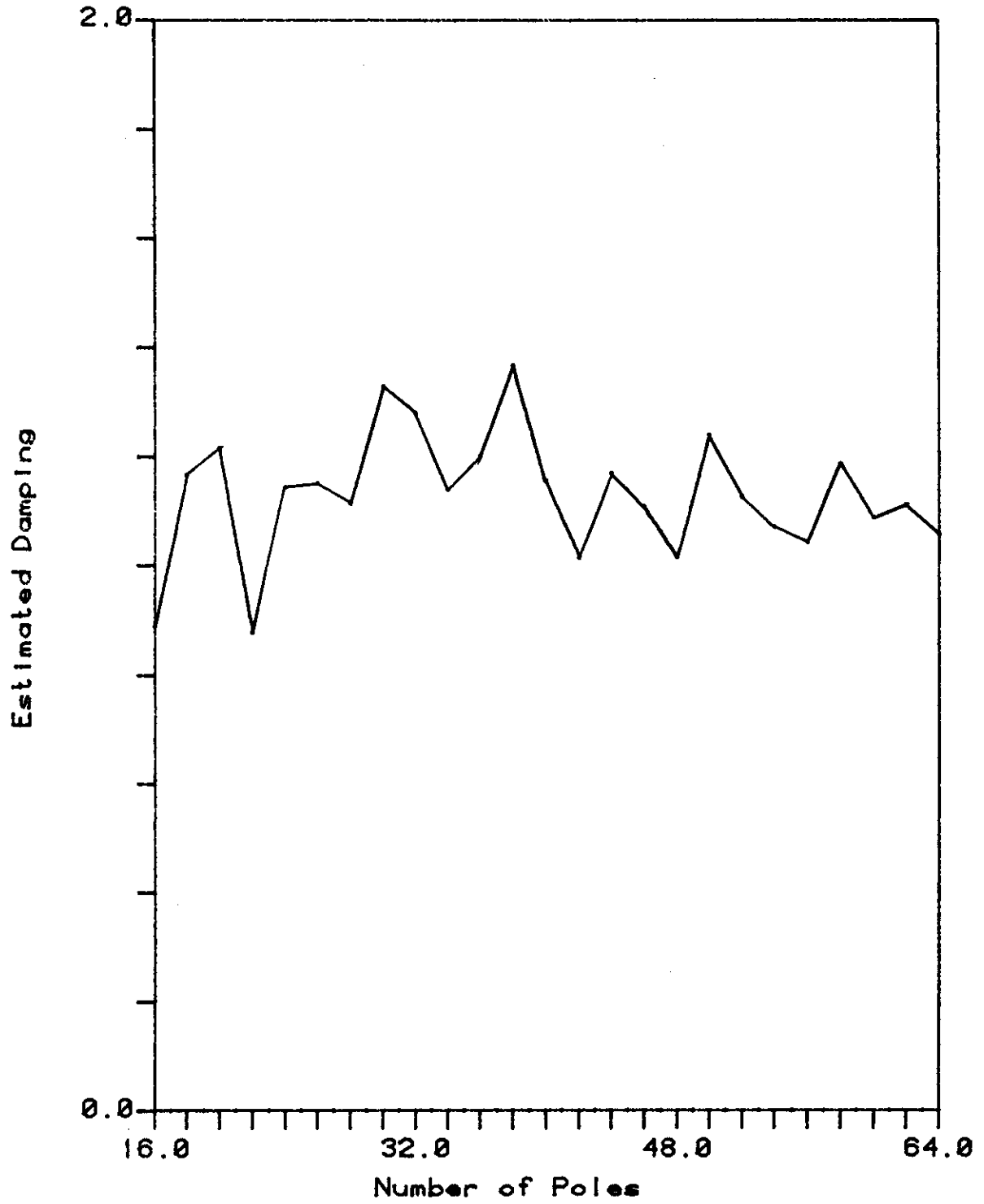


Fig VI-31: MEM Damping Estimates for 40 kt. Sea State

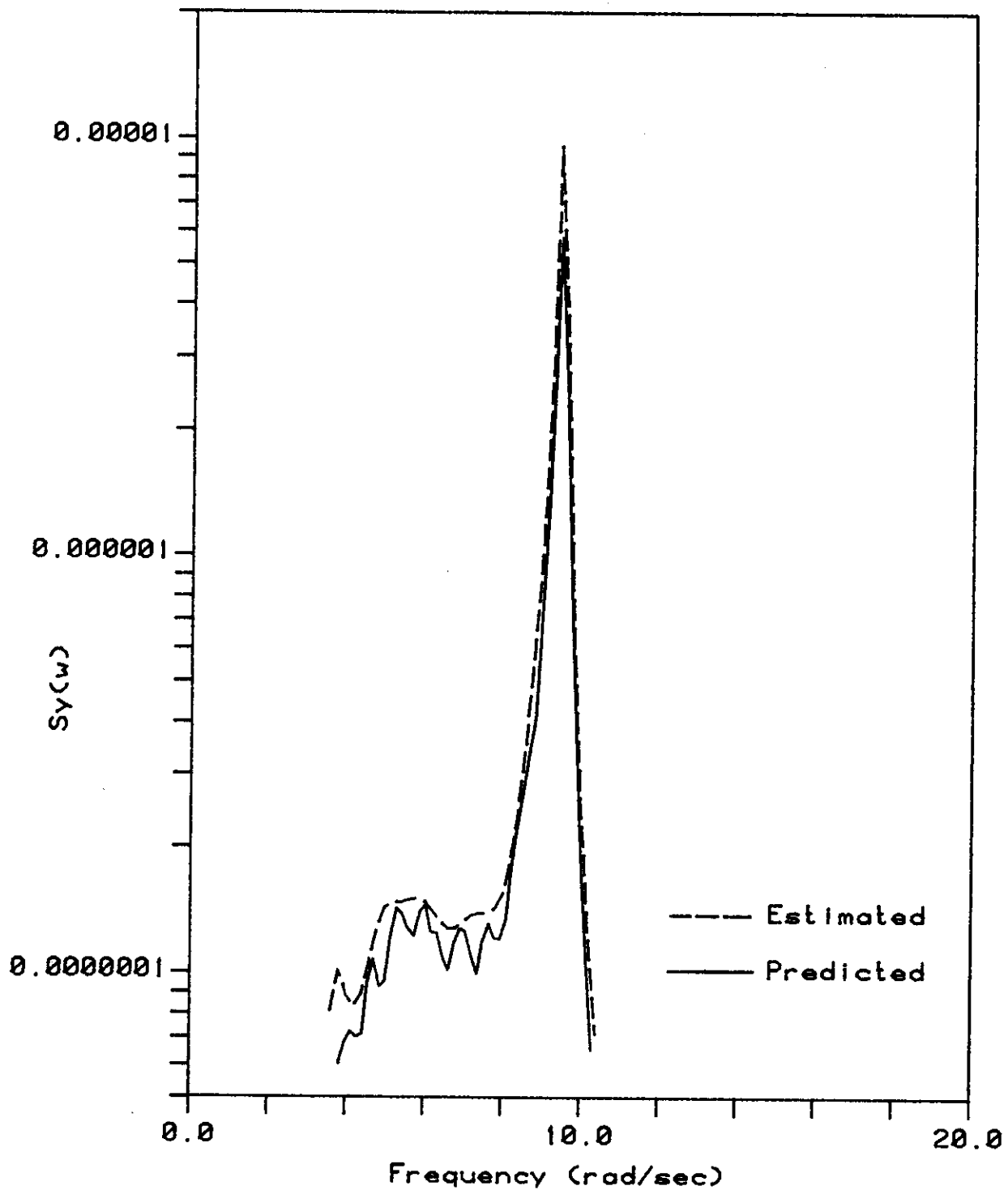


Fig VI-32: Cylinder Deflection Spec.
for 40 kt. Sea State

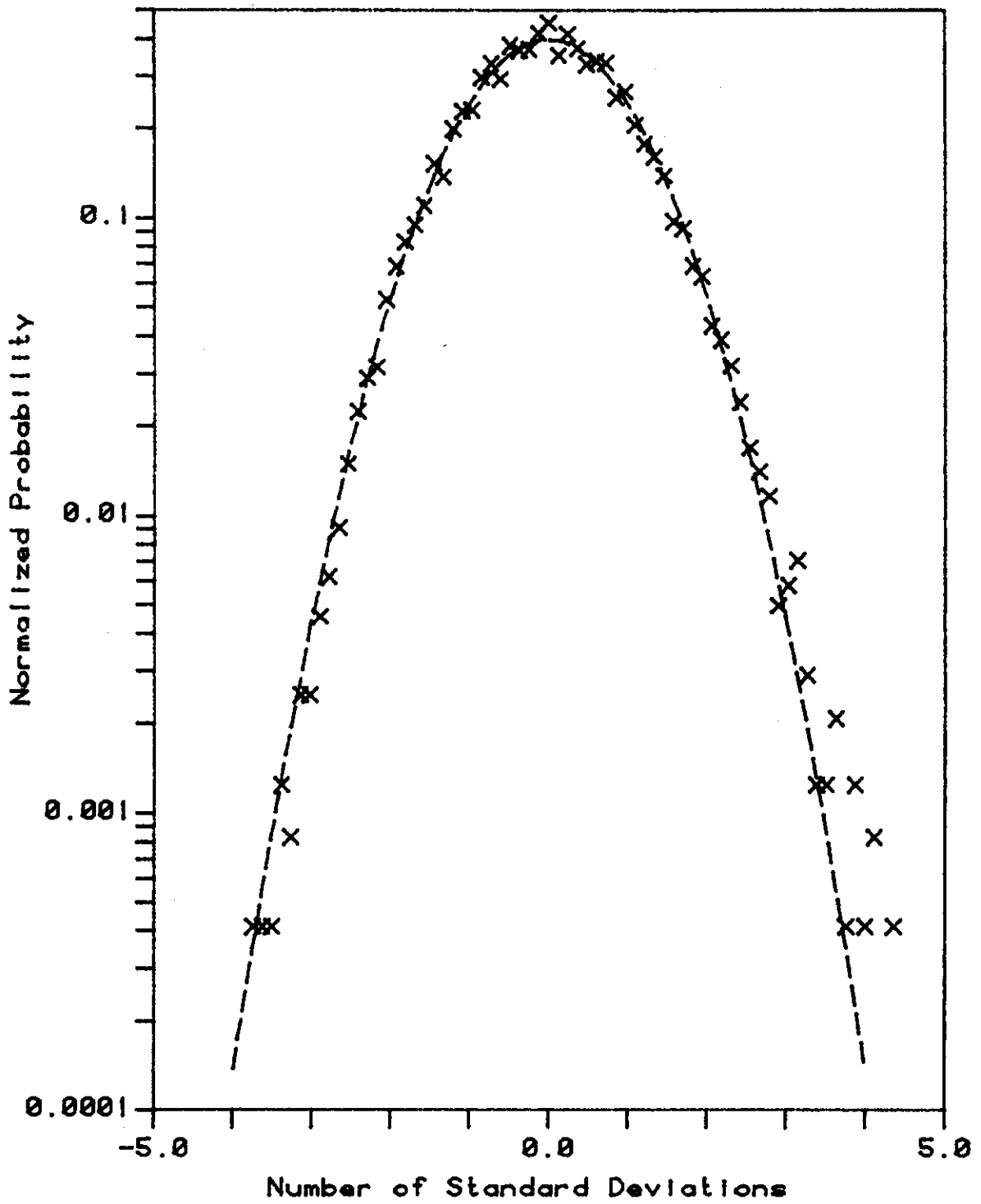


Fig VI-33: Wave Elevation Histogram for 50 kt. Sea State

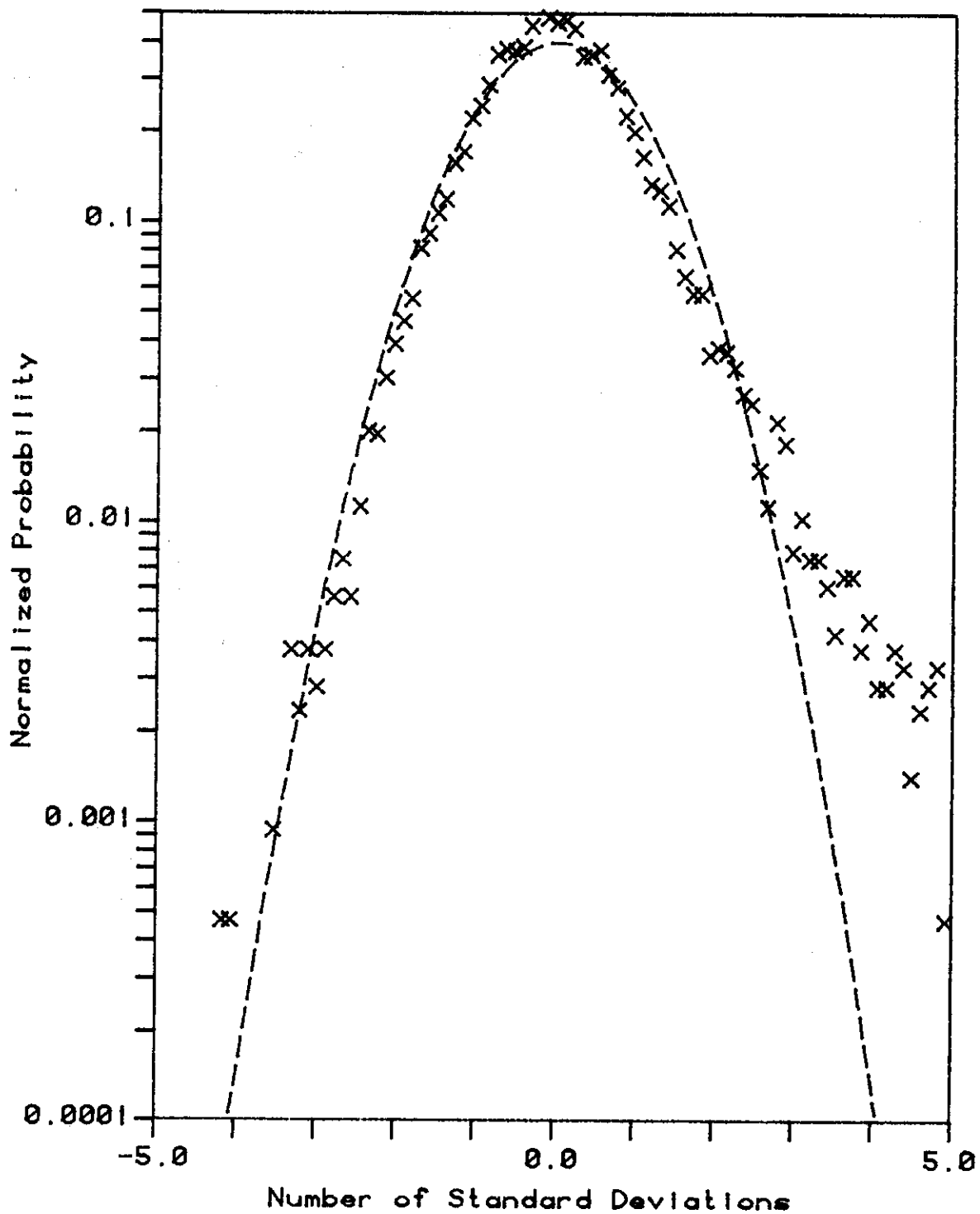


Fig VI-34: Wave Force Histogram for 50 kt. Sea State

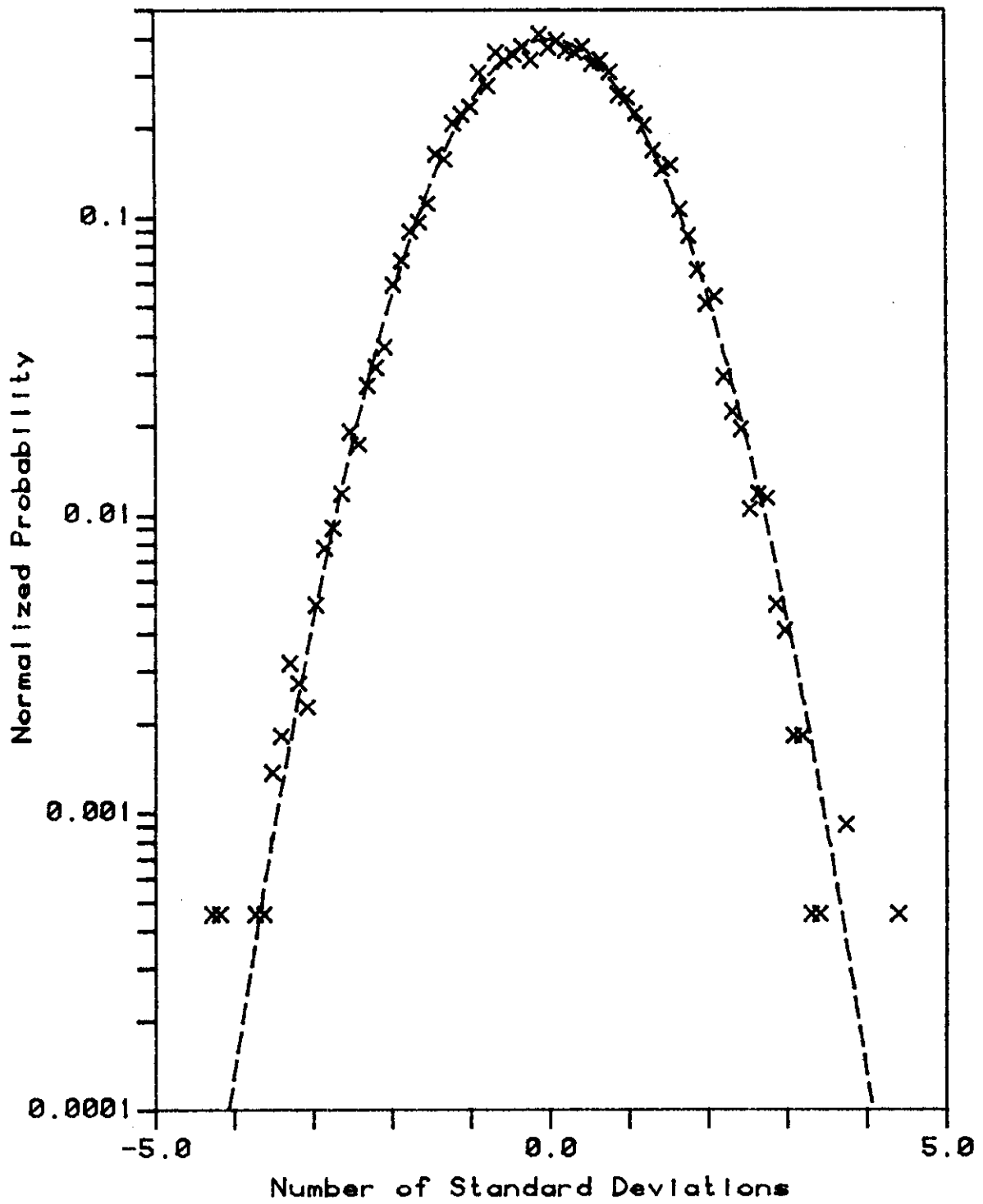


Fig VI-35: Cylinder Deflection Hist.
for 50 kt. Sea State

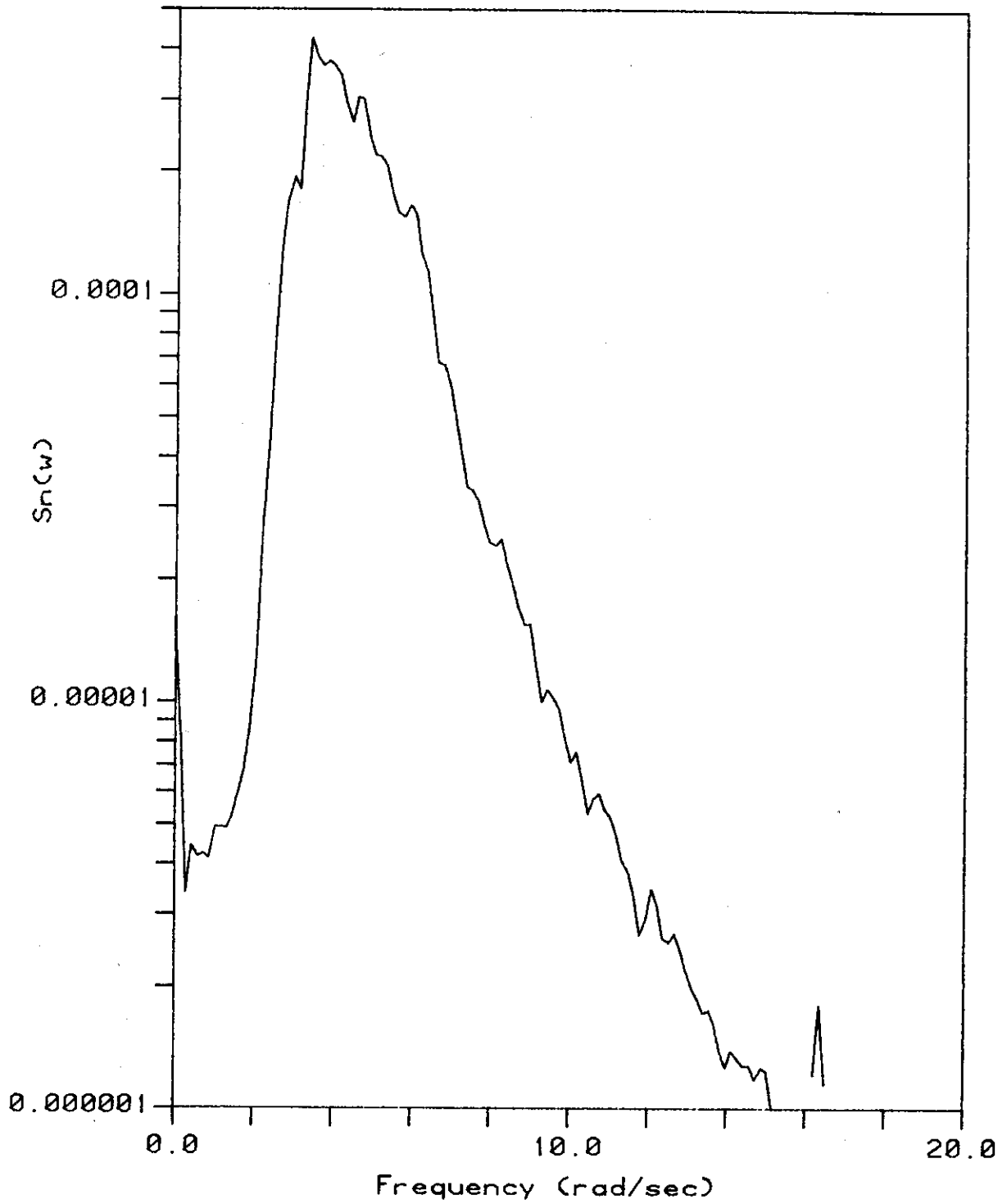


Fig VI-36: Wave Elevation Spectrum
for 50 kt. Sea State

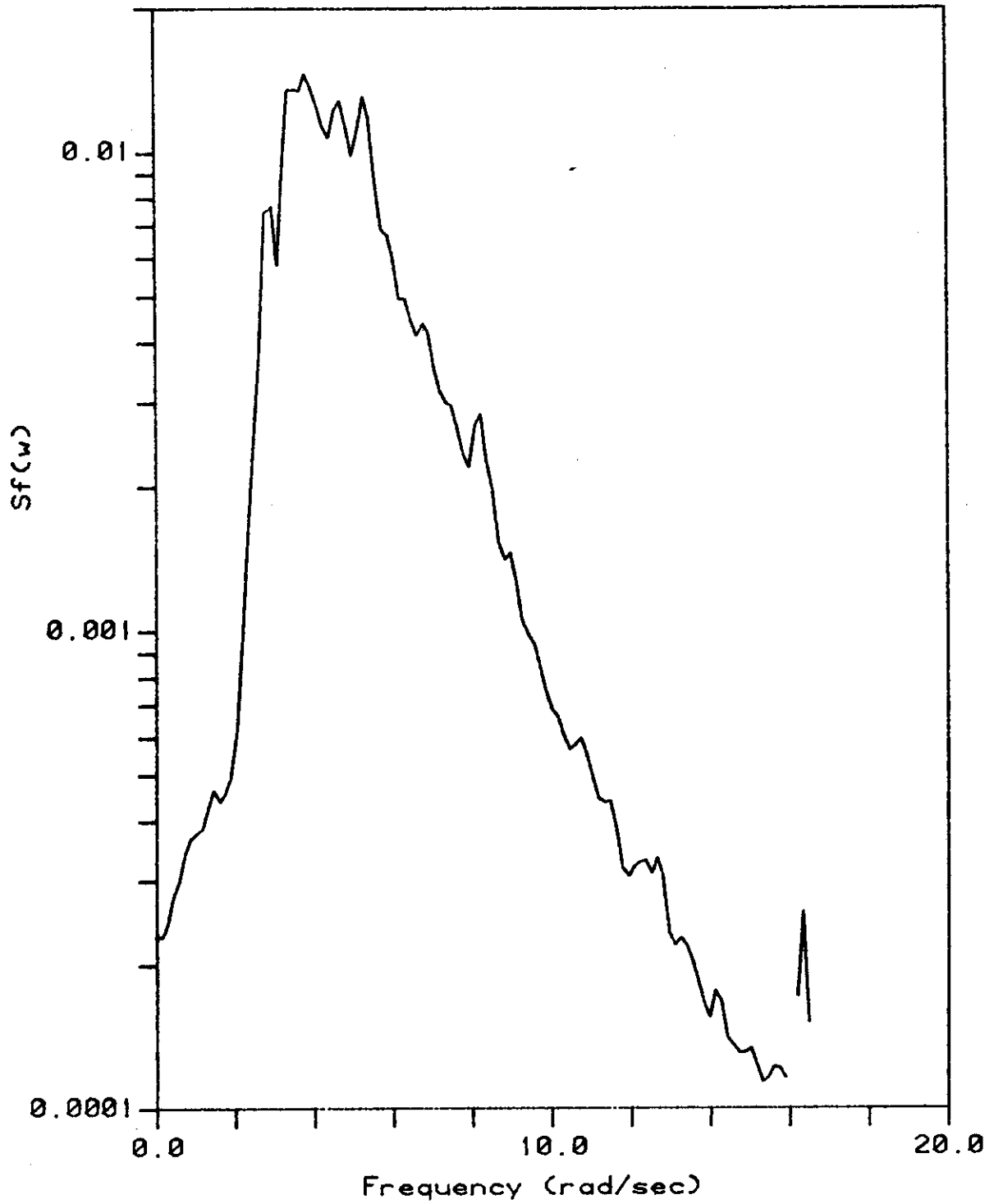


Fig VI-37: Wave Force Spectrum
for 50 kt. Sea State

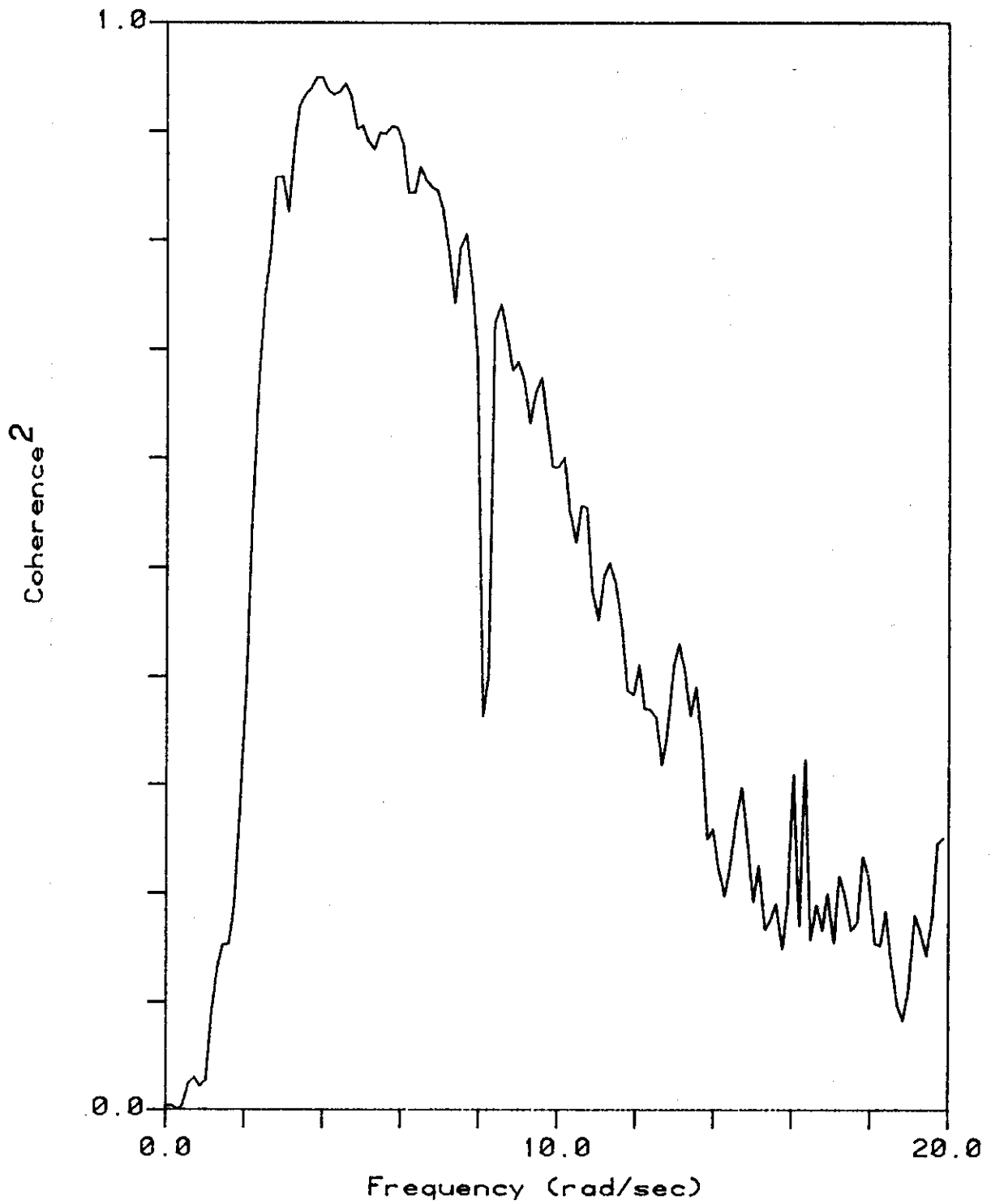


Fig VI-38: Wave Elevation/Force Coh.
for 50 kt. Sea State

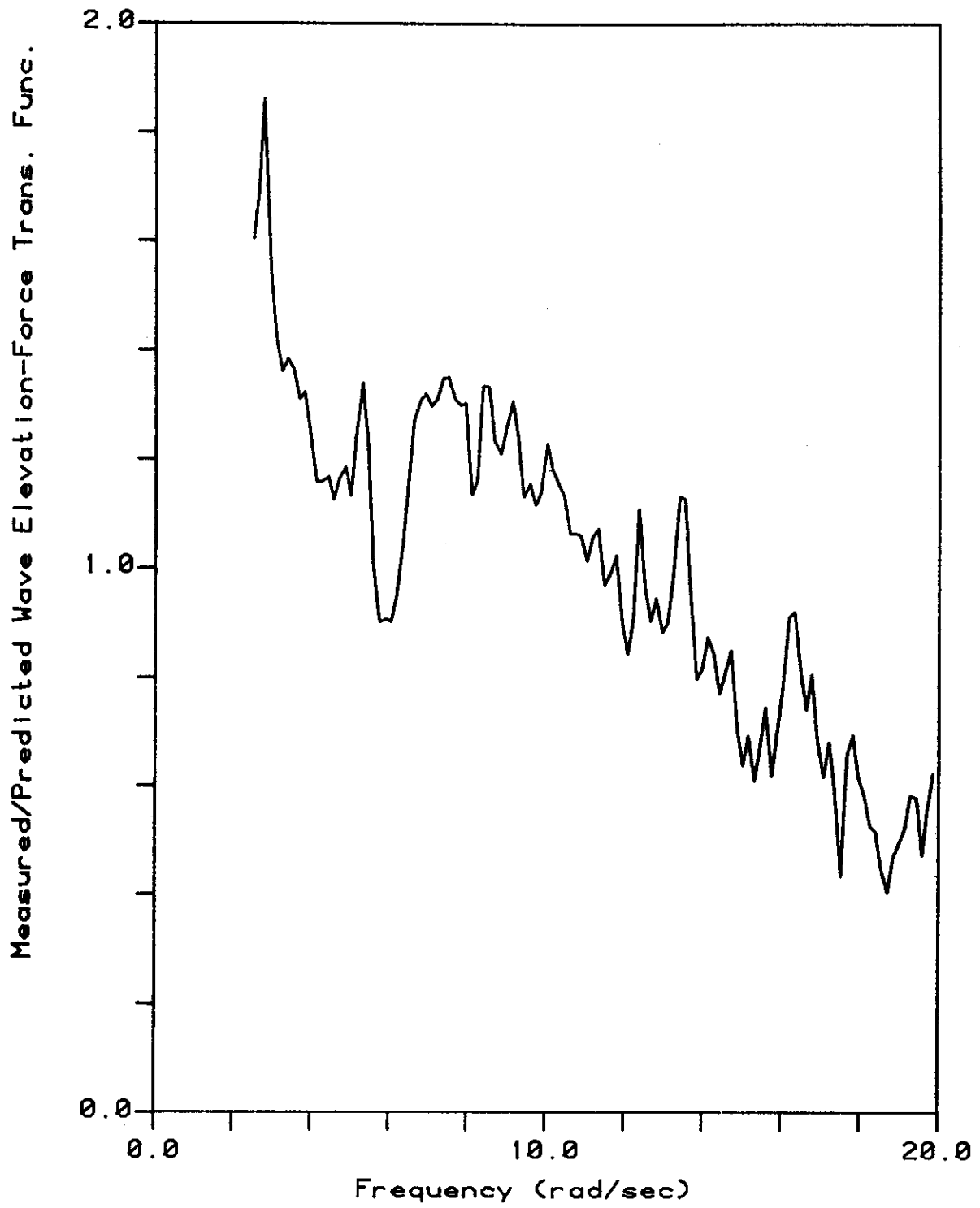


Fig VI-39: Inertial Force on Cylind.
for 50 kt. Sea State

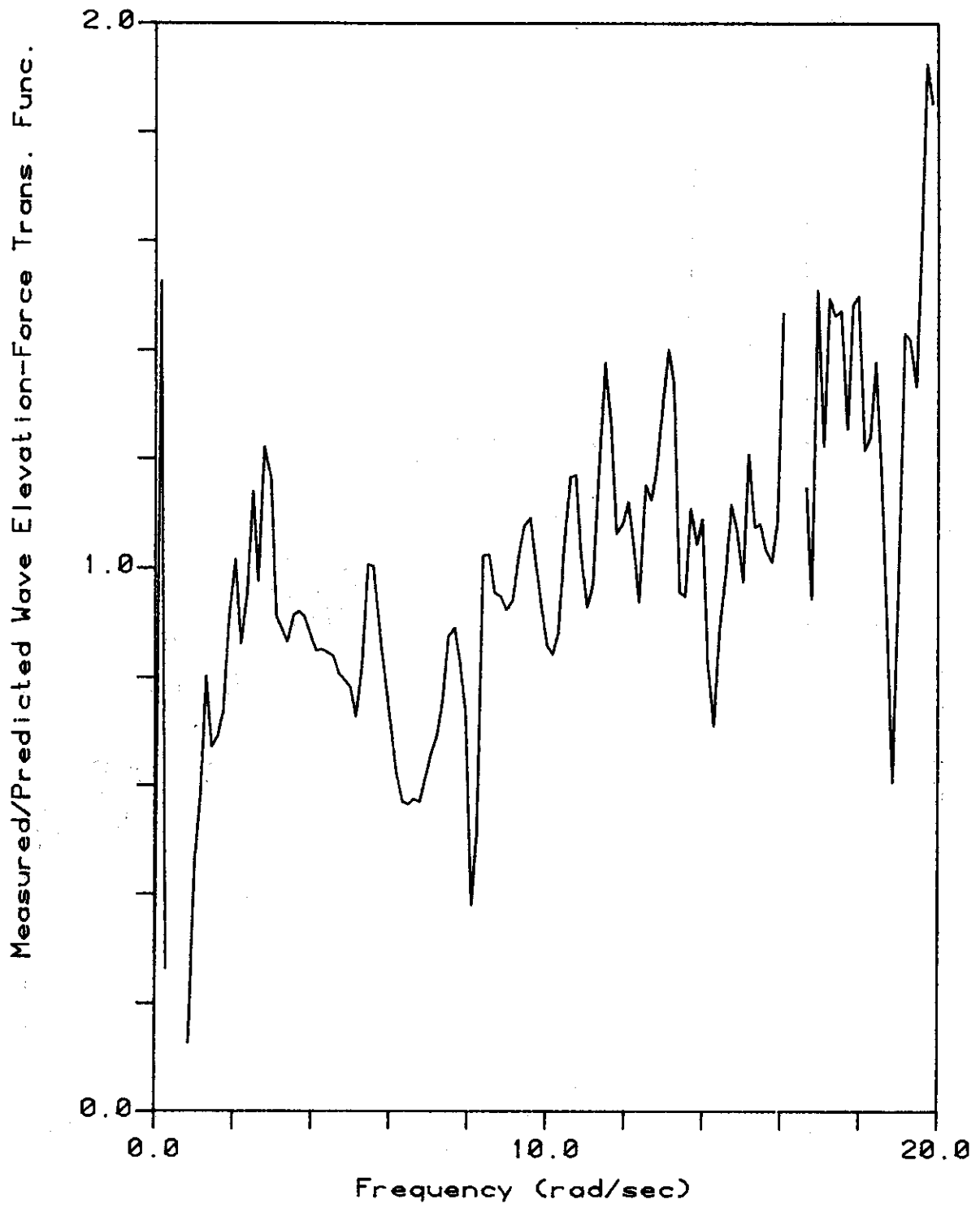


Fig VI-40: Drag Force on Cylinder for 50 kt. Sea State

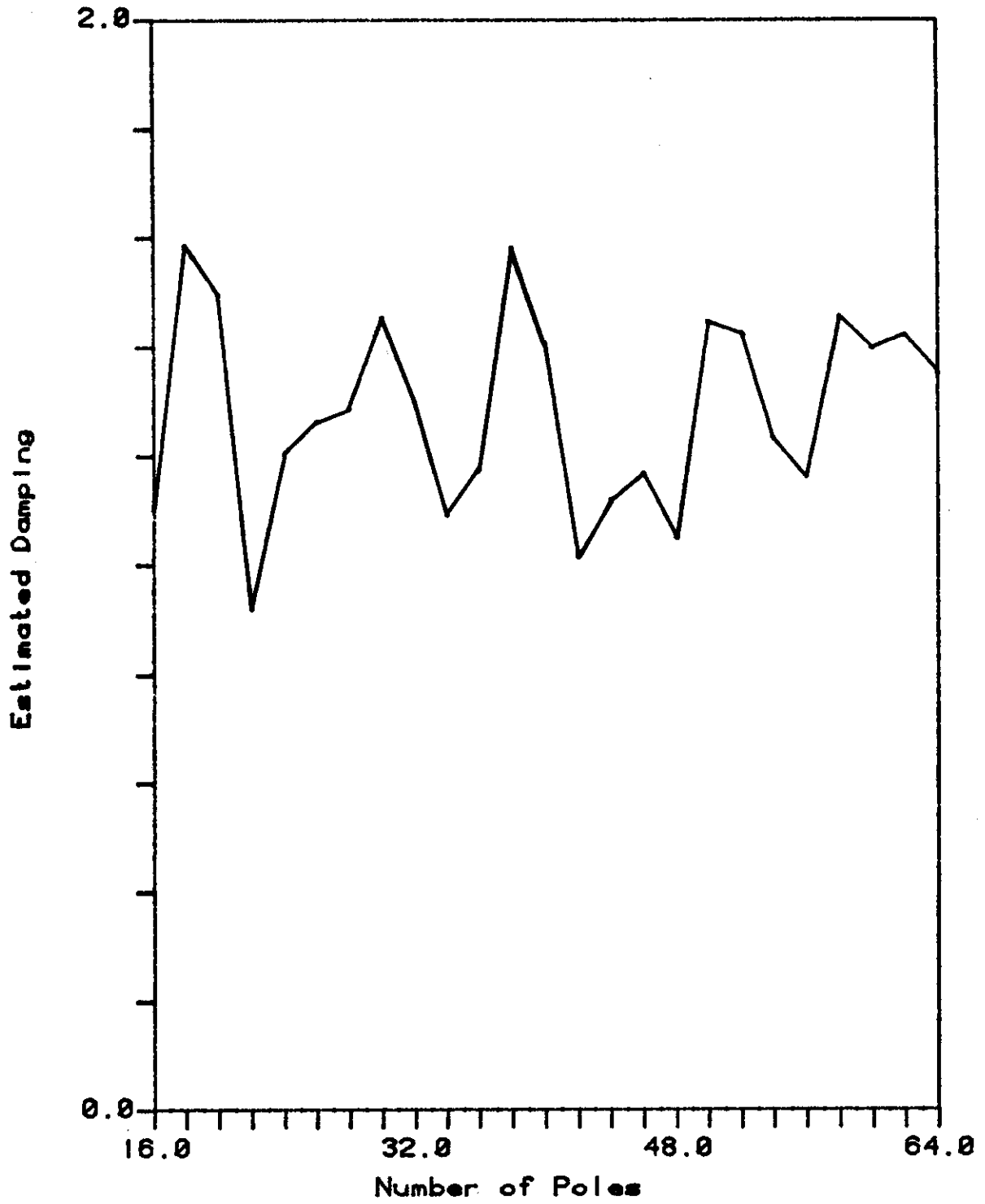


Fig VI-41: MEM Damping Estimates for 50 kt. Sea State

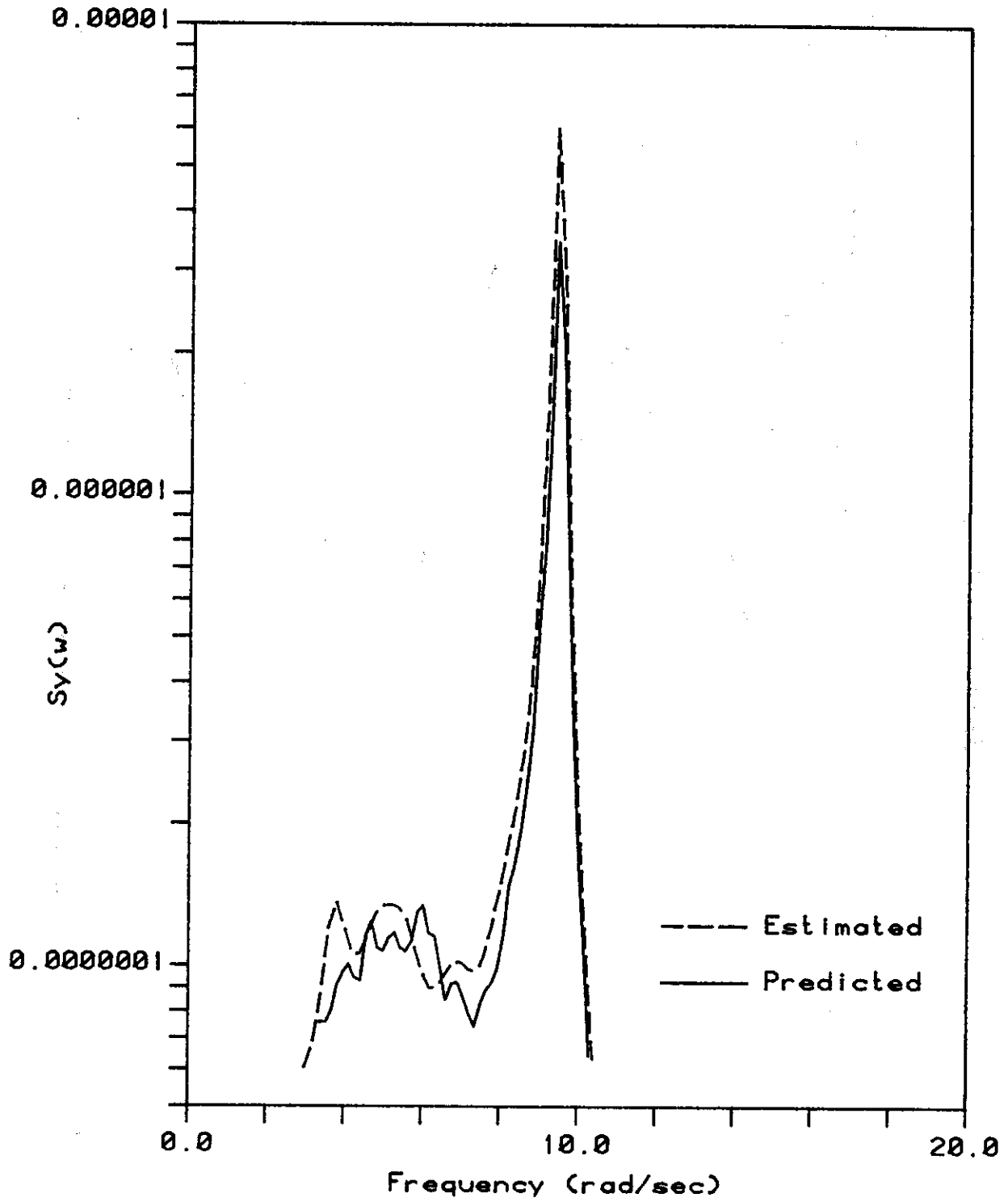


Fig VI-42: Cylinder Deflection Spec.
for 50 kt. Sea State

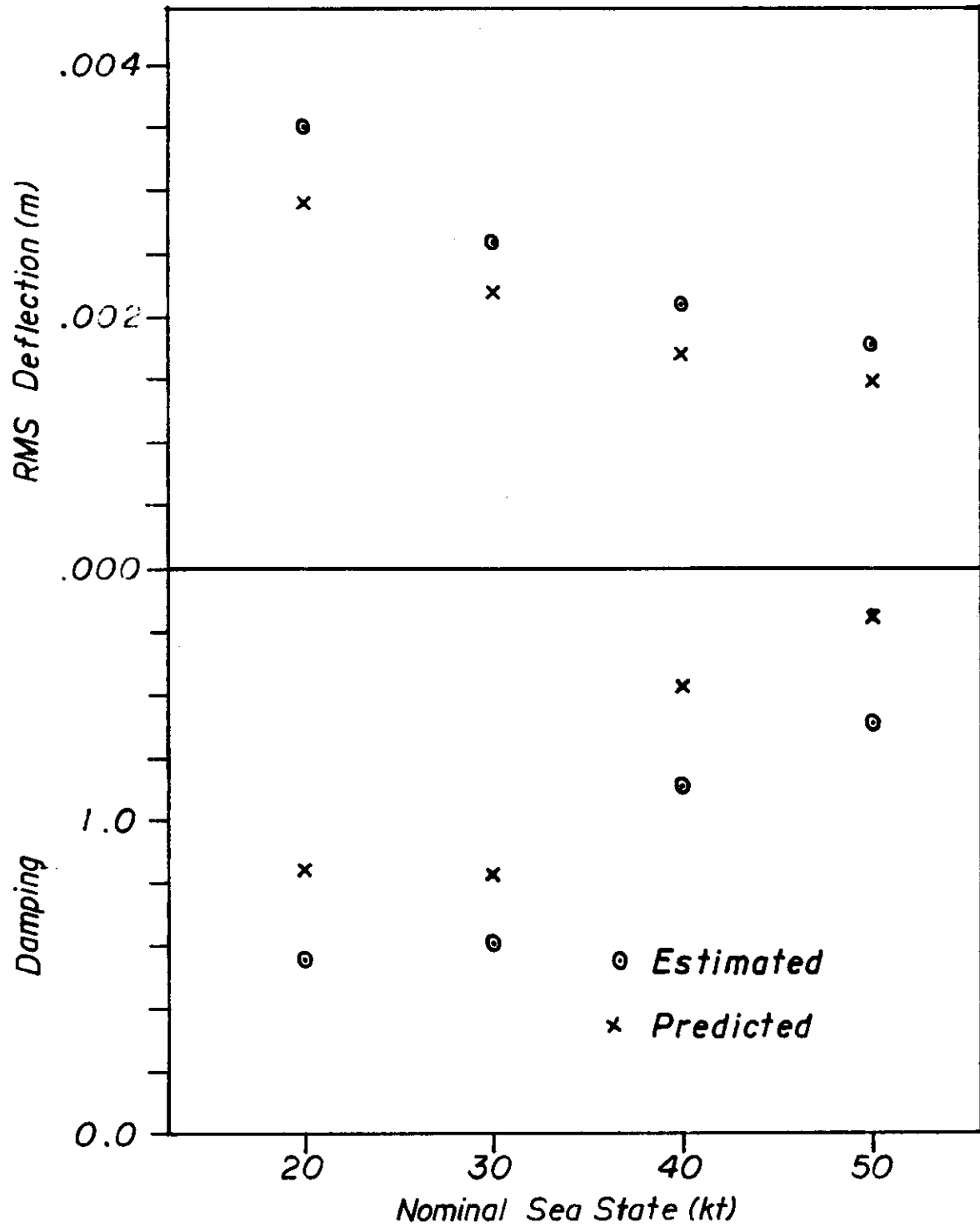


Fig VI-43: Estimated and Predicted Response versus Sea State

Nominal Sea State	20 kt.	30 kt.	40 kt.	50 kt.
Sig Wave Height (m)	0.050	0.072	0.118	0.132
Mean Frequency (rad/sec)	8.55	7.18	5.92	5.19
RMS Particle Velocity (m/sec)	0.121	0.130	0.174	0.172
Reynold's Number	3100	3300	4400	4400
Keulegan-Carpenter Number	3.5	4.5	7.3	8.2
RMS Force on Cylinder (N)	0.136	0.151	0.228	0.249
Cm Adjustment	0.95	0.95	1.10	1.20
Dc Adjustment	1.20	0.85	0.80	0.80
Predicted RMS Deflection (m)	.0029	.0022	.0017	.001
RMS Deflection of Cylinder (m)	.0035	.0026	.0021	.0018
MEM Estimate of Nat. Freq. (rad/sec)	9.356	9.387	9.431	9.456
Std. of Estimate	0.001	0.001	0.002	0.002
Predicted Damping (% of Crit.)	0.84	0.82	1.42	1.64
MEM Estimate of Damping (% of Crit.)	0.55	0.60	1.10	1.30
Std. of Estimate	0.07	0.08	0.12	0.12
# of Poles Used	46	44	44	64

Table VI-1: Summary of Results

VII. CONCLUSIONS

The purpose of this research has been to develop a method for predicting the motion spectra of an offshore platform in moderate seas. Particular emphasis was placed on the effect of the separated flow drag. To that end, a model of the behaviour of an offshore platform was developed which included separated flow drag through the relative velocity formulation of Morison's equation. Because the model was non-linear, and therefore could not be manipulated using standard random vibration techniques, predictions of the motion spectra were obtained using the approximate technique of Gaussian closure. Examination of the final relationship revealed that the non-linear, separated flow drag had approximately the same effect on the predicted spectra as an additional force on the structure, linearly related to the incident fluid velocity and an additional sea-state dependent hydrodynamic damping.

Two tests of the spectral predictor were performed. Spectra predicted using the derived relationship were compared to spectra estimated from sample time histories for a simple, hypothetical system modelled on a computer. Additional damping in excess of the specified system damping was observed in the sample time histories, in complete agreement with the hydrodynamic damping predicted. Similar results were obtained for a test of a small, spring-mounted cylinder excited by waves. Additional, sea-state dependent damping observed in the time histories agreed qualitatively with predicted hydrodynamic damping although the predicted values of damping always exceeded the observed values.

In conclusion, this research has demonstrated that separated flow drag leads to an effective hydrodynamic damping which is sea-state dependent. This additional damping was observed experimentally and predicted theoretically. The experimental results confirmed the suitability of the Gaussian closure technique in the solution of non-linear, random vibration problems of this type. It was also found that the relative-motion formulation of Morison's equation gave reasonable predictions of the hydrodynamic force on a cylinder in random waves, for judicious choices of the coefficients C_m and C_d .

The next logical step in this research is to apply the prediction equation to a real platform. One of the very large platforms, such as Cognac or Hondo, would be a good choice to study as these are the platforms most susceptible to fatigue damage through resonant response in moderate seas. The main effort required in order to predict response spectra or even modal damping for one of these platforms would be to transform the equations derived in this thesis into an efficient computational scheme. If it is found that hydrodynamic damping is significant, then estimates of modal damping from observed motion in a variety of sea states should be made to test the predictions. As an indication of the order of magnitude of hydrodynamic damping, hydrodynamic damping of the fundamental modes of Shell's South Pass 62C was predicted to be about 0.5% to 1.0% in a 40 kt. sea state, which compares to a total measured damping around 2.0%.

The model used for the hydrodynamic force, the relative-motion formulation of Morison's equation, introduced most of the uncertainty in the

accuracy of the predictions. Although a great deal of effort has been expended on measurement of hydrodynamic force in uniform, harmonic flow, very little has been directed to relating C_m and C_d so estimated, to appropriate values for use in random waves. The arguments presented in this thesis for choosing appropriate values of C_m and C_d are no substitute for an extensive program of measurements of forces in random waves. The near-surface region, where the relative-motion argument for including the motion of the structure fails, needs special attention. It is very important that forces in the near-surface region be accurately modelled since the fluid motion and hence the force per unit length is greatest in this region. Also, in view of the difficulty in manipulating a term of the form " $v|v|$ " as compared to a term of the form " $av + bv^3$ " and without justification that " $v|v|$ " is any better representation of nature in oscillating flows, it is proposed that future experimental work on separated-flow drag be directed at estimating values of a and b . Not only is this proposed form of the drag term easier to use, but it may be possible to more closely match predicted to observed forces because the number of parameters which can be adjusted has been increased by one.

In addition to the directions for future research noted, this research has a direct implication on the use of dynamic, finite element programs in the design of offshore platforms. The hydrodynamic component of the damping may be counted twice in the analysis. The modal damping input into one of these programs is normally based on measurements of modal damping estimated from observed motion of similar platforms. The estimated modal damping includes any effective hydrodynamic damping of

the existing platform. Many programs compute hydrodynamic forces using the relative motion formulation of Morison's equation. Therefore, the effective modal damping of the computer model of the platform equals the modal damping specified as input plus the hydrodynamic damping predicted in this thesis. Thus, the hydrodynamic damping is counted twice, once from the observed motion of similar platforms and once by the use of the relative motion formulation of Morison's equation. A more reasonable approach would be to subtract the predicted hydrodynamic damping from the estimate based on the observed motion before using it as input to a program.

APPENDIX A: A Change in the Form of the Drag Term in Morison's Equation

Morison's equation is rather difficult to manipulate mathematically because of the presence of the magnitude of the velocity in the drag term. In performing a non-linear stochastic analysis, some way must be found to get around this difficult problem. As has been pointed out by Dalzell [4], a term of the form " $v|v|$ " can be approximated with good results by one of the form " $av + bv^3$ ", with an appropriate choice of a and b. As demonstrated in Chapter IV, this latter form can be handled quite readily in a stochastic analysis.

The vector version of Morison's equation is shown in equation (A-1) and the proposed modified version in equation (A-2).

$$\frac{df_i}{dL} = (1 + C_m) \frac{\rho\pi D^2}{4} \dot{v}_i + \frac{C_{d\rho} D}{2} v_i |v_i| \quad (A-1)$$

$$\frac{df_i}{dL} = (1 + C_m) \frac{\rho\pi D^2}{4} \dot{v}_i + \frac{C_{d\rho} D}{2} v_i (a + bv_j v_j) \quad (A-2)$$

In the above equations, v_i is the incident flow velocity, which is assumed to be in a plane perpendicular to the axis of the cylinder.

Before deciding whether equation (A-2) is an acceptable substitute for equation (A-1), it is necessary to make a good choice of the two constants, a and b. A rational method by which to choose the constants is to minimize the "error" caused by using equation (A-2) instead of equation (A-1) in a particular problem. One formulation of the "error" is the integral of the magnitude squared of the difference in forces,

over all values of v_i , weighted by the probability density function of v_i . Equation (A-3) expresses this "error".

$$E = \iiint \left| \frac{df_i}{dL} - \frac{df_i}{dL} \right|^2 p(v_i) dv_1 dv_2 dv_3 \quad (A-3)$$

Equation (A-3) can be expanded by substituting in equations (A-1) and (A-2).

$$E = \left\{ \frac{C_d \rho D}{2} \right\}^2 \iiint (|v_i| - a - bv_j v_j)^2 |v_i|^2 p(v_i) dv_1 dv_2 dv_3 \quad (A-4)$$

To proceed from here, we will assume that only one velocity component is significant. This situation arises commonly in practice, such as for the vertical members of a structure subjected to a long-crested sea. In fact, the choice of values for a and b are not strongly affected by this assumption but the computational difficulty is greatly reduced. Equation (A-5) reflects the above assumption. Note also that the subscripts have been dropped as only one velocity component remains.

$$E = \left(\frac{C_d \rho D}{2} \right)^2 \int v^2 (|v| - a - bv^2)^2 p(v) dv \quad (A-5)$$

The type of problem for which it is desirable to use equation (A-2) is one in which an offshore structure is excited by waves of a random sea of low to moderate intensity. In such sea states, the probability distributions of the water velocity components fit the Gaussian distribution quite well. Equation (A-5) can thus be rewritten, substituting in a Gaussian probability density function.

$$E = \left(\frac{C_d \rho D}{2} \right)^2 \frac{1}{\sqrt{2\pi\sigma_v^2}} \int_{-\infty}^{\infty} v^2 (|v| - a - bv^2)^2 \exp \left[-\frac{v^2}{2\sigma_v^2} \right] dv \quad (A-6)$$

In equation (A-6), σ_v^2 is the mean square water velocity incident on the cylinder.

The procedure for choosing a and b is straightforward from this point. The integral can be split into positive and negative halves in order to eliminate the magnitude operator. The polynomials inside each integral can be expanded and the integrals evaluated using tables of definite integrals. Choosing a and b to minimize E then reduces to setting the partial derivatives of E with respect to a and b to zero. The resulting pair of linear equations can be solved for the two coefficients.

$$a = \sigma_v \sqrt{\frac{2}{\pi}} \quad (\text{A-7a})$$

$$b = \frac{1}{3\sigma_v} \sqrt{\frac{2}{\pi}} \quad (\text{A-7b})$$

Equation (A-2) can now be completed with the inclusion of equations (A-7a) and (A-7b).

$$\frac{df_i}{dL} = (1 + C_m) \frac{\rho \pi D^2}{4} v_i + \frac{C_d \rho D \sigma_v}{\sqrt{2\pi}} v_i \left\{ 1 + \left(\frac{v_j v_j}{3\sigma_v^2} \right) \right\} \quad (\text{A-8})$$

In figure A-1 are plotted the magnitudes of the drag terms of Morison's equation and the modified equation, both as a function of the magnitude of the velocity. As can be seen, the modified equation is a good approximation of the original equation over the range $0.5 \sigma_v$ to $3.5 \sigma_v$. Thus for a random vibrations problem involving separated flow, the only times when the force is not well modelled are when the velocity is low and during the infrequent times when the velocity is

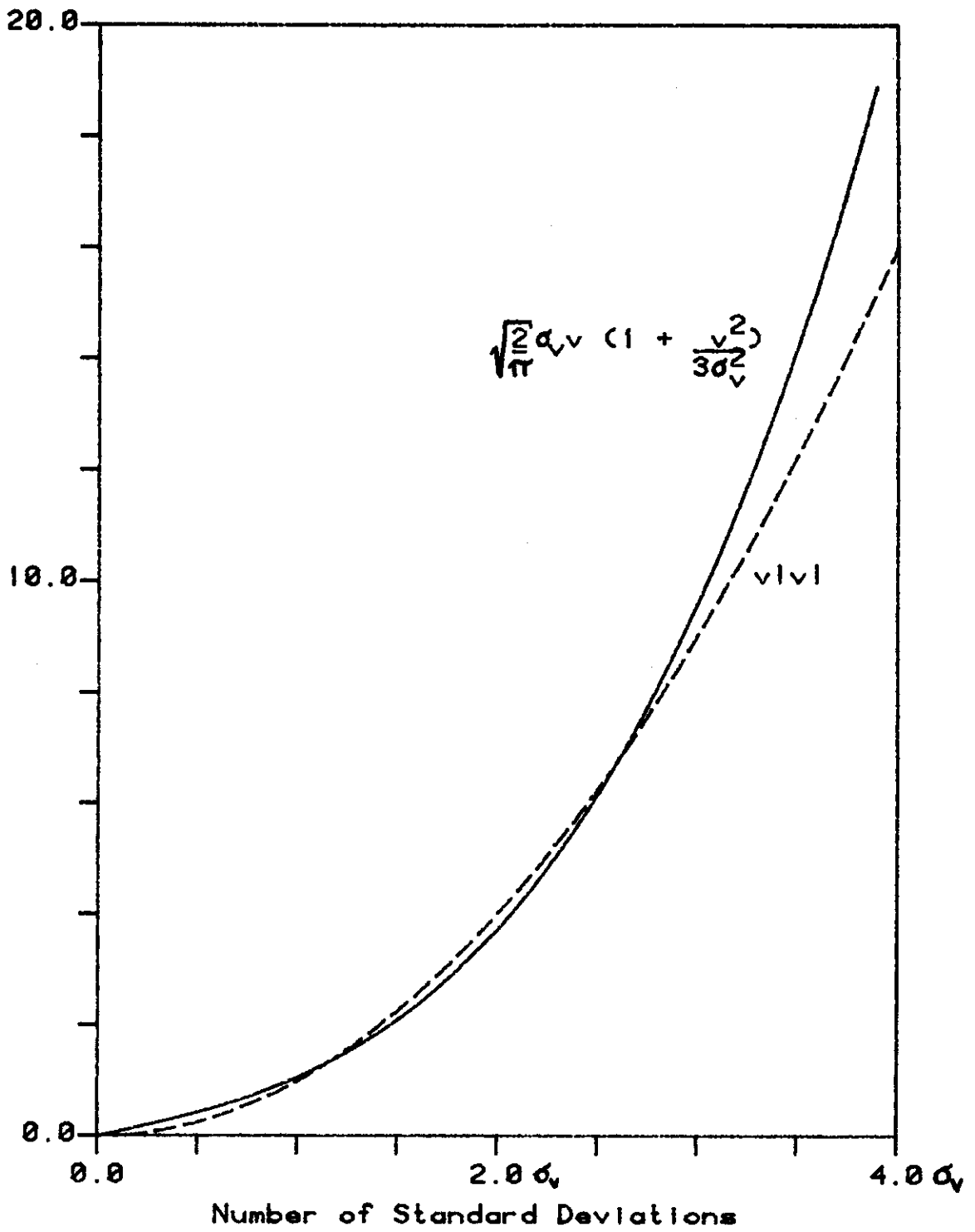


Fig A-1: Comparison of Modified Drag Term with $|v|$

high. If the purpose of this thesis were to predict extreme responses, then equation (A-2) would not be so useful, but since the goal is predicting motion for the purpose of fatigue estimates, the rare, extreme responses are not very important.

It is anticipated that the main influence of the separated flow drag term on the response of an offshore structure to low and moderate sea states will be to increase the apparent damping of the structure. It would therefore be useful to compare the two equations in a problem involving computation of apparent added damping. Most problems of this type are too difficult to solve using Morison's equation, hence the need for the modified version. However, there is one problem which can be solved using either equation, while still bearing a strong resemblance to the type of problem studied in the body of this thesis.

Consider the following simple problem. A cylinder is randomly oscillating with instantaneous velocity $w(t)$. The surrounding water is also randomly oscillating with an instantaneous velocity $u(t)$. The velocities $u(t)$ and $w(t)$ are independent, stationary, zero-mean, Gaussian, random processes with standard deviations σ_u and σ_w respectively. For simplicity, we will restrict u and w to motion along one axis. This problem is similar to the real problem of a segment of a member on a platform in a long-crested random sea. The main difference between the two problems is that u and w would not necessarily be independent in the real problem.

The object of the analysis of this problem is to compare the effective added damping predicted using Morison's equation versus that pre-

dicted using the modified version of the equation. The effect of adding a damper to the cylinder would be to cause a net flow of power away from the cylinder. Therefore, if the separated flow drag acts to effectively increase damping, there should be a net power flow away from the cylinder due to the separated flow drag. The course which will be followed is to predict the expected value of the power flow from the cylinder in this problem. The power flow will be calculated using Morison's equation as well as the modified form proposed in equation (A-8).

The instantaneous power flow per unit length from the cylinder to the water is equal to the negative of the hydrodynamic force acting on the cylinder multiplied by the cylinder's velocity.

$$\frac{d\pi}{dL} = -w \frac{df}{dL} \quad (A-9)$$

As mentioned in Chapter II, the relative velocity form of Morison's equation, and by the same reasoning the modified equation, should be used for the hydrodynamic force in the power flow calculation since the cylinder moves. The two power flows to be compared are found by substituting relative-velocity extensions to equation (A-1) and (A-8) into equation (A-9).

$$\frac{d\pi}{dL} = -w \left\{ (1 + C_m) \frac{\rho \pi D^2}{4} \dot{u} - \frac{C_m \rho \pi D^2}{4} \dot{w} + \frac{C_d \rho D}{2} v |v| \right\} \quad (A-10a)$$

$$\frac{d\pi}{dL} = -w \left\{ (1 + C_m) \frac{\rho \pi D^2}{4} \dot{u} - \frac{C_m \rho \pi D^2}{4} \dot{w} + \frac{C_d \rho D \sigma_v}{\sqrt{2\pi}} v \left(\frac{1+v^2}{3\sigma_v^2} \right) \right\} \quad (A-10b)$$

The following two equations relate the relative velocity to the velocities of the cylinder and water.

$$v = u - w \quad (A-11)$$

$$\sigma_v^2 = \sigma_u^2 + \sigma_w^2 \quad (A-12)$$

The instantaneous power flow is not so important as the expected value of the power flow.

$$E \left[\frac{d\pi}{dL} \right] = -(1+C_m) \frac{\rho\pi D^2}{4} E[w\dot{u}] + \frac{C_m \rho\pi D^2}{4} E[w\dot{w}] - \frac{C_d \rho D}{2} E[wv|v|] \quad (A-13a)$$

$$E \left[\frac{d\pi'}{dL} \right] = -(1+C_m) \frac{\rho\pi D^2}{4} E[w\dot{u}] + \frac{C_m \rho\pi D^2}{4} E[w\dot{w}] - \frac{C_d \rho D \sigma_v}{\sqrt{2\pi}} E \left[wv \left(\frac{1+v^2}{3\sigma_v^2} \right) \right] \quad (A-13b)$$

Note that u and w were defined to be independent so that the first term on the right side of each equation is zero. Also, the expected value of a stationary random process multiplied by its derivative is zero, so that the second term of each equation is also zero.

$$E \left[\frac{d\pi}{dL} \right] = - \frac{C_d \rho D}{2} E[wv|v|] \quad (A-14a)$$

$$E \left[\frac{d\pi'}{dL} \right] = \frac{C_d \rho D \sigma_v}{\sqrt{2\pi}} E \left[wv \left(1 + \frac{v^2}{3\sigma_v^2} \right) \right] \quad (A-14b)$$

The two expectations can be evaluated without much difficulty. It turns out that the two power flows are identical.

$$E \left[\frac{d\pi}{dL} \right] = E \left[\frac{d\pi'}{dL} \right] = \sqrt{\frac{2}{\pi}} C_d \rho D \sigma_v \sigma_w^2 \quad (A-15)$$

In conclusion, a modification to Morison's equation was proposed which eliminated the difficult mathematical problem of dealing with the magnitude of the velocity. The modified equation contained two parameters which could be adjusted so that the modified equation would best fit Morison's equation over some range of velocities. A method was described for choosing the two parameters which led to equation (A-8). A plot of Morison's equation and the modified equation showed that a good fit was made of Morison's equation by the modified version over the important range of velocities for any particular problem involving random flows.

To test how well the modified equation could predict effective, added damping, a simple problem was studied. The effective damping in this problem was predicted using Morison's equation and using the modified version. The two effective damping predictions were identical. Therefore, not only is the modified equation a good fit to Morison's equation over the important velocities for any random flow problem, but the modified equation also predicts the same effective hydrodynamic damping. Therefore, no problem is anticipated in using the modified equation in this research.

APPENDIX B: Selection of the Coefficients C_m and C_d for a Randomly Oscillating Flow.

When computing the hydrodynamic forces on a member of an offshore structure using Morison's equation, a question arises as to the values of C_m and C_d which should be used. Invariably, the flow around the member is a random process, whereas the majority of experiments performed to date to measure forces have employed harmonic flows. The purpose of the following discussion is to present a rational approach for the selection of C_m and C_d to use in a particular, random-flow problem based on the published values of C_m and C_d for harmonic flows.

Consider that the displacement of the water particles around a fixed cylinder is a very narrow band, stationary, zero-mean, Gaussian random process. If a random process has a very narrow bandwidth, individual cycles can be identified in sample time histories of the process, with the amplitudes of successive cycles being a slowly varying function of time. Over a few cycles, the hydrodynamic force is approximately equal to the force measured on a similar cylinder in an harmonic flow with the same frequency and amplitude of motion. Therefore, for a narrow-band, random process, it is possible to relate the hydrodynamic forces to the forces measured on cylinders in harmonic flows.

For cylinders in harmonic flows, the hydrodynamic force is normally related to the instantaneous fluid velocity, u , and acceleration, \dot{u} , through Morison's equation with the coefficients C_m and C_d dependent on the frequency of oscillation and the amplitude of the cycle. Therefore, the hydrodynamic force in random flows can also be related to the fluid

velocity and acceleration through Morison's equation, with the coefficients C_m and C_d varying from cycle to cycle. However, it is necessary for this and other work to be able to predict hydrodynamic forces in random flows from Morison's equation using constant coefficients C_m^* and C_d^* . The values of C_m^* and C_d^* must in some sense reflect the values of C_m and C_d appropriate for harmonic flows over the range of amplitudes encountered in a particular random process. When comparing the narrow-band random flow with harmonic flows, the same frequency of oscillation will be assumed in both cases.

A rational method for selecting appropriate values for C_m^* and C_d^* would be to minimize a measure of the difference between the predicted hydrodynamic force based on constant coefficients and based on coefficients which depend on the amplitude of the cycle. The particular measure which will be minimized is the expected value of the square of the difference in predicted forces, ΔF .

$$\Delta F = E[(f-f^*)^2] \quad (B-1)$$

$$f = (1 + C_m(A)) \frac{\rho\pi D^2}{4} \dot{u} + C_d(A) \frac{\rho D}{2} u|u| \quad (B-2)$$

$$f^* = (1 + C_m^*) \frac{\rho\pi D^2}{4} \dot{u} + C_d^* \frac{\rho D}{2} u|u| \quad (B-3)$$

In equation (B-2), $C_m(A)$ and $C_d(A)$ are the values of the added mass and drag coefficients appropriate for an harmonic flow with displacement amplitude A .

As a first step in evaluating equation (B-1), introduce the following change of variables:

$$u = A \bar{\omega} \sin \phi \quad (B-4a)$$

$$\dot{u} = -A \bar{\omega}^2 \cos \phi \quad (B-4b)$$

The random variable ϕ corresponds to the phase of the displacement cycle for a narrow-band random process. Introduction of the phase is useful, because A and ϕ are independent of each other. The amplitude, A , has a Rayleigh distribution with parameter σ_d , where σ_d is the RMS water particle displacement. The phase has a uniform distribution over the range $-\pi$ to π . The parameter $\bar{\omega}$ is the mean frequency of the random process.

Equation (B-1) may be expanded by substituting in equations (B-2) through (B-4b) and grouping terms. The expectation of the cross-terms between the inertial and drag components of the force is zero.

$$\begin{aligned} \Delta F = E \left[(C_m(A) - C_m^*)^2 \left(\frac{\rho \pi D^2}{4} \right)^2 A^2 \bar{\omega}^4 \cos^2 \phi + \right. \\ \left. + (C_d(A) - C_d^*)^2 \left(\frac{\rho D}{2} \right)^2 A^4 \bar{\omega}^4 \sin^4 \phi \right] \quad (B-5) \end{aligned}$$

Because A and ϕ are independent, equation (B-5) can be further simplified.

$$\begin{aligned} \Delta F = \left(\frac{\rho D^2}{4} \right)^2 \bar{\omega}^4 E[A^2 (C_m(A) - C_m^*)^2] E[\cos^2 \phi] + \\ + \left(\frac{\rho D}{2} \right)^2 \bar{\omega}^4 E[A^4 (C_d(A) - C_d^*)^2] E[\sin^4 \phi] \quad (B-6) \end{aligned}$$

In order to minimize ΔF , take the partial derivatives of ΔF with respect to C_m^* and C_d^* and set them to zero. The values of C_m^* and C_d^* for which the partial derivatives are zero are the optimum selections according to this method.

$$C_m^* = E[A^2 C_m(A)] / E[A^2] \quad (B-7)$$

$$C_d^* = E[A^4 C_d(A)] / E[A^4] \quad (B-8)$$

where:
$$E[g(A)] = \int_0^{\infty} g(A) \frac{A}{\sigma_d} \exp \frac{-A^2}{2\sigma_d^2} dA \quad (B-9)$$

The method of selection described reduces to taking a weighted average of the values of C_m and C_d appropriate for harmonic flows. The weighting function and hence the values of C_m^* and C_d^* depend on the particular random flow conditions through the probability density function of the amplitude. For a Rayleigh distribution, the probability density function is specified completely by the RMS displacement, σ_d . Therefore, C_m^* and C_d^* are functions of σ_d .

Just as C_m and C_d are related to the amplitude of the cycle for harmonic flows through the Keulegan-Carpenter and Reynolds number, C_m^* and C_d^* are related to the RMS displacement, σ_d , through equivalent non-dimensional parameters. The particular forms of the parameters used in this thesis are defined by equations (VI-1) and (VI-2). To parallel standard practise in the definition of Keulegan-Carpenter number, the random flow non-dimensional parameters are expressed in terms of σ_u , the RMS velocity rather than σ_d , σ_u being equal to σ_d multiplied by $\bar{\omega}$. In figures B-1 and B-2, C_m^* and C_d^* are plotted as functions of the random flow Keulegan-Carpenter number. The curves are plotted for a fixed value of β^* , 800, where β^* is defined by equation (B-10).

$$\beta^* = \frac{R^*}{N_{K-C}^*} = \frac{\bar{\omega} D^2}{2\pi \nu} \quad (B-10)$$

The curves were computed from equations (B-8) through (B-10). The functions $C_m(A)$ and $C_d(A)$ were taken from curves published by Sarpkaya [12]. A correction was applied to $C_d(A)$ at the lower Keulegan-Carpenter numbers in accordance with the work of Verley [14]. This correction was important because of the low Reynolds numbers in the experimental work in this thesis. For comparison, a second curve was plotted in each figure. These curves show the values of C_m^* and C_d^* which would be used if the selection were based on taking the values of C_m and C_d appropriate for an harmonic flow with the same RMS velocity as the random flow. The large differences point out the importance of carefully considering the method of selection of C_m^* and C_d^* . However, no method of selection based on experiments in harmonic flow is a proper substitute for experimental measurements of hydrodynamic forces in random flows.

The derivation of the relationship between the hydrodynamic force coefficients for harmonic flows and random flows was performed in the context of a very narrow-band, random process and a fixed cylinder. For lack of suitable alternatives, the relationship will be used independent of the bandwidth of the random process, on the understanding that the accuracy of the results probably degrades with increasing bandwidth. On the basis of the Navier-Stokes equation argument, the relationship can also be applied to problems in which both fluid and cylinder move by replacing the statistics of the incident flow, σ_u and $\bar{\omega}$, by the equivalent statistics of the relative motion between the fluid and the cylinder.

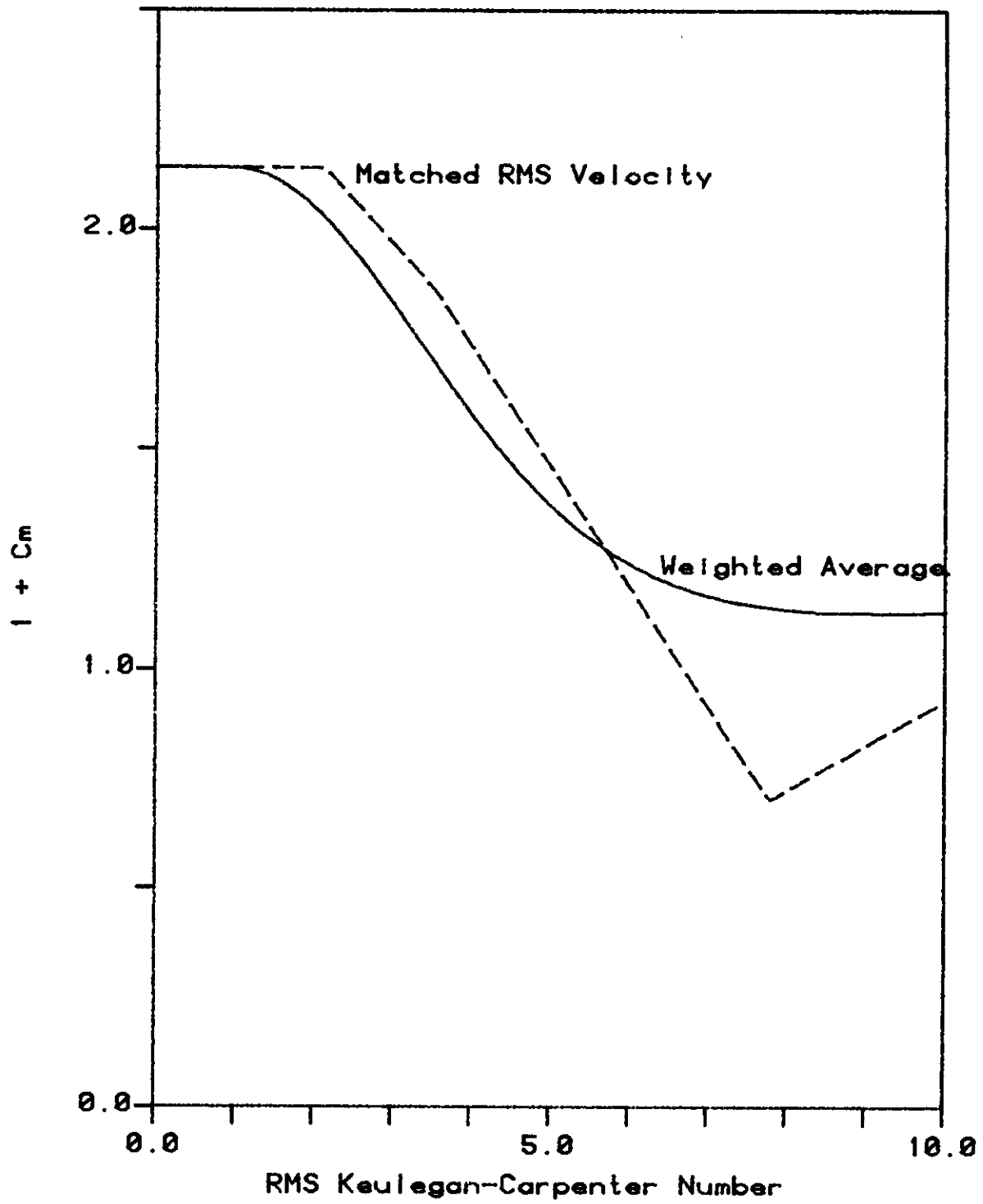


Fig B-1: Random Flow Added Mass

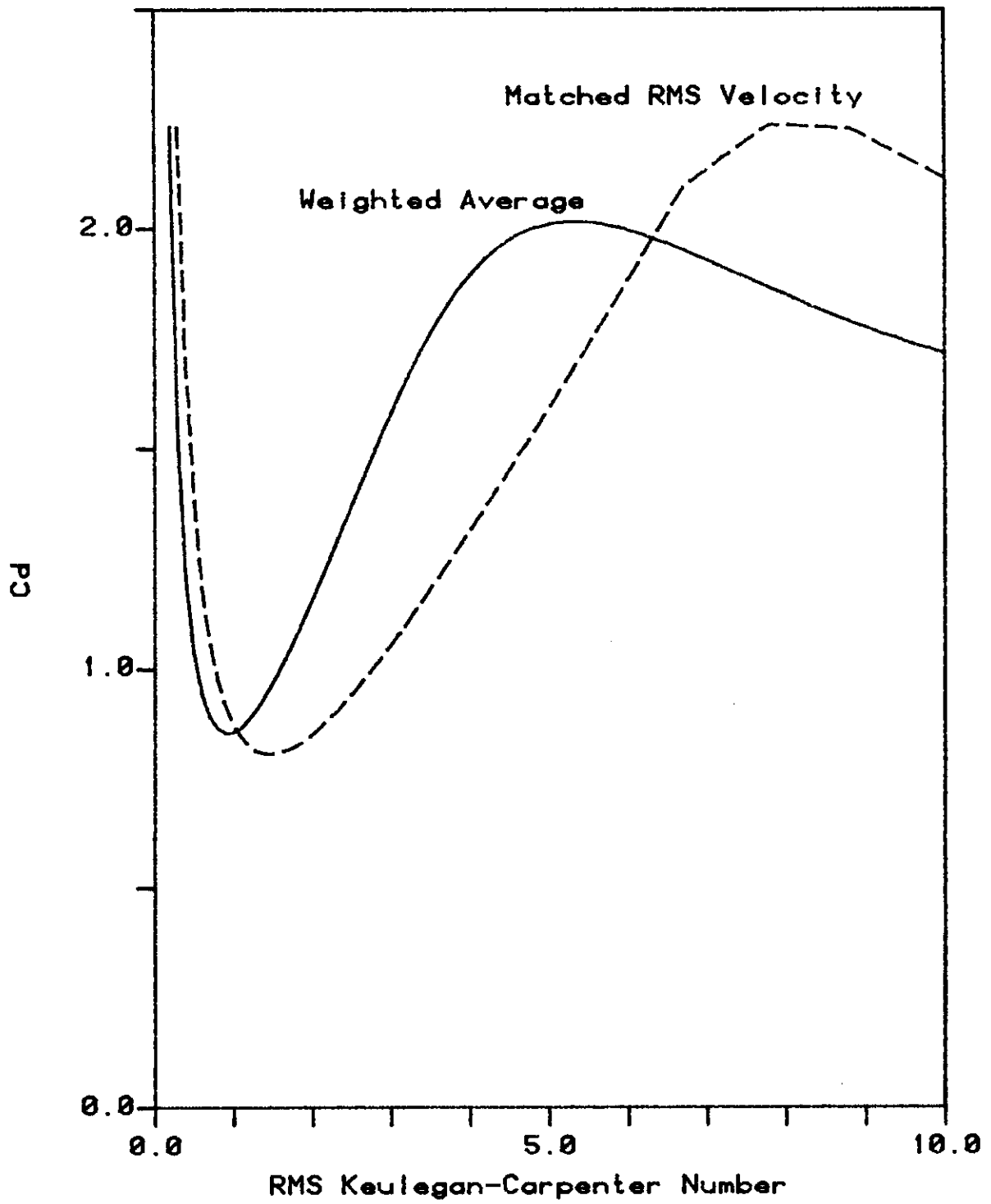


Fig B-2: Random Flow Drag Coeff.

REFERENCES

- [1] Borgman, L.E., "Random Hydrodynamic Forces on Objects," The Annals of Mathematical Statistics, Volume 38, 1967
- [2] Burke, B.G., Tighe, J.T., "A Time Series Model for Dynamic Behaviour of Offshore Structures", Society of Petroleum Engineers Journal, Dec. 1972
- [3] Campbell, R.B., "The Estimation of Natural Frequencies and Damping Ratios of Offshore Structures," Ph.D. Thesis, M.I.T., 1979.
- [4] Dalzell, J.F., "A Note on the Form of Ship Roll Damping," Journal of Ship Research, Volume 22, Number 3, Sept. 1978
- [5] Iyengar, R.N., and Dash, P.K., "Study of the Random Vibration of Nonlinear Systems by the Gaussian Closure Technique", Journal of Applied Mechanics, Vol 45, No. 2
- [6] Malhotra, A.K. and Penzien, J., "Non-deterministic Analysis of Offshore Structures", J. Engr. Mech. Division, ASCE, Vol 96, No. EM6, Dec. 1970
- [7] Moe, G., and Crandall, S.H., "Extremes of Morsion-Type Wave Loading on a Single Pile", ASME Paper No. 77-DET-82, Presented at the Design Engineering Technical Conference, Chicago, Sept. 1977
- [8] Moe, G., and Verley, R.L.P., "An Investigation into the Hydrodynamic Damping of Cylinders Oscillated in Steady Currents of Various Velocities," Report of the River and Harbour Laboratory, Norwegian Institute of Technology, June 1978

- [9] Morison, J.R., O'Brien, M.P., Johnson, J.W., and Schaff, S.A., "The Forces Exerted by Surface Waves on Piles", Trans. AIME, Vol. 189, 1950
- [10] Petrauskas, C., "Hydrodynamic Damping and Added Mass for Flexible Offshore Platforms", Coastal Engineering Research Center Report, Oct. 1976
- [11] Ruhl, J. A., "Offshore Platforms: Observed Behavior and Comparison with Theory", Proceedings of the 1976 Offshore Technology Conference, Paper No. 2553, Houston, May 1976
- [12] Sarpkaya, T., "Forces on Cylinders and Spheres in a Sinusoidally Oscillating Fluid", Journal of Applied Mechanics, ASME, Vol. 42, No. 1, March 1975
- [13] Vandiver, J.K., "Prediction of the Damping-Controlled Response of Offshore Structures to Random Wave Excitations", Society of Petroleum Engineers Journal, Vol. 20, No. 1, February 1980
- [14] Verley, R.L.P., "Oscillations of a Cylinder in Still Water", Report of the River and Harbour Laboratory, Norwegian Institute of Technology, May 1978
- [15] Vugts, J.H., and Kinra, R.K., "Probabilistic Fatigue Analysis of Fixed Offshore Structures", Journal of Petroleum Technology, April 1978

